THE INTERACTING BINARY WHITE DWARF SYSTEMS

APPROVED BY

DISSERTATION COMMITTEE:

_____

_____

_____

_____

_____

_____

THE INTERACTING BINARY WHITE DWARF SYSTEMS

by

JUDITH LUCILLE PROVENCAL, B.A., M.A.

DISSERTATION

Presented to the Faculty of the Graduate School of

The University of Texas at Austin

in Partial Fulfillment

of the Requirements

for the Degree of

DOCTOR OF PHILOSOPHY

THE UNIVERSITY OF TEXAS AT AUSTIN

May, 1994

Acknowledgments

There are a large number of friends who have helped me to realize my goal of a Ph.d. in astronomy. Don Winget has been a wonderful advisor, and has never given up on me despite my serious affliction of the imposter syndrome. Ed Nather has taught me how to observe, and provided me with much guidance in the study of the interacting binaries. Both of them have taught me the importance of doing everything to the best of your ability. The other members of my committee: Rob Robinson, Chris Sneden, and Jan-Erik Solheim have provided many helpful comments and discussions. I also want to thank the other students involved with the Whole Earth telescope group, and the XCOV bunny. I also need to thank Teresa Winget. She has been a wonderful friend, and has tolerated my ideosynchrises all these years. Her job is to "de-geek" Don's students, and I hope she succeeded. Finally, my family has been very supportive. I thank my parents for understanding when their 12 year old daughter would take her little telescope out into the snow and spend hours out there looking at Jupiter and Saturn.

Preface

Before embarking on these pages, I must comment on the usage of the "we" throughout this dissertation. While I wrote this dissertation, I collaborated with many people in this research, several of whom are my committtee members. This dissertation would have been impossible without the participation of the collaborators of the Whole Earth Telescope. It would have been impossible for me alone to collect the amazing amount of data presented in this dissertation and upon which my results are based. Because of this, I feel it appropriate to use "we" in this dissertation.

THE INTERACTING BINARY
WHITE DWARF SYSTEMS

Publication No. _____

Judith Lucille Provencal, Ph.D.
The University of Texas at Austin, 1994

Supervisor: Donald E. Winget

Interacting binary white dwarfs are believed to contain two white dwarfs of extreme mass ratio, one of which is filling its Roche Lobe, transferring material to its companion via an accretion disk. The defining characteristic of an IBWD is the nondetection of hydrogen in the system.

IBWDs represent the culmination of binary star evolution. In this final death dance, two degenerate objects are entangled, the massive white dwarf tidally stripping and devouring its helpless companion's outer layers. Because a white dwarf expands as it loses mass, the end result of this process is the complete absorption of one star by the other.

My goal in the examination of these systems is to understand their photometric behaviour and determine the best model of these objects. The IBWDs represent the endpoint of binary evolution. Knowledge of the physical properties of these objects will provide constraints on theories of binary evolution, white dwarf formation, the thermal and physical structure of accreting white dwarfs, and nucleosynthesis.

To achieve this goal, I have analyzed the most comprehensive high

speed photometric data sets available on 5 of the 6 known objects: AM CVn, PG1346+082, CP Eri, V803 Cen, and G61-29. AM CVn and PG1346+082 were targets of the Whole Earth Telescope in 1988 and 1990 respectively. We find a range of variation timescales, from minutes to days, and a range of physical behaviour. Most importantly, we measure a rate of period change of $\dot{P} = 1.68 \pm 0.03 \times 10^{-11}\ s\ s^{-1}$ for the dominant variation in AM CVn. We also find the differences in behaviour can be attributed to a difference in mass transfer rate that may be evolutionary in origin.

Finally, I discuss in detail the observational characteristics of each object, and overall properties of the IBWD family. In conclusion, I discuss past and future history of these objects, and touch on their possible influence on our knowledge of white dwarf evolution and formation. The IBWDs are possible progenitors of helium white dwarfs. If this hypothesis is correct, these systems represent a second entry point onto the white dwarf cooling curve.

Table of Contents

List of Tables

List of Figures

Chapter 1

A Profile in Psychosis: Stellar Cannibalism

1.1 Introduction

Stars are paradoxically fragile and violent creatures, successfully balancing on a tightrope stretched between unrelenting gravitational collapse and expansion into nothingness. Their stability is achieved through a complex dance partnering pressure and gravity, generating just enough energy via nuclear fusion to counteract the merciless inward drag of gravity but not releasing enough energy to cause the star to expand and cool, slowing the nuclear reaction rate. Stars owe their existence to this alliance of expansion and contraction.

Stars are not benign creatures. Flares, dynamos and chaotic magnetic fields resulting in a plague of spots resembling moldy fruit, convection and rotation are part of the everyday violence of stellar existence. Many stars who are members of multiple systems also expend their energies to participate in a most heinous crime: stellar cannibalism. They devour members of their own species. This thesis will take the reader on an amazing journey of discovery, as we examine objects believed to contain one star ravaging another.

Stellar cannibalism is a manifestation of two facts: 1) stars of different masses evolve at different rates, and 2) as stars evolve past the initial hydrogen burning main sequence, they in general expand. If the initial separation of two stars within a binary is within a range of parameters depending on the mass

ratio of the binary components, as the components of the binary evolve, the system will pass through several eras of mass transfer. The first episode begins when the more massive, or primary, star exhausts hydrogen in its core and expands, becoming extremely bloated. The less massive, or secondary, star, tidally disrupts and strips off the distended primary's outer layers, increasing its own mass and changing the mass ratio of the system. The originally more massive star will continue to evolve and eventually collapse to form a white dwarf, terminating the mass transfer. Meanwhile, the secondary star proceeds in its own evolution, eventually exhausting hydrogen in its own core, and expanding to form a red giant, providing the white dwarf with an opportunity to avenge itself as it strips off the bloated secondary's outer layers. Once the secondary passes through the giant phase and is on its way to becoming a white dwarf itself, it shrinks in size and the second episode of mass transfer ends.

The final primal struggle, the dance of death from which there must be only one survivor, commences. The white dwarfs, as prizefighters sizing each other up in an arena, spiral slowly together as they radiate gravitational radiation. Eventually, the two will become close enough together to begin the third and final era of mass transfer, in this instance from the less massive to the more massive star. Mass transfer from the less massive to the more massive star causes the separation of the two to increase (see section 1.3). A white dwarf is degenerate, and expands as it loses mass so the transfer will be self sustaining until the mass donor loses enough material to no longer qualify as a degenerate object. The transfer rate will decrease and gravitational radiation will again force the two together (Iben *et al.*, 1984). This decisive struggle will end only with the complete absorption of one star by the other. There will be

only one victor triumphant.

Interacting binaries passing through the different episodes of mass transfer share fundamental traits that group them together as a class. All such objects are characterized by their violent photometric activity on timescales ranging from days to seconds. All interacting systems, or cataclysmic variables, as they are sometimes called, are believed to be binaries with orbital periods ranging from minutes to days. The currently accepted model for these systems contains a white dwarf and a low mass secondary which is losing material to the white dwarf. The material is usually transferred via an accretion disk.

This thesis focuses on the photometric behaviour of a special subgroup of the interacting binaries. Typical interacting systems contain a white dwarf and a low mass, hydrogen rich main sequence star as the mass donor. The secondary is still on the main sequence, and is still evolving. The five cases featured in this work are different, they are best modeled with an evolved, low mass degenerate helium object in the role of mass donor. We would like to call the secondary a white dwarf, but that name implies a previous evolutionary path it is not clear these very low mass objects have followed. However, these systems are known as interacting binary white dwarfs (IBWDs) in the literature and will be labelled as such in this thesis. IBWDs are believed to be in the final phase of mass transfer of which the end result is a single white dwarf star.

There are several observational characteristics that define the IBWD family. The first, and most important, is the complete absence of hydrogen from the spectra. The spectra of all known IBWDs are dominated by broad lines, either in emission or absorption, of neutral helium. The lines are consistent

with formation in the atmosphere of a compact object or Doppler broadening in a swiftly rotating accretion disk (Robinson, *et al.*, 1975). All IBWDs are also photometric variables, altering their luminosity on timescales ranging from minutes to days. Some IBWDs undergo large 3 to 4 magnitude outbursts on a quasiperiodic timescale of two to three days. During these eruptions, the spectra of the object vary from absorption lines at maximum light to emission at minimum light (Wood *et al.*, 1987). There are no obvious eclipses detected in any of these systems. Finally, the IBWDs are not strong hard xray sources (Becker, 1981).

The theoretical history of the IBWDs is long and colorful. AM CVn was the first member of the class, discovered in 1946 (Humason *et al.*, 1947). Early models of the object ranged from a quasar to a massive helium star (Patterson, *et al.*, 1979). With the discovery of similar objects that, unlike AM CVn, undergo large magnitude outbursts, the model of the IBWDs evolved to consist of two degenerate objects in a close binary (Faulkner, *et al.*, 1972). The lower mass object is helium, is filling its Roche lobe (see Section 1.3) and transferring material to the more massive primary white dwarf.

The interacting binary white dwarfs provide an exciting avenue into galactic history, binary star evolution, stellar structure, and nucleosynthesis. These systems contain two evolved stars, one of which is being turned inside out by the mass transfer process. The material we observe in the accretion disk is processed material, ripped from the heart of what once was a main sequence star. The shredding of the secondary is a unique opportunity to observe open heart surgery performed on a star, to peer directly into a stellar core, and to actually observe the byproducts of stellar nucleosynthesis. The abundances of

elements present in the accretion disks of these objects will constrain current theories of stellar nuclear reactions (Marsh, *et al.*, 1991).

Determining the physical structure of white dwarfs in binaries will constrain models of binary evolution much as recent progress on the structure of solitary white dwarfs has challenged conventional stellar evolution theory (Winget *et al.*, 1992). The history of our galaxy is written in its white dwarfs, the cooling degenerate relics of former main sequence stars. Solitary field white dwarfs are relatively simple objects of similar mass and radius. Their nuclear fires have long since been quenched and their radiant energy is derived solely from the cooling process. Because they are simply cooling, white dwarfs of different ages have different temperatures. The number distribution of temperatures observed reveals the age of the galaxy and is a fossil record of star formation during different epochs in the history of the Milky Way (Liebert, *et al.*, 1986). Finally, white dwarfs have had a significant impact on stellar evolution. Some solitary white dwarfs with specific temperature values corresponding to the partial ionization of elements such as hydrogen and helium are observed to pulsate with multiple frequencies (Winget, *et al.*, 1981). Accurate knowledge of the pulsation frequencies of white dwarfs allow us to build accurate models of their structure, constraining theories of stellar evolution (Winget, *et al.*, 1992).

As solitary white dwarfs measure the pulse of stellar formation and evolution, the white dwarf components of cataclysmic variables are the fingerprints of stellar evolution within a binary environment. We do not clearly understand the effects being a member of a binary has upon the evolution of the stars contained in the system. Studies of the structure of white dwarfs in cata-

clysmic variables and comparisons with solitary field white dwarfs will provide valuable clues to constrain models of binary evolution, as well as mass transfer and diffusion theories. The IBWDs represent the greatest hope of determining the interior structure of an accreting white dwarf. Each of the IBWDs has a temperature of $\approx$ 20000 K (Patterson, *et al.*, 1992). At these temperatures, helium is partially ionized and provides an efficient mechanism for driving pulsation (Winget, 1981). Solitary helium rich (DB) white dwarfs with similar temperatures are observed to pulsate at multiple frequencies (Winget, *et al.*, 1987). Nonradial pulsation must play some role in the IBWDs as well, whether it be in the accreting star or in the disk (Van Horn, *et al.*, 1980). If even one of the mass accreting white dwarfs is pulsating, we are capable of using the pulsations to accurately measure the mass and internal structure of an accreting white dwarf (Bradley, 1993). We could answer such fundamental questions as whether white dwarf accretors have significantly thicker envelopes than solitary white dwarfs, and what can we learn about different accretion episodes from the structure of the star's outer layers?

1.2 The Plan of Presentation

There are six known IBWDs, five of which are featured in the following pages: AM CVn, PG1346+082, V803 Cen, CP Eri, and G61-29. The sixth is a newly discovered southern hemisphere object, and is not included in this thesis.

Each IBWD is believed to contain two helium degenerate objects, one of which transferring helium rich material via an accretion disk. Each system is a photometric and spectroscopic variable on timescales ranging from minutes

to hours. Each system has an assumed orbital period measured in seconds, but only G61-29 has an unambiguously identified orbital period of 2790 seconds.

The IBWDs are a complex group of objects. The currently accepted model is extremely simplified and does not explain the detailed behaviour we observe. Because of their complicated behaviour, we face a difficult task in identifying a unique model for all IBWDs. In this work, we will approach the problem from a different angle, and examine the observed photometric behaviour of each IBWD in a model independent, empirical manner, and let the data tell us if the model is a unique fit. We will begin our exploration with an introduction to the Roche model of the geometry and parameters of binary systems, followed by a brief description of the data reduction and analysis techniques involved in analyzing the photometric behaviour of each IBWD. We will then place the photometric behaviour of each object under a microscope, and examine models that best fit the observations, commenting on possible future work for each object. In the conclusion of this thesis, we will discuss the overall observational and theoretical characteristics of each object, pointing out family trends. We will conclude our investigation with a discussion of the place in evolutionary history of the IBWDs.

1.3 The Roche Model of the Structure of Binary Stars

Before delving into the intricate behaviours we observe in the IBWDs, we must first consider theoretical models of the structure of close binary systems. Consider a binary containing stars of masses M_1 and M_2. Each star in our hypothetical binary is spherically symmetric, giving rise to a r^{-1} gravita-

tional potential, resulting in an orbit about the center of mass best modelled by an ellipse. Kepler's third law relates the orbital period P to the binary separation a.

$$P^2 = \frac{4\pi^2}{G(M_1 + M_2)} a^3$$

The parameter a is the semi-major axis of the ellipse. The actual separation of the two stars is also a function of the eccentricity of the orbit, and varies from $a(1 + e)$ to $a(1 - e)$. For a circular orbit, the separation is simply given by a.

The 19th century French mathematician Edouard Roche first considered the problem of the behaviour of a test particle placed within a model of the potential created by two massive gravitating objects in the context of the survival of planetary satellites. His methods were later applied to binary star systems. The Roche approach to this problem contains three assumptions: 1) the test particle does not perturb the orbit of the two bodies, 2) the gravitating objects are centrally condensed, and 3) the orbits are circular and Keplerian.

Using the Roche approach, we can describe the gravitational potential field in our hypothetical binary in terms of imaginary surfaces of equal potential, the exact shapes of which are determined by the mass ratio ($\frac{M_2}{M_1}$) (Figure 1.1). At great distances from the binary, the surfaces are circular as the test particle sees the binary as a single mass. The equipotential surfaces very near the two stars are also circular, as the motion of the test particle in this region is dominated by the gravitational potential of the nearby star. The circular potentials surrounding each star are joined by a unique figure eight shaped surface that encompasses both stars. The part of the surface surrounding each

Figure 1.1: The surfaces of equal potential in a binary system. CM is the center of mass of the system, r_1 and r_2 are the distances of stars M_1 and M_2 from CM, L_1, L_2, L_3 are the inner and outer Lagrangian points. L_4 and L_5 are points of local potential maxima.

star is known as the Roche lobe. Any material within the Roche lobe of each star is dominated by the gravity of the nearby star. The lobes are joined at the inner Lagrangian point (L_1), which behaves as a mountain pass between two valleys. If any material within a Roche lobe near the inner Lagrangian point is perturbed, it finds it easier to travel to the other Roche lobe through L_1 than to escape outside the Roche lobes altogether. The points labelled L_2 and L_3 in Figure 1.1 are the outer Lagrangian points.

This visual image of the geometry of a binary has important consequences for models of mass transfer. If the two stars are both small in radius, and their stellar surfaces do not touch their imaginary Roche lobe surfaces, the material comprising each star is dominated by the gravity of each star, and the binary system is said to be detached. If either star evolves and expands, or if the binary separation decreases via gravitational radiation, the surface of either star may come in contact with its Roche lobe, and the star then fills its Roche lobe. Material near L_1, if perturbed, will travel through L_1 into the Roche lobe of the other star. Such a binary is said to be semi-detached and mass transfer will continue as long as the donor's stellar surface remains in contact with its Roche lobe.

In the reference frame of the accretor, L_1 acts as the nozzle of a hose, continuously spraying material as it whirls around the primary at the orbital period. The incoming material carries significant angular momentum which must be lost before the material can accrete onto the surface of the accretor. For the Roche model, the circularization radius, or the radius at which the material will form a ring around the accretor, depends on the mass ratio, and hence the angular momentum, of the binary (Frank *et. al*, 1985). Unless the accretor is very distended, or a strong magnetic field is present, the material will form a ring around the primary.

$$\frac{R_c}{a} = (1+q)[0.500 - 0.227log(q)]^4$$

where R_c is the circularization radius, a is the binary separation, and q is the mass ratio $\frac{M_2}{M_1}$.

An accretion disk provides an efficient mechanism for losing angular momentum and allowing material to accrete onto the primary. Unfortunately, we do not understand the actual viscous mechanism responsible for angular momentum loss, so models of accretion disks parameterize this important mechanism within the parameter α, believed to be between 0 and 1 (Shakura *et al.*, 1973). The disk energy, be it through collisions, viscosity, shocks or whatever. The only way the material within the disk can respond to this loss is to sink deeper into the potential well of the star, which requires the material to lose angular momentum. The net result is most material will spiral inward to impact on surface of the accretor while the outer parts of the disk will gain angular momentum and spiral outwards, carrying angular momentum with it. The size of the accretion disk is limited by tidal forces.

Mass transfer, in addition to its influence on the evolution of each star, will cause the binary parameters to change. If we model mass transfer assuming a constant total mass, the mass ratio of the two stars will either increase or decrease, resulting in a change of separation and orbital period (Frank *et. al.* 1985). The effect of mass transfer on separation depends on whether the donor is the more or less massive component of the binary. If the more massive star is the donor, the mass ratio will become less extreme and move closer to unity, the separation will decrease, and the binary period will decrease. If the less massive star is losing material, the mass ratio will become more extreme, the separation will increase, and the binary period will become longer. The lobe radius will increase as well, requiring our model to include some mechanism to keep the stellar surface in contact with the Roche lobe if mass transfer is to be sustained. æ

Chapter 2

Data Reduction and Analysis Tools

High speed photometry is an observational technique designed to monitor short period variations in the luminosity of a variable star, and is the primary observational tool we employed in this thesis. Raw, unreduced photometric data consists of long lists of numbers obtained over periods of time. Hidden within these lists is valuable information concerning the brightness of a star as a function of time. This chapter describes the techniques we used in retrieving the information and transforming the lists of counts into knowledge of the periodic behaviour of the star we observed.

2.1 Data Reduction Techniques

The standard two (or three) channel photometer (Nather, 1973) attached to the end of a telescope generates a series of times and number of counts detected from a variable star (Ch 1) and a constant brightness comparison star (Ch 2) observed to monitor photometric conditions. The number of counts is a measure of the number of pulses the photomultiplier tube produces as light strikes the tube's photocathode. Ideally, the number of pulses is a measurement of the number of photons arriving, through a small aperture, from the star, striking the photocathode, and producing pulses. Unfortunately, the photons do not come solely from the star; the sky, moon, atmospheric extinction,

scintillation, weather conditions, fireflies, and instrumental noise contribute to the observed signal. These effects must be carefully removed to unmask the actual brightness variations of the star.

The observed angular size of our variable star on the sky fluctuates due to changing seeing conditions, and most telescopes do not track with extreme precision. Because it is vitally important to always include all the light from the star, the aperture through which the light beam travels is of necessity larger than the angular diameter of the star on the sky. The contribution, from background sources such as the small patch of sky background immediately adjacent to the star, to the number of counts detected is termed the "sky".

Sky pollution, including any moonlight present, is measured with either of two techniques. If the observer is fortunate enough to possess a three channel photometer, the third channel continuously monitors the sky background by observing a patch of sky near the variable star. If a two channel photometer is employed, measurements of the stars in both channel 1 and channel 2 are briefly interrupted in a nonperiodic manner to move the telescope off the variable and comparison stars to measure sky background. Of course, continuous sky measurements are preferred, because the sky may vary significantly within minutes, a timescale identical to the variations we are searching for in the star. If measurements of the variable star must be interrupted to sample sky, the process must be accomplished in a nonperiodic matter, and on a timescale longer than the periodicities we are interested in. Periodic gaps in the variable's light curve will introduce artifacts into the analysis.

If a continuous sky channel is available, the sky curve is smoothed

and subtracted point by point from the light curve of the variable star. When only occasional sky measurements are available, an approximate sky curve is produced by fitting a straight line between consecutive sky measurements and subtracting this piecewise linear fit from the variable star's light curve.

The fractional contribution of sky to the total number of counts in the variable star's light curve is a primarily a function of the magnitude of the star. In the case of AM CVn ($m_b = 14.4$), sky brightness is responsible for up to 40 percent of the total counts on a 36 inch telescope with a two millimeter aperture. For PG1346+082 in low state ($m_b = 17.6$), the sky accounts for up to 80 percent of the photons, and in high state ($m_b = 13.6$) contributes about 25 percent of the total counts. When sky contributes such a large fraction of the total number of observed counts, a three channel photometer, with its continuous sky record, provides much better results than the two channel photometer.

During the course of a night of observing, the altitude of the star in the sky will change, increasing or decreasing the amount of atmosphere between the telescope and the variable. During a star's prime observing season, it is visible at dusk low on the horizon, viewed through a large amount of atmosphere, rises through the meridian, where it is viewed through a minimum of atmosphere, and sets again at dawn, again viewed through a large amount of atmosphere. The variation of amount of atmosphere along our line of sight results in atmospheric extinction, producing a characteristic change in the number of photons arriving at the telescope (Figure 2.1). To remove the effects of extinction, an extinction fit is calculated for each nightly light curve and then subtracted from the light curve. If the variable star maintains a constant mean magnitude and the observing conditions during the night were

good, the resulting light curve will have a constant mean number of counts.

The removal of sky and extinction is not the final step of the reduction process. Symptoms of nonphotometric weather are sometimes present in the light curve. Clouds, lightning, and gross fluctuations in the observed angular size of the star will mask the actual variations of the star. In this situation, the second channel comparison star plays an important role. The comparison star is unvarying in brightness (although in a few instances, we have accidently chosen variable stars for our comparison star), and after removal of sky and extinction, its light curve should be flat if weather conditions were photometric. If cloud was present, or the quality of seeing varied, the comparison light curve will not be flat. If the discrepancies are extreme, the light curve of the variable star is suspect, as it will also contain variations not physically present in the variable. Such data should not be used in further analysis.

The removal of sky, extinction, and nonphotometric data leaves us with light curves corresponding to the number of counts received from the variable star corrected to above the earth's atmosphere. To facilitate in stringing light curves from different nights, and in many instances, different telescopes, together, each is divided by the average number of counts to give a mean of zero. We assume that the star maintains a constant mean magnitude, a condition which is violated for several stars in this study. As will be explained, special steps have been taken in the analysis of these objects.

The placement of each light curve on a uniform time base is the final step in data reduction (see Kepler *et al.*, 1982 for a more detailed account). The time standard used during observation is UTC, which is converted to ephemeris

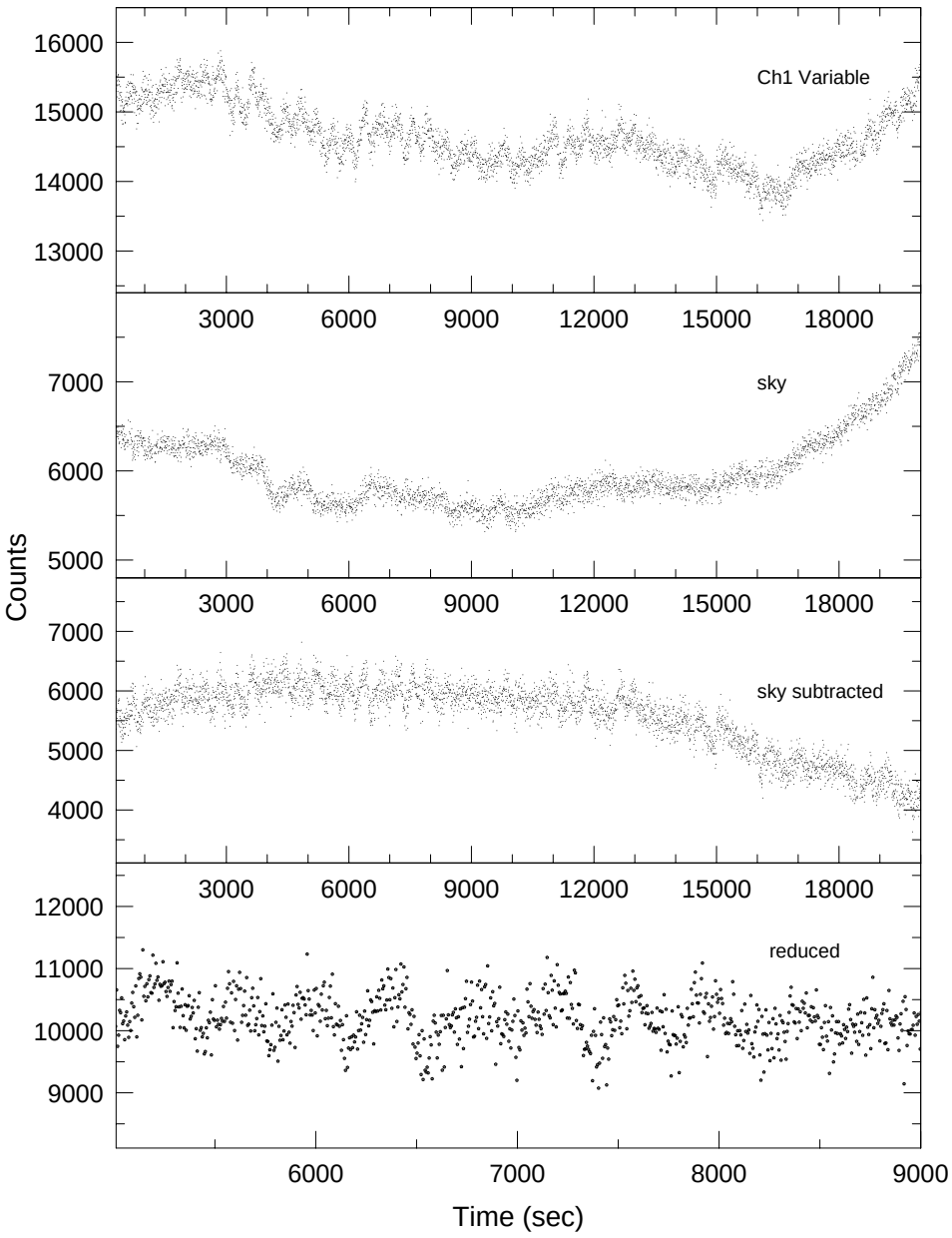

Figure 2.1: Data Reduction techniques for a three channel data run. The first panel displays the variable and the sky channel, the second panel shows the effects of extinction, and the last panel is a portion of the reduced light curve.

time, with due account taken of leap seconds. To remove the motion of the earth about the sun and correct the time of each observation to the barycenter of the solar system, we calculated the barycentric correction for each run start and applied it to each point in the run. One of the Fourier techniques we employ in analysis requires equally spaced data, therefore we did not calculate the barycentric correction for each point in each run. This results in a systematic effect mimicking an unimportant timing error of up to two seconds through the course of a run. Finally, the barycentric times for observed points in each run are then converted to Julian ephemeris date. Each run in each observing year is referenced to a time corresponding to the beginning of the observing season. Placing each run of each observing season on a standard timescale allows us to string together all of the individual light curves obtained during each observing season for analysis, giving us the timebase necessary to adequately examine multiperiodic variables (see section 2.3).

Traditionally, we have employed the units "mmg" (millimagnitudes) to describe the relative amplitudes of the variations we measured. However, this unit is misleading, as the term "magnitude" implies a logarithmic scale, while the amplitudes we measure are linear, relative intensities. Therefore, we have adopted the unit of modulation intensity recently introduced by Winget *et. al* (1993). Modulation intensity (mi) is a linear representation of fractional intensity of modulation, employing a linear rather than logarithmic scale. We will also employ the corresponding units of modulation power $mp = (mi)^2$ as our unit of power (traditionally defined as $(mmg)^2$).

2.2 Non-Linear Least Squares

With the successful reduction of the raw light curves, we are now ready to proceed with data analysis. Our principle goal in the analysis of an object's brightness variations is the identification of any periodic behaviour in its light curve. We wish to fit a sine curve of given period to the data and evaluate the "goodness" of, or how much we can believe in, the fit. One of the primary tools we employ in this analysis is the non-linear least squares fitting technique.

All non-linear least squares techniques use the same basic method, choosing a a model and a merit function to determine the agreement between the data and the model to be fit. We adjust the parameters of the model with the incentive of identifying the best fit between the model and the data. When we find the minimum value of the merit function, we have found the best fit for our model to the data.

To leap into mathematics for a moment, the standard model used in most least squares techniques is a linear combination of a series of functions of x. In general, the standard model has the form

$$y(x) = \sum_{k=1}^{M} a_k X_k(x)$$

where $X_1(x) \ldots X_M(x)$ are the basis functions. We note that the term "non-linear" does not refer to the linearity of the functions of x, but comments only on the model's dependence on the parameters $a_k, k = 1, 2, ...N$.

The non-linear least squares technique we chose to employ in this

dissertation, uses χ^2 as its merit function.

$$\chi^2(\vec{a}) = \sum_{i=1}^{N} \frac{\left(y_i - y(x_i;\vec{a})\right)^2}{\sigma_i}$$

(For a detailed discussion of fitting methods, see Numerical Recipes, p. 499.)

We are searching for periodic behaviour in the light curves of variable stars, and therefore choose sine functions as our model for the light curves. Of course, our sine model is an ideal, noiseless generalization and will never exactly match the original light curve. High speed photometry is dominated by scintillation noise, created as atmospheric cells of differing size pass between the star and the telescope. Scintillation noise "smears" the light curve, allowing the non-linear least squares program to fit, with nearly equal confidence, a series of sine curves of slightly different period. The noise in effect introduces a range, or error, in our knowledge of any period actually present in the light curve.

Non-linear least squares fitting is an iterative process. The nonlinear dependence of the model on the parameters a_k eliminates the possibility of directly solving the problem. We begin with an initial guess of the period of variation. The non-linear least squares program takes the initial guess, compares it to the data, and decides on improvements. The new guess will become the initial guess, and the program will iterate again. Once the value of χ^2 ceases to decrease with each iteration, the current guess becomes the model best fitting the data. This solution is recorded for use by the user.

The non-linear least squares program must decide, after comparing our input guess with the data, how much to change the guess and in what direction before proceeding to the next iteration. The size of each step in the

iteration, or the distance from the initial guess to the improved guess, is scaled according to the behaviour of a scaling factor λ. λ is increased if χ^2 increases from the previous value and decreased if χ^2 is less than the previous value.

A helpful mental model is to picture yourself as a person travelling in mountainous country corresponding to frequency space. It is difficult to climb the mountains, and you try to avoid them. Running into a small bump in frequency space will cause χ^2 to increase. λ will increase the step size, avoiding getting stuck trying to climb the bump. It is also not unusual for χ^2 to wander, with small variations, near the minimum of a flat valley, spending a great deal of time calculating directions of maximum decent in the generally flat region. In practice, iteration ceases when χ^2 decreases by a negligible amount.

The covariance matrix calculated by the non-linear least squares program samples the dependence of each parameter on the others. The structure of the matrix is quite simple. The diagonal terms are the squares of the variances of each individual parameter. The other elements are the covariances, demonstrating the dependence of each parameter on the others. If our data are normally distributed, the errors of each parameter will be independent, the matrix will be symmetric about the diagonal and the covariance terms will equal zero. On the other hand, if the values of the covariances are comparable to the diagonal elements we will need to re- examine our data set. In this case, the model parameters are not normally distributed and the error of the fit is underestimated. For example, in fitting a sine function to a light curve, the covariance matrix contains information on the errors in the period, amplitude and phase. The diagonal matrix elements are the separate errors in the period, amplitude and phase. The nondiagonal elements contain information

on the dependence of the errors of period on the phase and amplitude, on the dependence of the errors of the amplitude on the phase and the period and the dependence of the errors of the amplitude on the period and the phase. If these terms are not close to zero, than the period, amplitude and phase are not orthogonal, but are correlated. If we want to accurately determine any period of variation in the light curve, we need to go back to the telescope and get more data.

2.3 The Fourier Transform and its Applications

We use nonlinear least squares techniques to fit sine waves to a series of data. This technique is very descriptive if we have prior knowledge of a rough value of the periods of variation in the stellar light curve. It would be painstaking, however, if we did not know if the star were variable at all, and wanted to explore all of frequency space for possible variations. This situation is the dominion of the Fourier transform, using sine functions as a basis set.

We can describe any physical waveform in terms of a series of sinusoidal components. In other words, any physical function of time may be transformed to a function of frequency describing the sinusoidal constituents of the original function of time. This concept forms the cornerstone of the Fourier transform (FT). Because of the FT's ability to identify periodic signals, we use the FT as a bulwark of high speed data analysis. In all of the work in this thesis, the term Fourier transform (FT) refers to a transform using sine functions as a basis set.

Our high speed photometric data sets sample the intensity of the

star as a function of time. A Fourier transform of a light curve describes the frequency, amplitude and phase of the light curve's periodic and quasiperiodic sinusoidal components (see Bracewell, 1965 for a detailed discussion of the properties of Fourier transforms). Identifying periodicities present in the data is the first step towards realizing a sensible physical model of the object of interest. For example, many white dwarf stars pulsate simultaneously at hundreds of different frequencies. As bells made of different metals ring with different tones, stars with dissimilar structures will oscillate with different frequencies. If we can accurately identify these frequencies, we can build a detailed model of the white dwarf's interior structure (Winget *et al.*, 1992).

Unfortunately, as we will discuss in the next section, the high speed photometric data we obtain at the telescope are not continuous, but are recorded at discrete intervals as the photometer counts photons for a certain length of time, records the number, and begins counting again. We have no knowledge of the behaviour of the light curve on timescales shorter than the counting, or integration, time, reducing the ability of the FT to construct a perfect model of the sinusoidal components of the light curve. The absolutely critical sampling frequency for a sine wave is two points per cycle. The FT is not sensitive to variations in the data with frequencies greater than the limiting frequency Nyquist frequency

$$f_c = \frac{1}{2\Delta t}$$

where Δt is the integration time (Bracewell, 1965). We must choose an integration time with care, depending on the timescale of the variations of interest. If all the variations in the light curve are at frequencies smaller than the integration frequency, the FT of the light curve can be considered an accurate

representation of the data. If power is present at frequencies larger than the integration frequency, we cannot retrieve this information with the data in hand because of the characteristics of the way we took the data. Power will be reflected into the FT of our under-sampled data, but will not represent the variations physically present in the star and lead to erroneous interpretations. We must carefully choose the integration frequency to be far larger than any physical frequencies possibly present in the light curve.

The white dwarf stars which form the centerpiece of this thesis, are variable at more than one frequency simultaneously. To be helpful in our analysis, we must be able to use the FT to separate and isolate individual frequencies in the light curve. The ability of a FT to distinguish closely spaced individual frequencies is dictated by the length in time, or timebase, of the light curve. Formally, the resolution of a FT is defined as

$$R = \frac{1}{2t}$$

where t is the time length of the data set (Bracewell, 1965). If we calculate the FT of data containing periodic signals with frequency differences greater than this resolution, separate, isolated peaks will be present. If the frequency difference is smaller than the resolution, the peaks will blend together and appear as a distended, perhaps strangely shaped, peak in the FT.

The width of an individual peak in a FT is also a function of the length of the input light curve. If we continually calculate and recalculate a FT of a light curve that is perpetually increasing in length, we can watch the resolution of the FT increase and the widths of each peak decrease. This

decrease in width translates into an increasingly better knowledge of the actual frequency of variation and a decrease in the associated errors.

The number of frequency points we calculate to adequately sample the shape of a FT is also a function of the timebase of the input light curve. The resolution defined above defines the separation in frequency of adequately resolved peaks in the FT. The number of frequency points we actually calculate to describe the FT must exceed that required by the resolution of the data set. If we were to calculate a FT using only the number of points defined by

$$N = \frac{\text{freq range}}{R}$$

then one peak in the FT will be assigned two points. We have no guarantee, however, that each point will lie exactly on the maximum or exactly in the valley of each peak. If we try to measure the amplitude of a peak in such a FT by interpolating between points, our measurement will be underestimated. Our estimation of the frequency of the peak will also be in error. The number of points actually calculated must be sufficient to adequately define the shape of the peak profile. We calculated all the FTs in this thesis using a number of points defined by of

$$N = \frac{\text{freq range}}{R_{10}}$$

where $R_{10} = \frac{1}{10t}$. In this instance, all peaks are oversampled by five times to define their shapes and amplitudes.

2.4 The Whole Earth Telescope

This section deals with what is really an observational tool. The description of WET is included here simply because the enormity of the prob-

lem which led to its birth could not be clearly understood without a bit of explanation of Fourier transform techniques.

The basic theoretical properties of the Fourier transform are characterized by the Nyquist frequency and the resolution. However, in the real world the characteristics of the data set itself will have profound effects on the resulting FT and our ability to extract useful information from it. The ideal light curve is an infinitely long series of measurements with no gaps in the record. Unfortunately, we do not live on a static world, but rather on a dynamic, living planet. The sun rises every morning, clouds sometimes cover the sky, and winds occasionally blow hard enough to make further observations impossible until the following evening. These hardships introduce imperfections, in the form of periodic gaps, into the data record. The gaps manifest themselves in a FT as a forest of additional peaks surrounding the actual peak representing the variation, and separated from it by the frequency at which the gaps appear in the data. These peaks are aliases, artifacts of our inability to continuously monitor the star's variations and do not represent physical processes arising in the star. For example, single site observations are dominated by one-day aliases resulting from unavoidable sunrise, where the frequency difference between the aliases is $11.57 \mu Hz$, corresponding to the inverse of 86400 seconds, the number of seconds in each day.

Every physical periodicity at which a variable star is changing its luminosity will have this alias forest associated with it in the FT of the light curve (Figure 2.2). Variations closely spaced in frequency will create an interwoven web of aliases that is impossible to untangle. Overlapping alias patterns may create a peak in the transform that is larger than the actual power, making

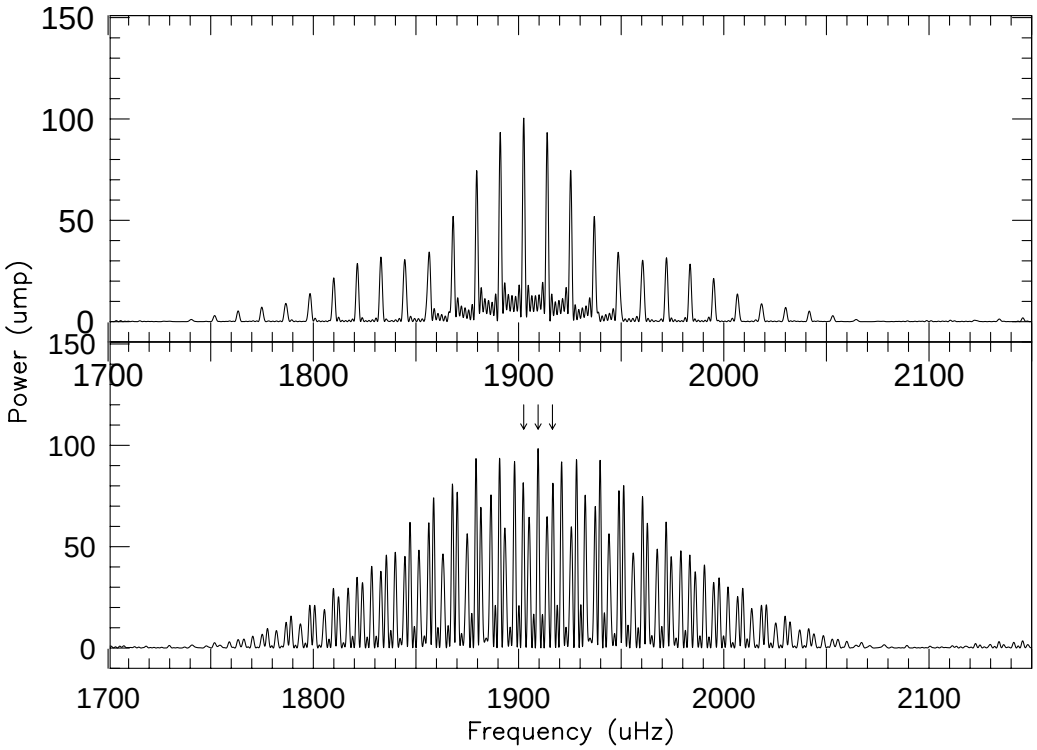

Figure 2.2: The effects of gaps in the data set. The top panel is a spectral window, the pattern created by a single sinusoid sampled as if it were observed every night for one week. The additional peaks are aliases, created by the daily data gap. The bottom panel shows the same data set with three closely spaced frequencies. Which are the real ones? (arrows)

it possible to misidentify the real power present in the data. Frustration with this problem led to the conception of the Whole Earth Telescope (WET).

The Whole Earth Telescope (WET) is a collaboration of astronomers around the globe assembled to combat the problem of gaps in the data. During a WET observing run, multiple telescopes situated at strategic longitudes strive to obtain continuous coverage of the target variable star. As the star sets for one observer, another further west is preparing to "pick up the ball" and avoid creating a breach in the data record. WET tries to organize as much

redundant coverage as possible, allowing a pinch-hitting observatory to step in if another can not continue to observe the primary target. To maximize the advantages of redundant coverage and to make best use of the multiple telescopes, during a WET campaign data we reduce data in real time, and we also maintain a command post at all times. We contact, usually via telephone, each observatory at the beginning of their night to ascertain weather conditions and assign targets to observers. If all observatories are clear, WET can maintain coverage of both the primary target and a secondary target simultaneously. If the station observing the primary target clouds over during the night, the observers contact WET headquarters, and the site monitoring the secondary target is switched to the prime target.

The result of all this ambitious organization has been some of the most spectacular, nearly continuous data sets ever obtained on a variety of targets, ranging from DO variable white dwarf stars to an intermediate polar. The elimination of alias peaks and the greatly improved signal to noise of the FTs have led to the best identification of the masses of a hot pre-white dwarf star and a helium rich white dwarf to date (Winget *et al.*, 1992, 1993), the measurements of rotation rates, the detection of magnetic fields of order of thousands of gauss, the detection of differential rotation in a white dwarf, and measurements of the structure of a helium rich white dwarf. WET observations challenged traditional dogma of white dwarf formation and structure, stellar evolution and nucleosynthesis. WET is the cutting edge of observational techniques.

The Whole Earth Telescope has observed three of the five interacting binary white dwarf systems: AM CVn, PG1346+082, and V803 Cen. The data sets on AM CVn and PG1346+082 form the centerpiece of our observational

analysis of the interacting binary white dwarf systems.

2.5 The Analysis of the Fourier Transform

To extract useful information from the Fourier transform, we must first understand how physical processes occurring in the star's light curve would manifest themselves in the frequency space sampled by the FT. If we know the fingerprints to search for, our analysis chores will be much easier.

Many astrophysically interesting activities, such as pulsation, rotation, and in some cases amplitude modulation, manifest themselves in a FT as a series of peaks equally spaced in frequency or in period. Several standard techniques to search for such characteristics exist, such as the KS test (Press, *et al.*, 1987). However, these tests are biased in that the tester is required to pick peaks beforehand to use in the test. We wished to develop an unbiased method of searching a FT for peaks of equal frequency splitting.

We developed an automated technique of exhaustively searching an entire FT for peaks with equal frequency spacing. The method involves both the FT and its spectral window. The spectral window is the pattern in a FT created by a single, noiseless sinusoid sampled exactly as the original data. Our method functions because the structure of alias peaks in the spectral window is independent of the frequency of the sinusoid creating the window. The spectral window of a 200 second variation is identical to the spectral window of a 15000 second period.

The window is used to create a template containing two peaks separated by the frequency splitting of interest. This template is formed by adding,

in both frequency and phase, two spectral windows, one of which is offset in frequency with respect to the other, by the frequency difference being searched for. It is critical to include phase information to adjust the amplitudes of the alias peaks properly.

The template is compared with the pattern of power surrounding every peak in the FT above an amplitude threshold decided upon by the user. The technique determines the sum, for all peaks in the FT about the amplitude limit, of the square of the differences between the template and the regions surrounding the actual peaks, and derives average differences for the entire FT for every frequency difference being searched for.

$$D_{peak} = \sum_{i=1}^{npks} (A_{FT} - A_{temp})^2$$

$$Av_{split} = \frac{D_{npks}}{N_{npks}}$$

After each peak has been tested for a certain frequency splitting, a new template is created with a slightly different frequency splitting and the process is repeated. If a certain frequency splitting occurs in the FT a multiple of times, the template will be a good fit to the region surrounding the peaks split by this frequency. The average difference for that frequency splitting will be less than the average for other splittings. The difference we calculate for that splitting will be a minimum.

This new technique is in some ways superior to our two standard techniques to search for equal frequency or period spacings; the Kolmogorov-Smirnov (KS) test and the FT of the period transform (period spacings) (Winget, *et al.*, 1992). As we have discussed, the KS test requires prior choice of peaks

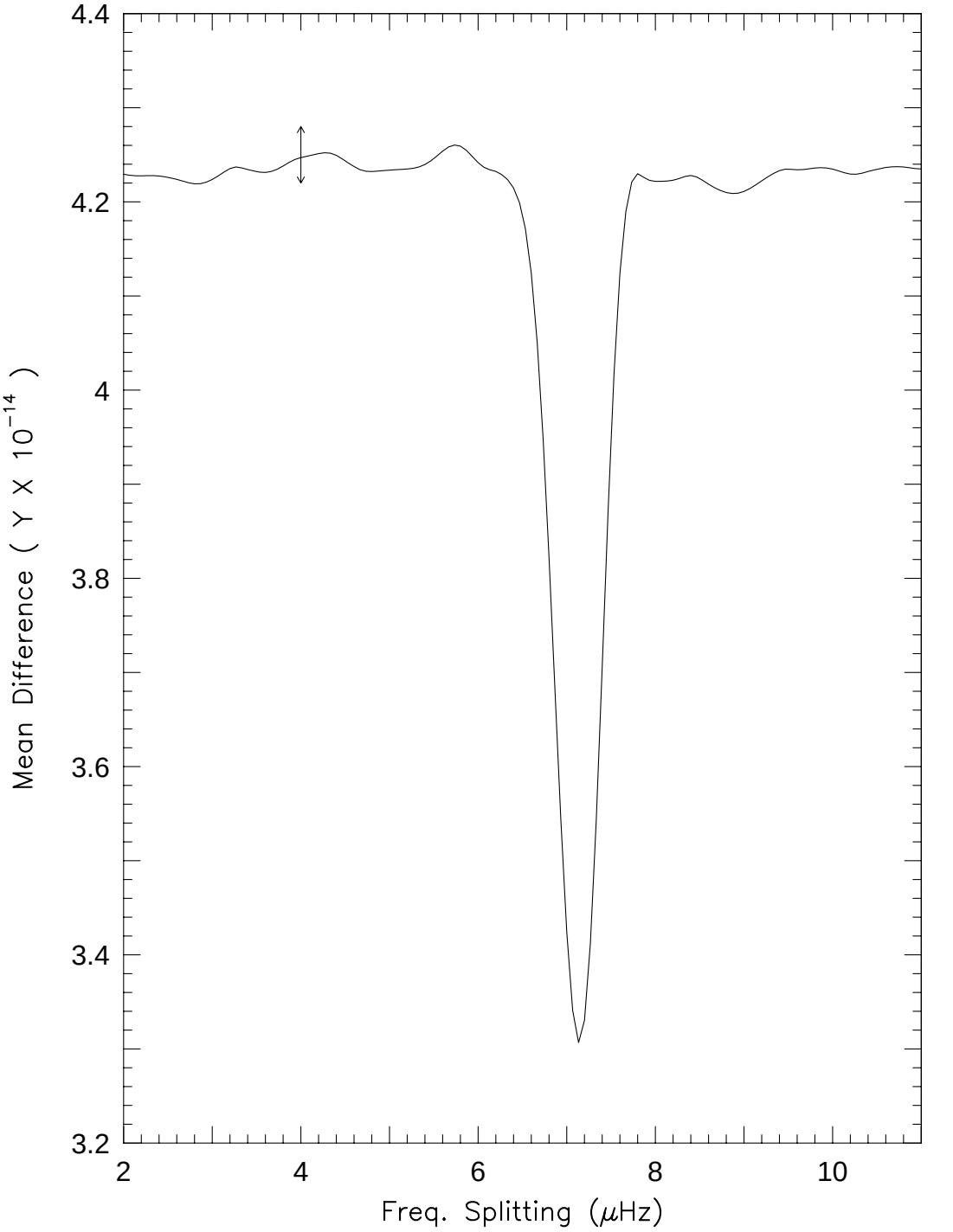

Figure 2.3: The frequency splitting present in a region of the FT of the DOV star PG1159+035, as detected by the template method. The one sigma errors are given by the arrows. The minimum at $\approx 7.0\mu Hz$ tells us this frequency splitting is present in the FT. This is confirmed by visual inspection of the data set, and corresponds to rotationally split l=2 nonradial g-modes.

as input. This test is biased. Because the peak profiles in the period transform are highly nonsinusoidal, the FT of the PT introduces harmonics of the equal spacings. This can confuse the issue of the actual period spacings present. However, the template method does not yet function well in searching for period spacings because of problems in normalizing the results for each peak and period spacing. The equal period spacing template for each peak in an FT is a different size, unlike the situation for equal frequency splitting. We have not yet successfully overcome this problem.

The template technique to search for equal frequency splittings functions best when the aliases present in each FT are reduced, as in WET data. Aliases are always the same frequency away from the main peak, and therefore will be detected by this technique. A solution to this problem is to use the technique on the window itself. We can then eliminate any equal frequency spacings found in the spectral window when the test is used on the actual data set.

Chapter 3

The Unusual Variable Star AM CVn

We have completed our discussion of the reduction and analysis techniques we will use in this thesis, and it is now time to delve into the exciting, complex observed behaviour of the IBWDs. We will begin our exploration with AM CVn, the first IBWD, and perhaps the best hope for finally understanding these fascinating objects.

AM CVn (HZ-29, WD 1232+37, PG1232+379) was discovered by Humason and Zwicky in 1946 (Humason *et al.*, 1947). Its peculiar spectrum, characterized by shallow, asymmetric, neutral helium absorption lines and a complete lack of hydrogen, was first noticed by Greenstein and Matthews (1957). AM CVn has been demonstrated to vary its brightness, at the one percent level, at two independent frequencies; the double humped 1051 s ($951.2\mu Hz$) dominant variation and also at 1011 s ($988.7\mu Hz$) (Smak, 1967 and Solheim, *et al.*, 1984). Flickering, the classic signature of mass transfer, was first reported in AM CVn's light curve in 1972 (Warner and Robinson, 1972). The object maintains a constant mean amplitude (14.3 m_b). No large magnitude outbursts, such as those seen in dwarf novae, have ever been observed in AM CVn.

Since its discovery, a plethora of papers have been published attempting to explain the enigma of AM CVn. Proposed models encompass everything

from a quasar to a massive helium star (see Patterson, *et al.*, 1979). The consensus today models AM CVn as an interacting binary consisting of two helium white dwarfs of extreme mass ratio (Faulkner *et al.*, 1972, see Wood *et al.*, 1987 for convincing arguments). The less massive component fills its Roche Lobe and transfers material to the primary via an accretion disk. This model is based on the hydrogen depleted spectrum, the photometric variability, the lack of x-ray emission and the presence of flickering in the light curve.

Fundamental questions concerning the behaviour of AM CVN persist. The light curve has consistently been described in terms of a dominant 1051 s period with a double-humped pulse shape. No conclusive evidence exists, however, to determine whether the true cycle of repeatability is $951.3\mu Hz$ (1051.2 s) (Smak, 1967) or $1902.5\mu Hz$ (525 s), as suggested by Solheim *et al.* (1984). Despite the $951.2\mu Hz$ variation's presumed orbital origin, no correct ephemeris has ever been presented, casting doubt on the frequency and amplitude stability of this variation.

We must also consider the multiperiodic nature of AM CVn. Solheim *et al.* (1984) reported the presence of significant power in AM CVN's Fourier transform at $988.7\mu Hz$ (1011.4 s). We observe amplitude changes in this period on timescales of months.

In an attack on AM CVn, we have organized all the high speed photometry available to us, spanning 1976 to 1992. Through careful examination of the Fourier transforms (FTs), pulse shapes and phase information of this vast collection of data we will attack the question of the true physical period in this object and attempt to sort out the confusion surrounding the mystery

of AM CVn.

3.1 Observations and Reductions

The observations consist of 289 hours of white light and multicolor high speed photometry obtained in 1976, 1978, 1982, 1987, 1990, and 1992 (see Chapter 2 for detailed discussions of the techniques and equipment). The multicolor data were taken with Johnson U, B, and V filters. The filters, plus one setting containing no filter, were rotated through the light beam to obtain information in each filter bandwidth. The sites and telescopes which contributed are given in Tables 3.1 to 3.3. Over half of the data was taken in 1990, during a two week Whole Earth Telescope run (Nather *et al.* 1990). All the individual runs employed either 3, 5, 6 or 10 second integration times.

The method of reduction is that employed by Winget *et al.* (1992) and discussed in Chapter 2. No attempt was made to differentiate individual runs by telescope aperture, and the individual light curves were not tapered. Our best example of a reduced light curve is given in Figure 3.1.

3.2 The Fourier Transforms

We constructed a Fourier Transform (FT) of the light curves from each year (Figure 3.2). With the exception of 1990, these seasonal FTs are calculated using data obtained from a single site, spanning several nights, and therefore have gaps in coverage. Gaps create cycle count ambiguities and result in the production of additional peaks, or aliases, in the FT. The frequency, amplitude, and quantity of the aliases produced are influenced by the number

Table 3.1: 1976-1982 Journal of Observations

Run	Telescope	Date	Run Start	Length	Integration
r1722	36 inch	27 May 76	3:49:54	2.1	5.0
r1724	36 inch	28 May 76	3:28:44	1.95	5.0
r1727	36 inch	29 May 76	3:29:00	2.4	5.0
r1730	36 inch	30 May 76	3:27:32	2.57	5.0
r2093	30 inch	8 Mar 78	7:27:00	4.1	10
r2098	30 inch	9 Mar 78	5:53:00	5.33	10
r2104	30 inch	10 Mar 78	8:38:00	2.43	10
r2106	30 inch	11 Mar 78	5:04:00	6.71	10
r2109	30 inch	12 Mar 78	3:39:00	6.32	10
r2112	30 inch	13 Mar 78	3:22:00	3.18	10
r2123	82 inch	17 Mar 78	8:17:50	2.10	3
r2126	36 inch	1 Apr 78	5:48:00	1.40	5.0
r2130	36 inch	3 Apr 78	3:28:20	1.45	5.0
r2131	36 inch	3 Apr 78	6:09:20	3.79	5.0
r2137	30 inch	11 Apr 78	2:47:00	1.84	5.0
r2138	30 inch	11 Apr 78	7:01:00	2.79	5.0
r2141	30 inch	12 Apr 78	4:45:00	4.70	5.0
r2146	82 inch	13 Apr 78	7:27:31	2.75	5.0
r2149	82 inch	15 Apr 78	7:23:00	1.00	5.0
r2151	82 inch	17 Apr 78	6:31:16	0.51	5.0
r2156	36 inch	7 May 78	4:34:20	2.36	5.0
r2163	36 inch	9 May 78	4:07:40	3.22	5.0
r2170	36 inch	12 May 78	3:35:20	3.46	5.0
r2190	36 inch	5 June 78	4:01:20	1.61	5.0
r2205	82 inch	8 June 78	5:06:57	0.81	5.0
r2352	30 inch	4 Dec 78	10:13:10	1.05	5.0
r2354	30 inch	23 Dec 78	9:19:00	3.15	5.0
r2358	30 inch	24 Dec 78	11:07:30	1.32	5.0
r2362	30 inch	25 Dec 78	11:29:20	1.04	5.0
r2632	36 inch	24 Jan 82	9:05:32	3.34	5.0
r2638	36 inch	27 Jan 82	9:24:08	2.77	6.0
r2641	36 inch	28 Jan 82	9:08:11	3.37	6.0
r2666	30 inch	22 May 82	3:16:33	3.27	5.0
r2677	36 inch	17 June 82	3:33:26	1.36	5.0

Table 3.2: Journal of Observations

Run	Telescope	Date	Run Start (UT)	Length (hr)	Int (s)
run31	36 inch	2 Feb 87		4.53	5.0
run35	36 inch	3 Feb 87		4.05	5.0
run36	36 inch	4 Feb 87		4.65	5.0
run8	36 inch	4 Mar 87	5:38:30	2.96	5.0
run26	36 inch	5 Mar 87	6:21:40	2.22	5.0
run28	36 inch	5 Mar 87	8:52:00	2.98	5.0
run45	36 inch	6 Mar 87	6:17:50	2.23	5.0
run47	36 inch	6 Mar 87	8:47:50	2.93	5.0
run64	36 inch	7 Mar 87	6:14:40	2.23	5.0
run66	36 inch	7 Mar 87	8:43:30	2.98	5.0
run68	36 inch	8 Mar 87	5:18:10	1.43	5.0

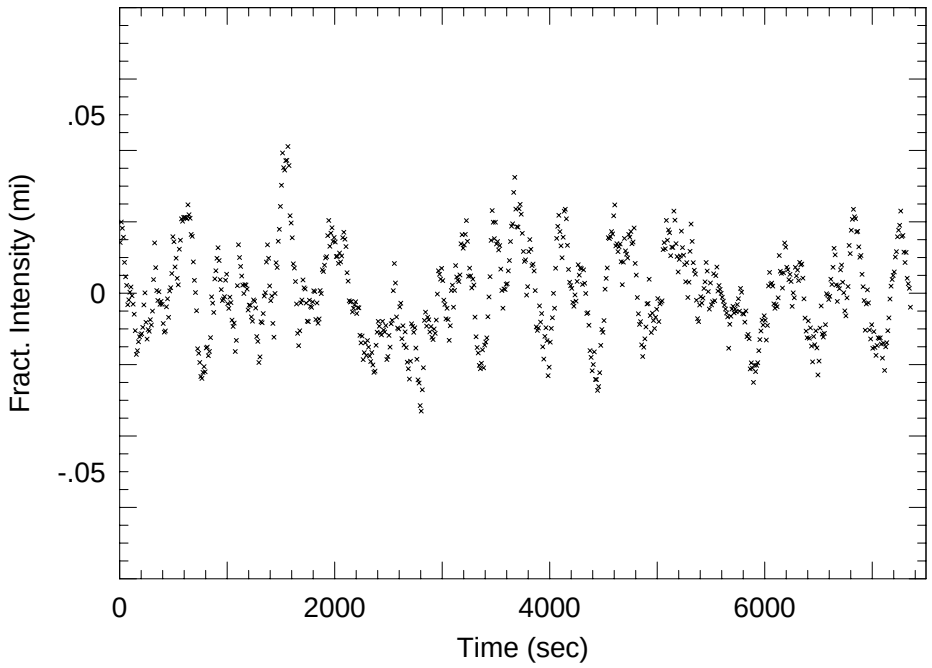

Figure 3.1: Light Curve of AM CVn taken with the CFHT 3.6m telescope. The 525.6 second variation is clearly visible.

Table 3.3: 1990 Journal of Observations

Run	Telescope	Date	Run Start (UT)	Length (hr)	Int (s)
pab24	30 inch	22 Mar 90	4:57:00	6.69	10
a210	24 inch	23 Mar 90	7:28:00	7.80	10
ren-0071	1m	23 Mar 90	21:49:00	4.86	10
ren-0072	1m	24 Mar 90	17:53:30	8.79	10
a212	24 inch	25 Mar 90	11:39:00	3.38	10
ren-0073	1m	25 Mar 90	17:38:00	9.01	10
pab-0029	82 inch	26 Mar 90	5:13:30	6.28	10
ren-0074	1m	26 Mar 90	17:23:30	9.18	10
a213	24 inch	27 Mar 90	6:30:00	8.87	10
ren-0075	1m	27 Mar 90	17:16:10	9.05	10
a215	24 inch	28 Mar 90	12:40:00	2.45	10
ren-0077	1m	29 Mar 90	00:12:10	2.13	10
en-001	36 inch	29 Mar 90	6:01:08	1.60	10
en-002	36 inch	29 Mar 90	8:06:44	2.64	10
a217	24 inch	29 Mar 90	12:56:00	2.23	10
gv-0071	OHP 2m	30 Mar 90	1:46:57	2.05	10
a220	24 inch	30 Mar 90	12:56:00	2.09	10
gv-0075	OHP 2m	31 Mar 90	1:39:40	2.117	10
en-0003	36 inch	31 Mar 90	2:29:33	6.60	10
cfc20	24 inch	31 Mar 90	7:22:20	6.07	10
fbv-002	CFHT 4m	31 Mar 90	13:07:57	2.04	10
gv-0079	OHP 2m	1 Apr 90	6:09:10	1.94	10
cfc23	24 inch	1 Apr 90	5:35:30	9.05	10
cfc24	24 inch	2 Apr 90	5:35:30	9.55	10
cfc25	24 inch	3 Apr 90	5:50:20	4.25	10
jlp-081	36 inch	14 Jan 92	07:05:33	2.00	5.0
jlp-082	36 inch	14 Jan 92	09:09:43	3.00	5.0
jlp-084	36 inch	15 Jan 92	08:07:00	2.94	5.0
jlp-085	36 inch	15 Jan 92	11:07:50	0.94	5.0
jlp-091	36 inch	4 Apr 92	3:11:30	8.37	5.0
jlp-092	36 inch	6 Apr 92	8:44:21	2.32	5.0
jlp-093 UBVC	36 inch	7 Apr 92	2:54:50	6.50	5.0
jlp-094 UBVC	36 inch	9 Apr 92	2:36:10	3.69	5.0
jlp-096	36 inch	28 May 92	7:42:00	0.93	5.0
jlp-0100	36 inch	1 Jun 92	4:46:20	2.52	5.0
jlp-0103	36 inch	3 Jun 92	3:56:00	2.13	5.0
jlp-0104	36 inch	3 Jun 92	6:07:30	0.54	5.0
jlp-0105	36 inch	3 Jun 92	6:46:20	0.48	5.0

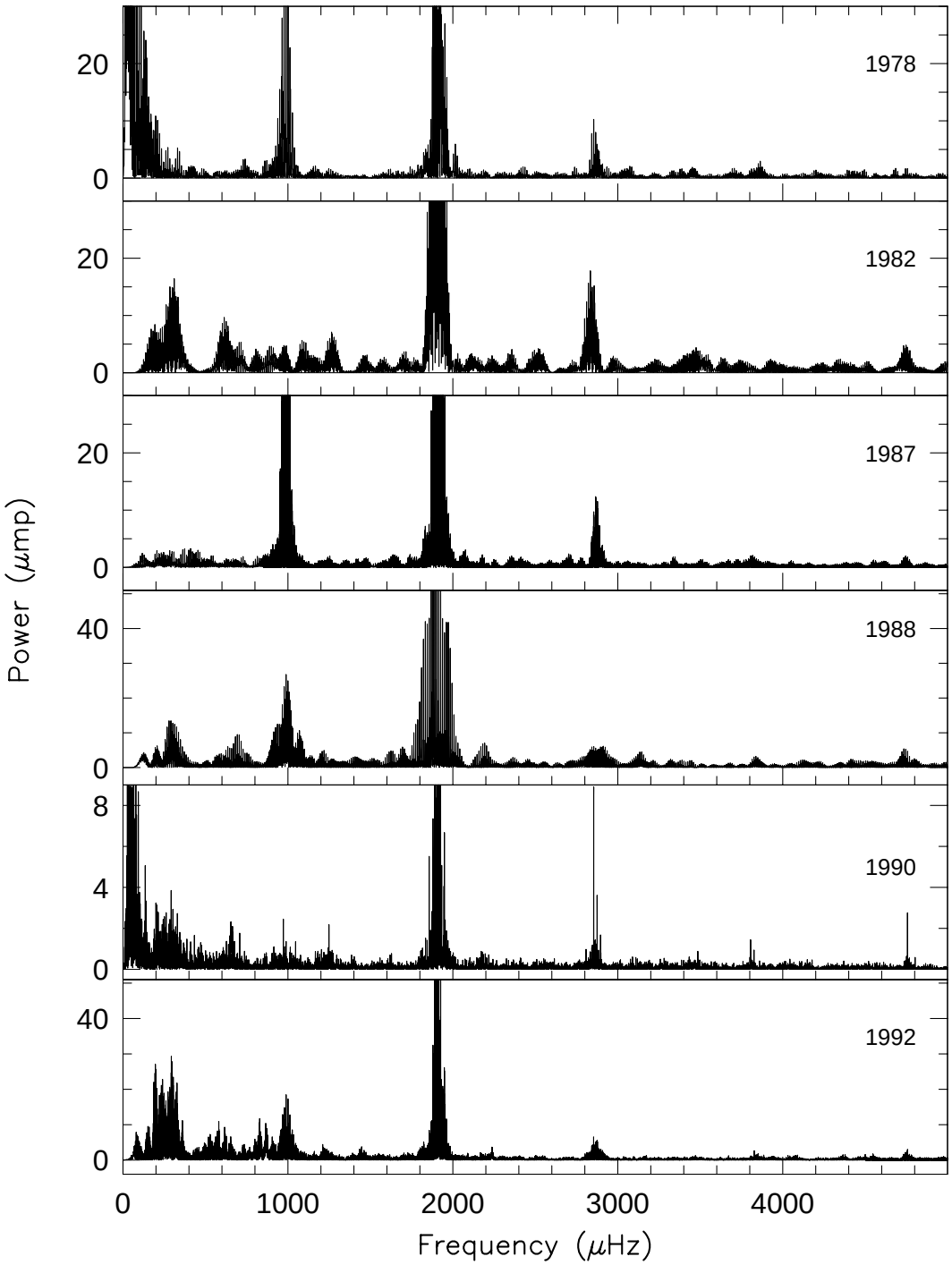

Figure 3.2: The seasonal Fourier transforms of AM CVn. The dominant power is at 1902.6, 2853.9, 3813.9, 4756.4, and 988.7 μHz, (525.6, 350.4 262.2, 210.2, 175.2 and 1011.4 seconds). The power at 988.7 μHz is capable of dramatic amplitude changes.

and length of periodic gaps in the coverage (see the detailed discussion on aliasing in section 2.4 and in Nather *et al.*, 1990). Excluding the 1990 seasonal FT, this group of Fourier transforms is dominated by 24 hour aliases created by the daily sunrise.

The basic similarities and underlying differences of each FT are evident. The dominant power is consistently at $1902.5\mu Hz$ (525.6 s), with additional peaks appearing at $988.7, 1248.8, 2853, 8, 3805.2, 4756.4$, and $5707.8\mu Hz$ (1011.4, 800.8, 350.4, 262.8, and 175.2 s). No power is detected at $951.2\mu Hz$, the reported period of variability. Solheim *et al.* (1984) express a difficulty in differentiating between 988.7 and $951.2\mu Hz$ because $951.2\mu Hz$ is near a 3 cycle per day alias of $988.7\mu Hz$. This is not the case in any FT presented in Figure 3.2. The frequency difference between 988.7 and $951.2\mu Hz$ 37.4 μHz, corresponding to a period of 0.31 days. $951.2\mu Hz$is $2.6 \pm 0.1\mu Hz$ away from the three cycle per day alias. The seasonal FTs have sufficient timebase to resolve this frequency difference. In no case is significant power present at $951.2\mu Hz$.

With the exception of the 988.7 and large amplitude peaks in the seasonal FTs are integral harmonics of the reported period of $951.2\mu Hz$, exact to within measurement error. The amplitudes of the $1902.5, 2853.8, 3805.2, 4756.4$, and $5707.8\mu Hz$ are stable, within measurement error, in all the FTs (Figure 3.3).

Closer examination of these supposed harmonics of $951.2\mu Hz$ (1051 s) demonstrates that the power at $1902.5, 2853.8$ and $3805.2\mu Hz$ does not consist of isolated peaks, but rather is associated with intricate structure. Figure 3.4 presents a closeup of the area around the $1902.5\mu Hz$ power for each year. The

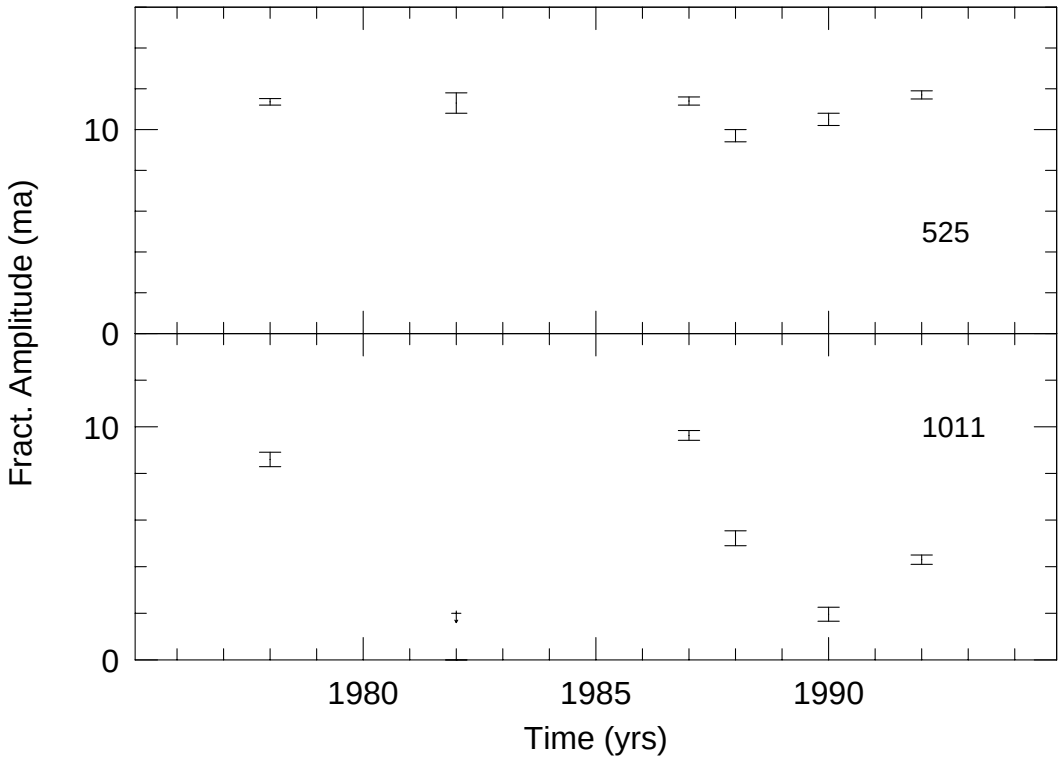

Figure 3.3: Amplitude of 525.6 (top panel) and 1011.4 (bottom panel) second peaks each observing season. The 525.6 second peak is stable to within 2σ, while the 1011.4 second peak may vary significantly.

spectral window, the pattern created in an FT by a single sine wave sampled exactly as the actual data, is given in the corner of each FT. The window is not plotted on the same frequency scale as the FT, but serves to illustrate the pattern of aliases created by a single frequency.

The FTs of the $1902.5\mu Hz$ region contain structure that is the signature of the presence of multiple periodicities. This is clearly demonstrated in the 1987 data, where a second window pattern is entangled on the high frequency side of the dominant window pattern. The 1976 FT bulges on the low frequency side at the bottom of each peak, an example of two spectral windows superimposed that are not resolved.

The nearly continuous coverage obtained in 1990 by WET (see section 2.4 for a detailed discussion of WET) has effectively eliminated aliases in the FT, and reveals a second small peak on the high frequency side of the dominant peak, labeled by the arrow in Figure 3.4. The additional small peaks present on both sides of the large $1902.5\mu Hz$ peak are residual aliases. The labeled peak is not part of the alias web, and is over 7 sigma above the FT's noise level. The $1902.5\mu Hz$ region in this case contains at least a doublet, and possibly a triplet. Similar complex structure is evident in the 2853.8 (Figure 3.5) and $3805.2\mu Hz$ regions in each year. The frequency difference between the dominant peak and the second component (and third, in some cases) is $20.77(\pm 0.04)\mu Hz$ in every instance. In each example, the "harmonic peak" is the lowest frequency and highest amplitude component of the multiplet.

The power in the 988.7 μHz (1011 sec) region appears to be independent of the 1902.6 μHz (525.6 sec) peak and its harmonics. It characteristically

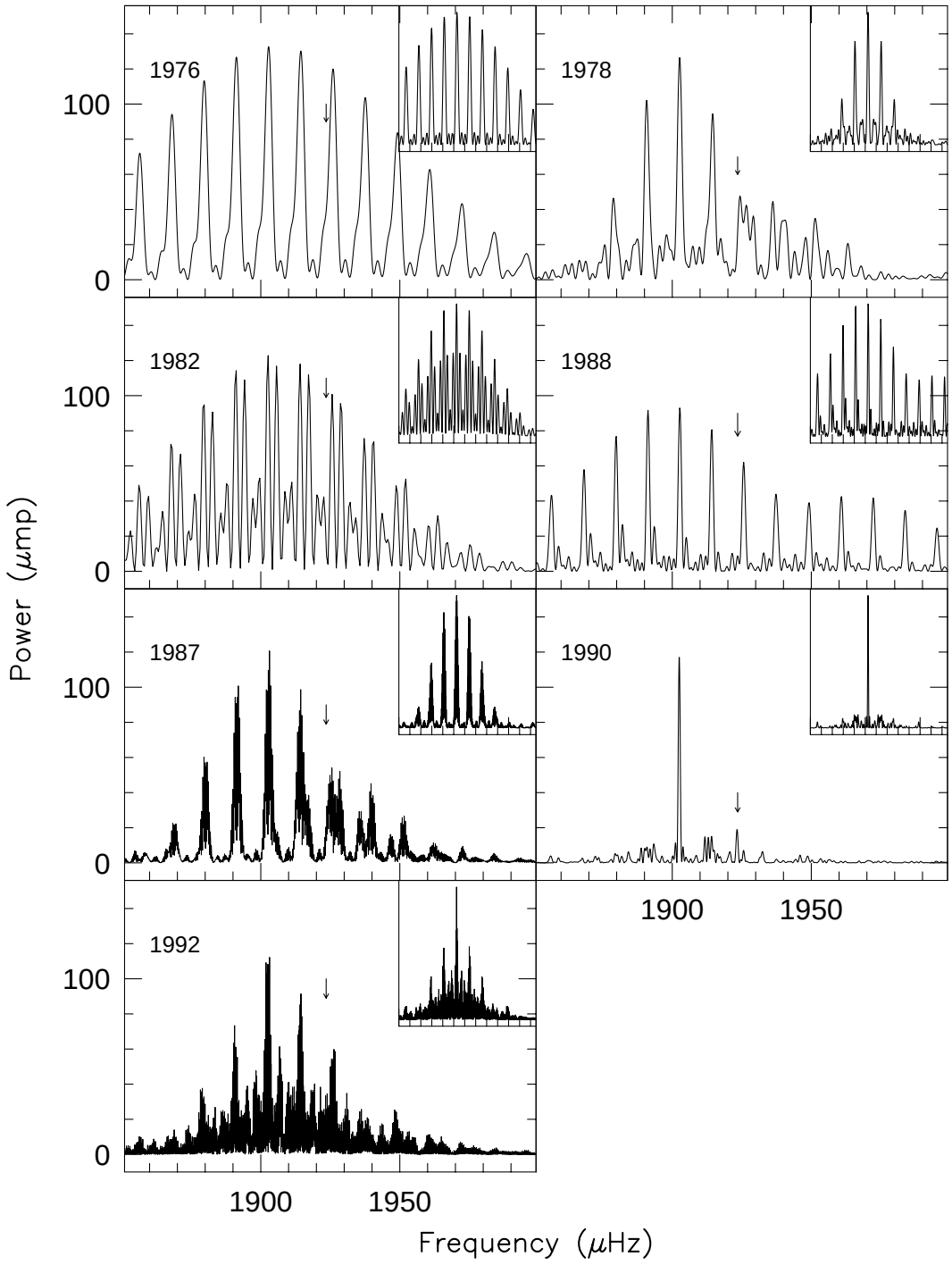

Figure 3.4: The $1902.5\mu Hz$ (525.6 s) region of AM CVn's FT in each season. The spectral window, the pattern generated by a single sine, is given in each corner. The arrow marks the location of the doublet peak.

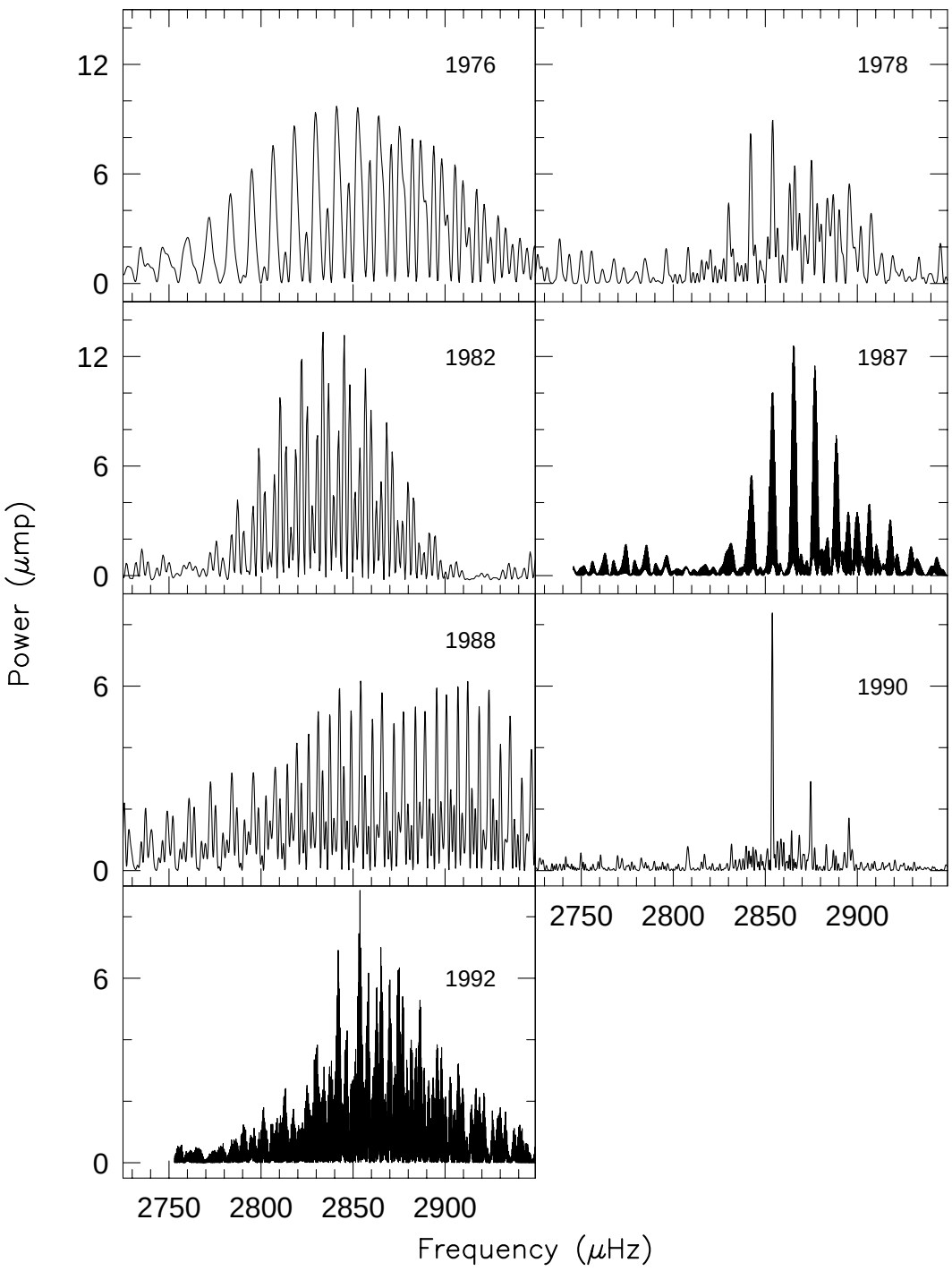

Figure 3.5: The 2853.8μHz (350.4 s) region in each season's FT of AM CVn. The window spectrum is given in Figure 3.4. Each season's FT is consistent with the presence of the triplet clearly resolved in 1990.

displays a simpler structure than the harmonics (Figure 3.6). The pattern in most FTs corresponds to that of a single frequency, and provides a good example of the problems of aliasing and the choice of the period of the variation responsible for the power. Whether $988.7\mu Hz$ or its one day alias at $977.1\mu Hz$ (1023.4 s) is the actual periodicity has been the subject of some controversy (Solheim *et al.*, 1984). The data from 1990, lacking strong aliases, settles this question definitively. The true period is $988.7\mu Hz$ (see Figure 3.6). Unlike the $1902.5\mu Hz$ power, the $988.7\mu Hz$ frequency exhibits strong amplitude variability (Fig 3.3). Power is conspicuously absent in this region in 1982 and present at very low amplitude in 1990. The $988.7\mu Hz$ variation had an amplitude nearly equivalent to the $1902.5\mu Hz$ variation in 1987, and a intermediate amplitude in 1988. It was present at very significant amplitude in January of 1992, but had again disappeared by June. The $988.7\mu Hz$ power is capable of dramatic amplitude variations on timescales of months, although its frequency does not vary outside measurement errors.

There is an elaborate network of power near 1250 μHz in several of the transforms (Figure 3.7). The period of the largest amplitude peak in the 1990 FT is 800.84 seconds. This power is also present in 1976, 1982, 1987, and 1992. The largest amplitude peak in the 1982 FT does not correspond to 800.84 seconds, but rather to 788.87 seconds, almost exactly 525.6×1.5, the first demonstration of power, besides 1011.4 seconds, that is not an integer relation to 1051 seconds. In addition, 800.84 seconds is $19.6\mu Hz$ away from 788.87 seconds, a frequency difference similar to the $20.7\mu Hz$ structure associated with the 525.6, 350.4 and 262.8 second periods. In this instance, however, 800.84 seconds is *minus* $19.6\mu Hz$ from 788.87 seconds. The difference between

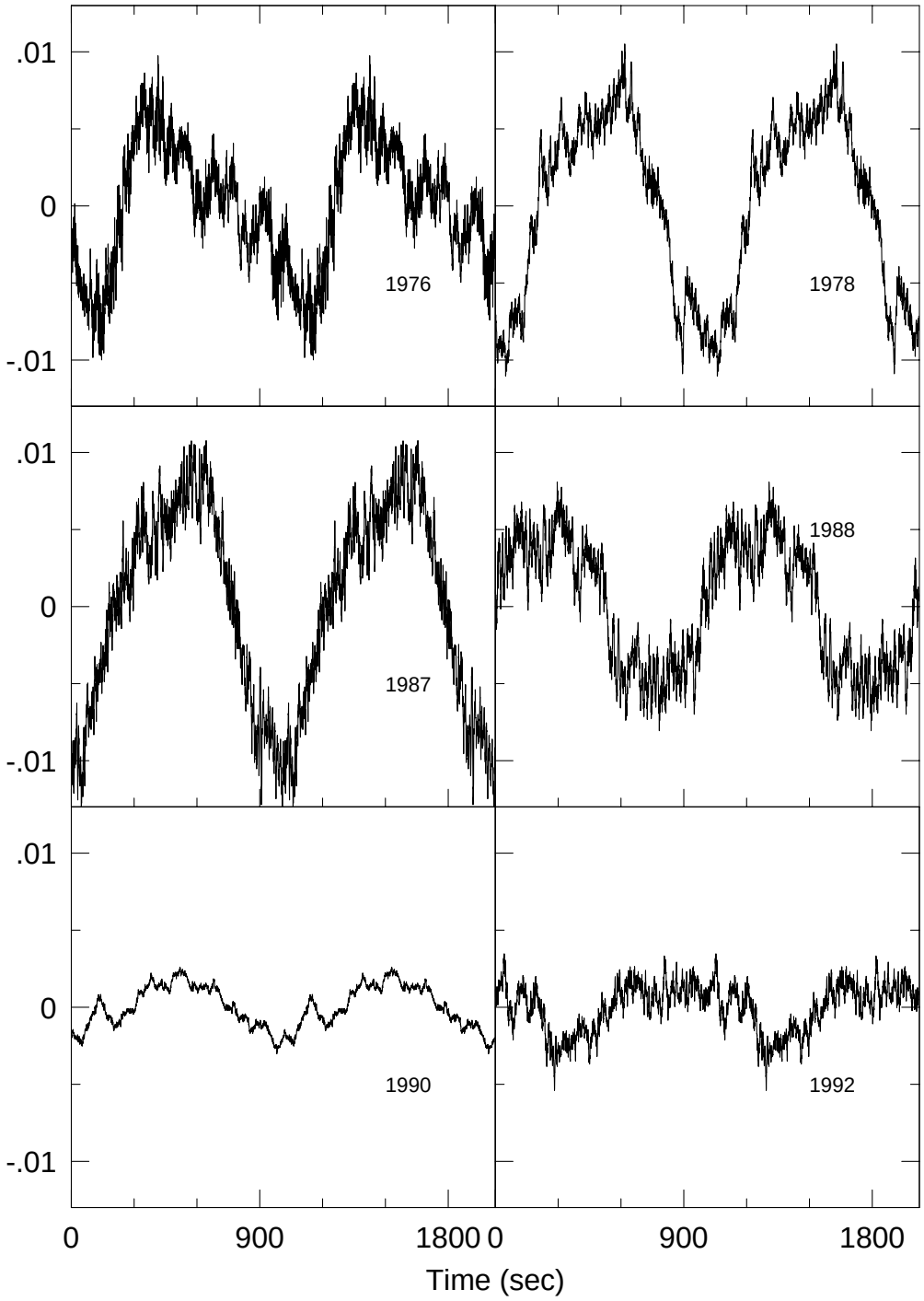

Figure 3.6: The 988.7μHz (1011.4 s) region of each seasonal FT of AM CVn. The location of 1051.2 seconds is given by the arrow. No significant power is detected at 1051.2 seconds.

$20.7\mu Hz$ and $19.6\mu Hz$ may be marginally significant, the timebase required to resolve the two is the length of the 1990 data set. In all other instances where the $20.7\mu Hz$ structure is present (525.6, 350.4 and 262.8 seconds), the multiplets are in every case on the high, not low, frequency side of the supposed harmonic peak. This region of power also differs in the behaviour of its amplitude from the 525.6, 350.4 and 262.8 second regions. The largest amplitude peak switches between 788.87 seconds and 800.84 seconds. Also, its general behaviour is reminiscent more of the 1011 second power than that of the other variations. If the power at 800 seconds is related to the 525.6 second power, we must explain these differences.

We do not find any evidence for other stable periodicities. Other peaks which could be termed as significant appear in each FT, but do not repeat. These short lifetime, non repeating variations may be related to the reports of flickering in AM CVn (see Warner, 1972). Some authors have mentioned power at around 289 seconds (Patterson *et al.*, 1991). A substantial peak at 285.96 does appear in the FT of an individual short run taken with the CFHT but is not seen in any other FT. This FT also has power at 25.78 and 26.33 seconds, at an amplitude of 0.5 mmi. This period is commensurate with that noted by Patterson (*et al.*,1979). This power does not appear in any other transform we examined. The amplitude of the 26 second power would, however, be just barely above noise level in other FTs.

The $20.7\mu Hz$ frequency splitting lead us to search for additional examples of equal frequency splitting in AM CVn's FT. We employed the template technique described in Chapter 2 to search all peaks above a certain amplitude threshold for a range of frequency splittings (Figure 3.8). Although

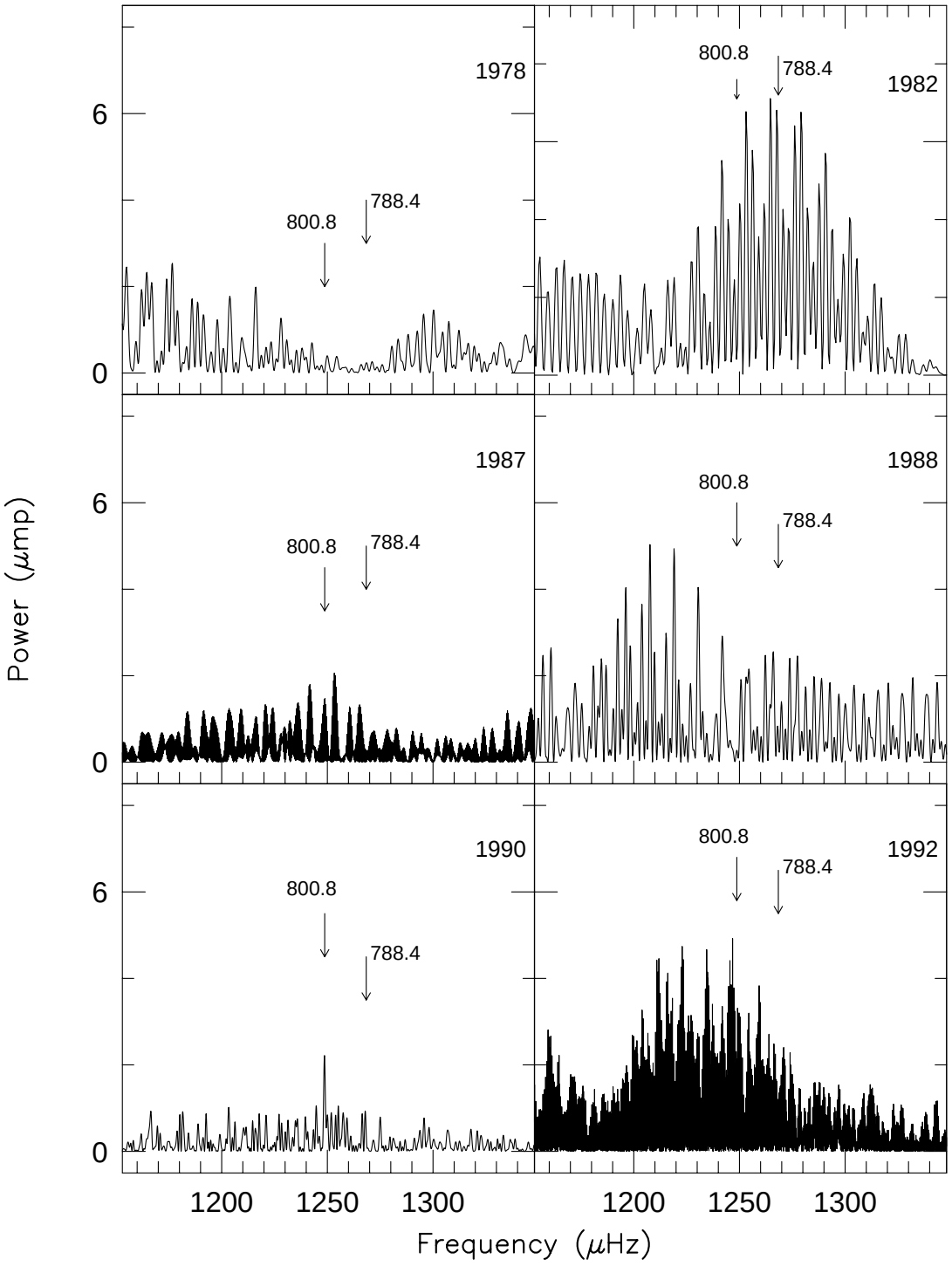

Figure 3.7: The 800.8 second region in each season's FT of AM CVn.

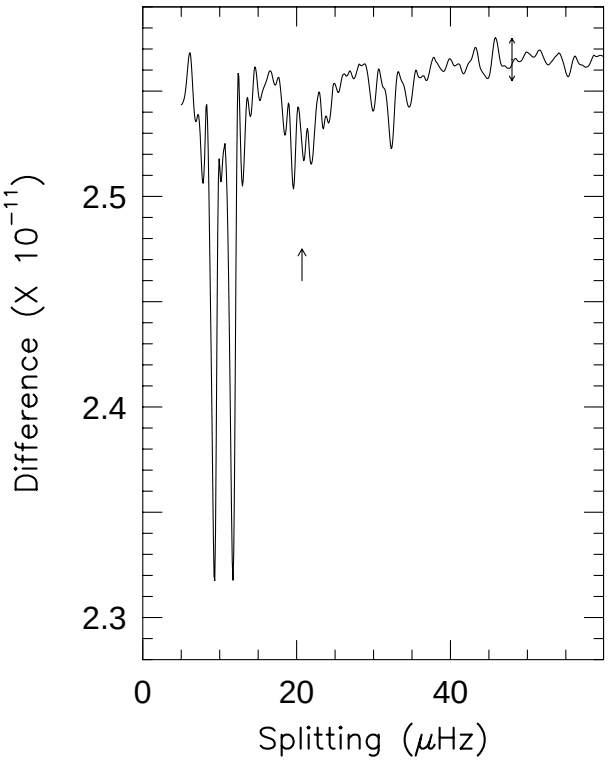

Figure 3.8: Equal frequency splittings in the 1990 AM CVn FT. The deepest minima are window artifacts. The minima at $20.7\mu Hz$ is the fine structure associated with the 525.6, 350.4 and 262.2 second periods.

the deepest minima are window artifacts, the $20.7\mu Hz$ fine structure is also detected. The feature at $32\mu Hz$ is also a window artifact. There are no additional examples of equal frequency splitting in AM CVn's 1990 FT.

3.2.1 The Case for 1051 seconds as the Physical Photometric Period

One of our primary concerns is the identification of the physical photometric period(s) of AM CVn. The evidence presented in the FTs clearly

points to a solution to this question. It is possible to create a waveform that the FT process will translate into a series of harmonics of the true period of repeatability (see Figure 3.16). On first glance, the presence of such a series of exact harmonics of 1051 seconds suggests this is the physical period, not 525 seconds. Unfortunately, the situation is not so simple. A harmonic is defined as

$$H_n = n\nu_o$$

where H and ν_o are frequencies and n is an integer. The first three members of AM CVn's supposed harmonic series, 525.6, 350.4 and 262.8 seconds, are not single peaks. Each are multiplets, comprised of up to three individual peaks, each component separated by $20.7\mu Hz$. While complex structure of harmonics is possible, if the harmonics are due to pulse shape distortions, the frequency splitting in each harmonic should increase as the harmonic number increases.

$$F = \nu + \Delta\nu$$

$$2F = 2\nu + 2\Delta\nu$$

The constant $20.7\mu Hz$ observed in AM CVn is not consistent with the hypothesis that these periodicities are simple harmonics of 1051 seconds.

A fatal blow to the hypothesis of simple harmonics of an unseen fundamental period is struck by the 800 second power. This region contains indications of the similar $20.7\mu Hz$ structure as the harmonics, but is itself not a harmonic of 1051 seconds. Therefore, the 525.6, 350.4, 262.8, 210.2 and 175.2 second peaks present in each seasonal FT of AM CVn are not simple harmonics of 1051 seconds, but arise via a more complex mechanism.

3.2.2 The Case for 525.6 Seconds as the Photometric Period

The FTs of AM CVn have seven main periodicities to account for: 525.6, 350.4, 262.8, 210.2, 175.2, 800.8, and 1011.4 seconds, as well as the complex, $20.7\mu Hz$ structure associated with several of them. There is no convincing evidence to conclude that 1051 seconds is the physical period present in AM CVn. The next logical step is to designate 525.6 seconds as the period of repeatability, or ν_o. Proceeding with this assumption, 262.8 seconds and 175.2 seconds become the first and second harmonics of ν_o, corresponding to frequencies of $2\nu_o$ and $3\nu_o$.

The list of unaccounted periodicities has shrunk to 350.4, 210.2, 800.8 and 1011.4 seconds. The 350.4 second region is different from the 210.2 and 1011.4 second power. It is fairly large amplitude, and consists of a distinct triplet with $20.7\mu Hz$ splitting. Because the $20.7\mu Hz$ frequency splitting is identical to that demonstrated by the 525.6 second peak, we designate the 350.4 second power as a second distinct period, although its frequency is numerically related to 525.6 seconds and therefore may arise via the same mechanism. The same basic argument applies to 800.4 seconds, although its amplitude behaviour is reminiscent more of the 1011.4 second power than the 525.6 second power.

The list of unexplained periods has shrunk to just two, 210.2 and 1011.4 seconds. The 210.2 second peak has no harmonic and no associated complex structure. Its frequency, however, is the sum of the frequencies corresponding to the 525.6 and 350.4 second periods and so may be linear combination, not an independent periodicity. The 1011.4 second peak is not numerically related to any other periodicity, does not appear to contain complex structure,

and exhibits large changes in amplitude on timescales of months. We designate this as a fourth frequency, but also as the only frequency numerically independent of the 525.6 second variation.

The FTs of AM CVn contains power at seven frequencies: 1011.4, 800.8, 525.6, 350.4, 262.8, 210.2, and 175.2 seconds. Each of these frequencies may be accounted in terms of one completely independent periodicity, 3 numerically related, possibly independent periodicities, two harmonics, and one linear combination.

$$\nu_o = 1902.5\mu Hz \text{ (525.6 sec)}$$

$$\frac{3}{2}\nu_o = 2853.7\mu Hz \text{ (350.4 sec)}$$

$$\frac{2}{3}\nu_o = 1268.3\mu Hz \text{ (800.8 sec)}$$

$$2\nu_o = 3805.0\mu Hz \text{ (262.8sec)}$$

$$\nu_o + \frac{3}{2}\nu_o = 4757.4\mu Hz \text{ (210.2 sec)}$$

$$3\nu_o = 5707.5\mu Hz \text{ (175.4 sec)}$$

$$\nu_2 = 1011.4 \text{ sec}$$

The above interpretation of the frequencies neatly relates all the observed power. The next step is to consider the $20.7\mu Hz$, and investigate whether this model of the frequencies is consistent with the presence of fine structure. The power at 525.6, 350.4, 800.8, and 262.8 seconds each consists of multiplets containing the same 20.7 μHz frequency splitting. As discussed in the case of 1051 seconds, this is not consistent with the interpretation of these periodicities as simple harmonics of 1051 seconds. Our alternative interpretation of the variations in AM CVn designates 525.6, 350.4 and 800.8 as

numerically related, yet independent frequencies rather than harmonics of an unseen fundamental period, so each may contain the same frequency splitting (Winget, *et al.*, 1992). The only possible problem lies with the 262.8 second region. Our above interpretation designates 262.8 seconds as a harmonic of 525.6 seconds. We note that the frequency of the second component of the 262.8 second structure, at 261.4 seconds, is *exactly* the sum of the frequencies of the 525 second doublet. The $20.7 \mu Hz$ structure associated with the 262.8 second peak is therefore a coincidence, resulting from the linear combination of the frequencies of the 525 second peak and its doublet companion.

Our original quest was to account for the seven main periodicities, as well as the $20.7 \mu Hz$ structure, present in the FTs of AM CVn. The best accounting neatly describes all the structure present in terms of three related multiplets, 800.8 (or 788.87), 525.6, and 350.4 seconds, their associated harmonics, two linear combinations and one unrelated period (1011.4 seconds). The problem of equal 20.7 μHz structure for multiple harmonics is resolved in this interpretation.

3.3 The Pulse Shape

The pulse shape, the average waveform constructed by folding light curves at a period of interest, furnishes another tool with which to examine the stability of the 525 second periodicity. The pulse shape contains no information not present in the FT, but is a convenient way to interpret the harmonic structure associated with a variation. Harmonics, periodicities with integer relations to another variation, may arise in two ways: a nonsinusoidal variation

will produce pulse shape harmonics in the FT, or the harmonics may be independent periodicities in their own right. Coherent harmonics present in the data will have an effect on the pulse shape of the fundamental period. Other noncommensurate periodicities present in the data will not have a significant effect on the pulse shape of interest if the data covers a time base much greater than the resolution time, defined as the inverse of the frequency difference, of the periodicities. The maxima and minima of such variations will fall at different points in the pulse shape as each cycle is folded in, for example one cycle of the noncommensurate periodicity's maximum may coincide with another cycle's minimum as the data is folded at the period of interest. In this manner, the net influence of such variations will average out if the light curve spans a timescale greater than the resolution time of the periodicities.

The 525.6 second pulse shape (Figure 3.9) is nearly sinusoidal, with a modest asymmetry. These departures from a sinusoid are responsible for the harmonics of 525.6 seconds in the FT. To investigate the possibility that the 525 second variation was composite, similar to eclipses in dwarf novae where the disk and then the hot spot are eclipsed, we first subtracted the best fit of a sinusoid from the pulse shape, assuming that the primary variation is sinusoidal (Figure 3.10). The result is not satisfying, and resembles a failed attempt to remove an emission line from a spectrum, in which the observed emission line is at a different frequency than the subtracted line. The sinusoid removes too much in some areas of the pulse shape, and doesn't do enough in other areas. We conclude that our assumption of an underlying sinusoidal variation is wrong.

To avoid this assumption, we attacked the problem using a second

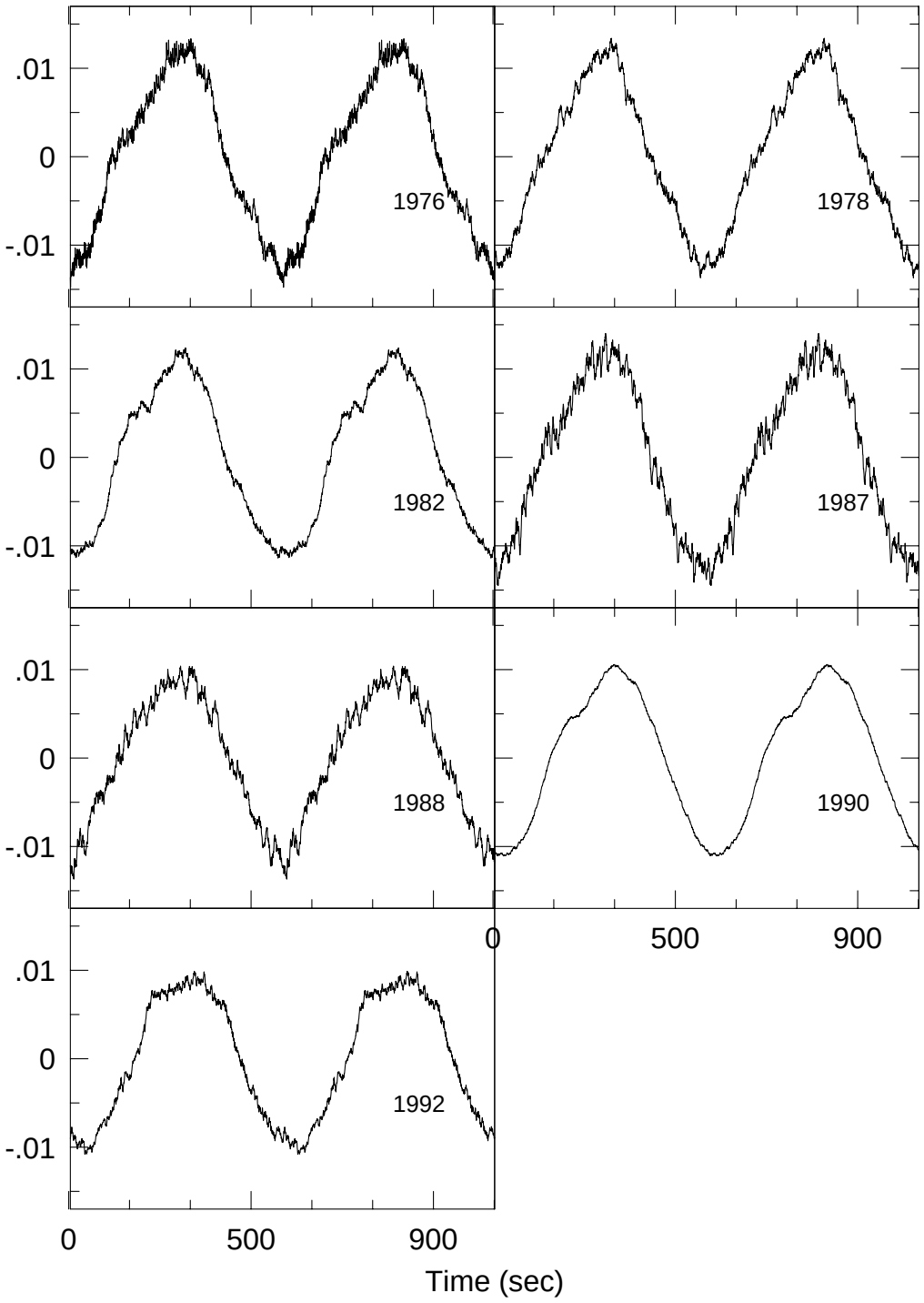

Figure 3.9: The seasonal pulse shape of the 525.6 second variation of AM CVn, created by folding each year's light curve at 525.6 seconds. The amplitudes are nearly identical, as is the general profile of each pulse.

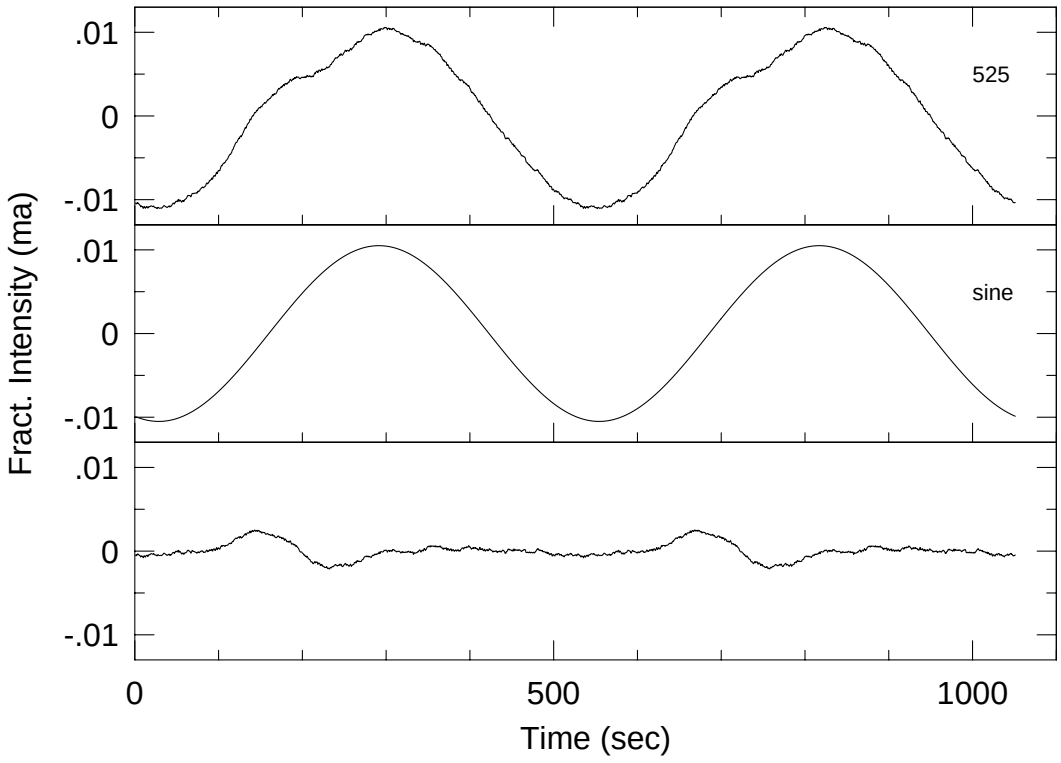

Figure 3.10: The 1990 seasonal 525.6 second pulse shape minus a sine wave.

method, which assumed the down slope of the pulse shape to be uncontaminated by the mechanism producing the asymmetry. A pulse shape was created using the mirror image of the descending half of the 525 pulse shape as a model for the first half. This model was subtracted from the 525 pulse shape (Figure 3.11). This result is more appealing, as the asymmetry may be modeled by an excess of brightness on the rising slope of the pulse.

Pulse shapes are influenced by any period that is an integral multiple of the period of interest. Equivalently, pulse shape harmonics will appear in FTs if the dominant variation departs from a sinusoid. We investigated which of the harmonics of the 525.6 second period could be attributed to these effects by creating a light curve employing the 525.6 second pulse shape obtained in 1990 and calculating the FT of this simulated light curve. This FT had peaks at 525.6, 262.8, and 175.2 seconds. We then incorporated the 350.4 and 210.2 pulse shape. This resulted in an FT remarkably similar to that of AM CVn, with power at 525.6, 350.4, 262.8, 210.2, and 175 seconds at amplitudes commensurate with those in the original transforms. This test demonstrates that the harmonics at 262 and 175 seconds are undoubtedly pulse shape manifestations of the 525.6 second period, but the power at 350.4 and 210.2 can not be simply pulse shape harmonics of 525.6 seconds. If 525.6 seconds is the physical periodicity of AM CVn, at least one other frequency must be present as well.

We also constructed similar yearly pulse shapes for the 1011 second period, when it was present in the seasonal FT (Figure 3.12). The 1011 periodicity does not maintain a stable shape, in contrast to the 525 second variation. For example, the 1976 pulse shape is very different from all the others. It is

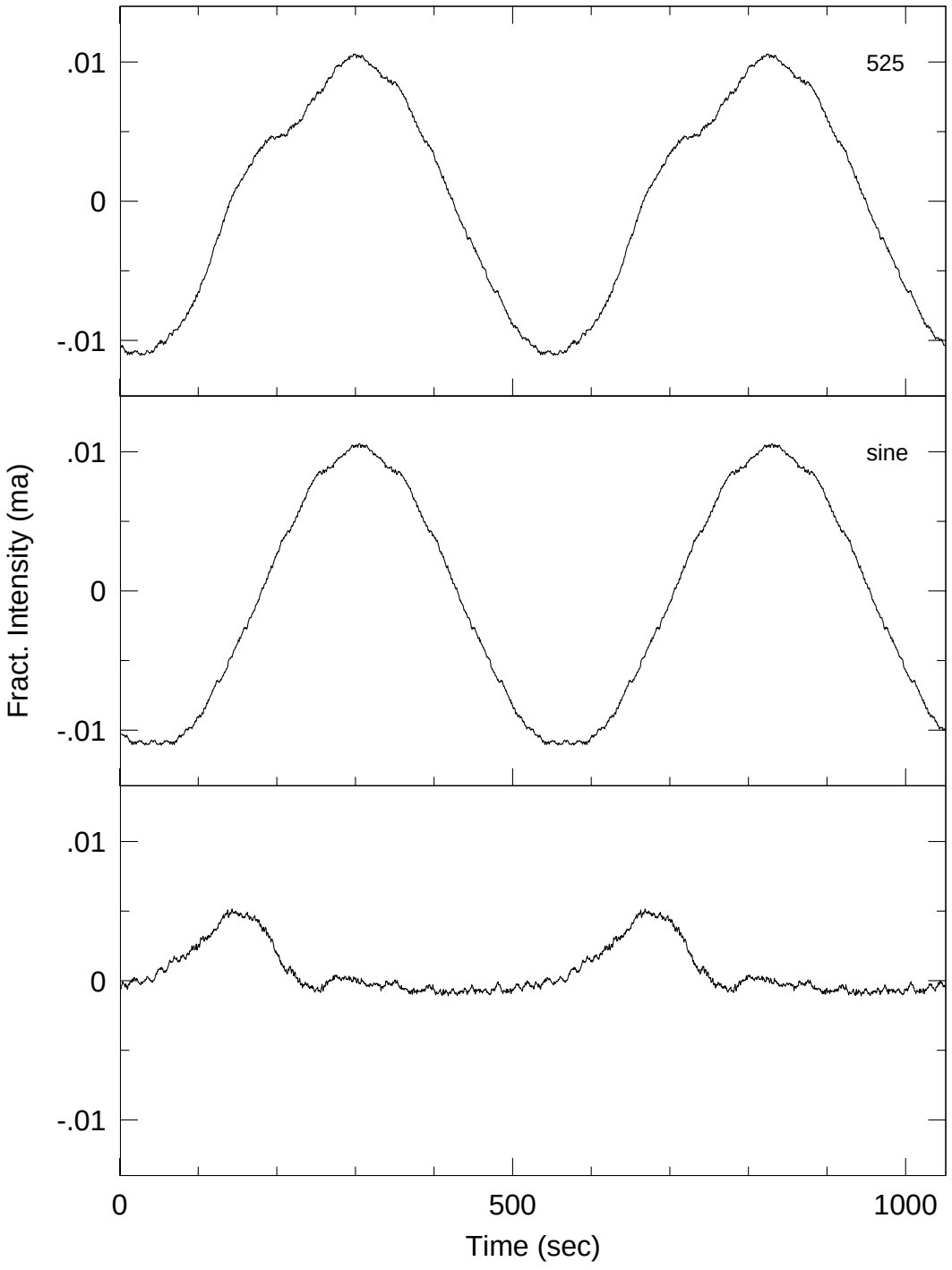

Figure 3.11: The 1990 seasonal 525.6 second pulse shape minus a simulated pulse assuming the down slope is a mirror image of the up slope. This indicates the 525.6 second pulse has excess brightness on the upward portion of the pulse.

almost a mirror image of the 1987 pulse shape. The mechanism responsible for the 1011 variation is clearly different from that resulting in the 525 second periodicity.

3.4 Simultaneous Multicolor Photometry

Several of the individual light curves of AM CVn are multicolor (UBVC) observations, obtained by rotating a set of Johnson U,B, and V filters and one clear aperture through the light beam . Our primary purpose behind these observations was the examination of the relative behaviour of the 525 second variation as a function of color to help distinguish between possible mechanisms. The light curves were obtained predominately in 1992, with one run from 1982. The Fourier transforms of each color employing the 1992 data are given in Figure 3.13. There are obvious differences between the FTs. The amplitude of the 525.6 itself is nearly constant (Figure 3.14), but the amplitude of the 988.7μHz (1011.4 s) peak varies greatly. Also, the 1250μHz (800 s) and 2857μHz (350 s) peaks have their largest amplitude in the U band. Significant power at 1600 μHz (625 seconds) is present only in the FT of the U band data.

We constructed pulse shapes at 525.6 seconds for each color (Figure 3.14). Each pulse shape was given the same time of zero in the figure. All the pulse shapes have the same amplitude, phase and general shape. A hint of difference appears in the U pulse shape. There appears to be a feature on the descending slope that is not present in the other pulse shapes (Figure 3.15). The multicolor observations were made with a 36 inch telescope, with a series of rotating filters, resulting in a fairly low signal to noise ratio. The possibility

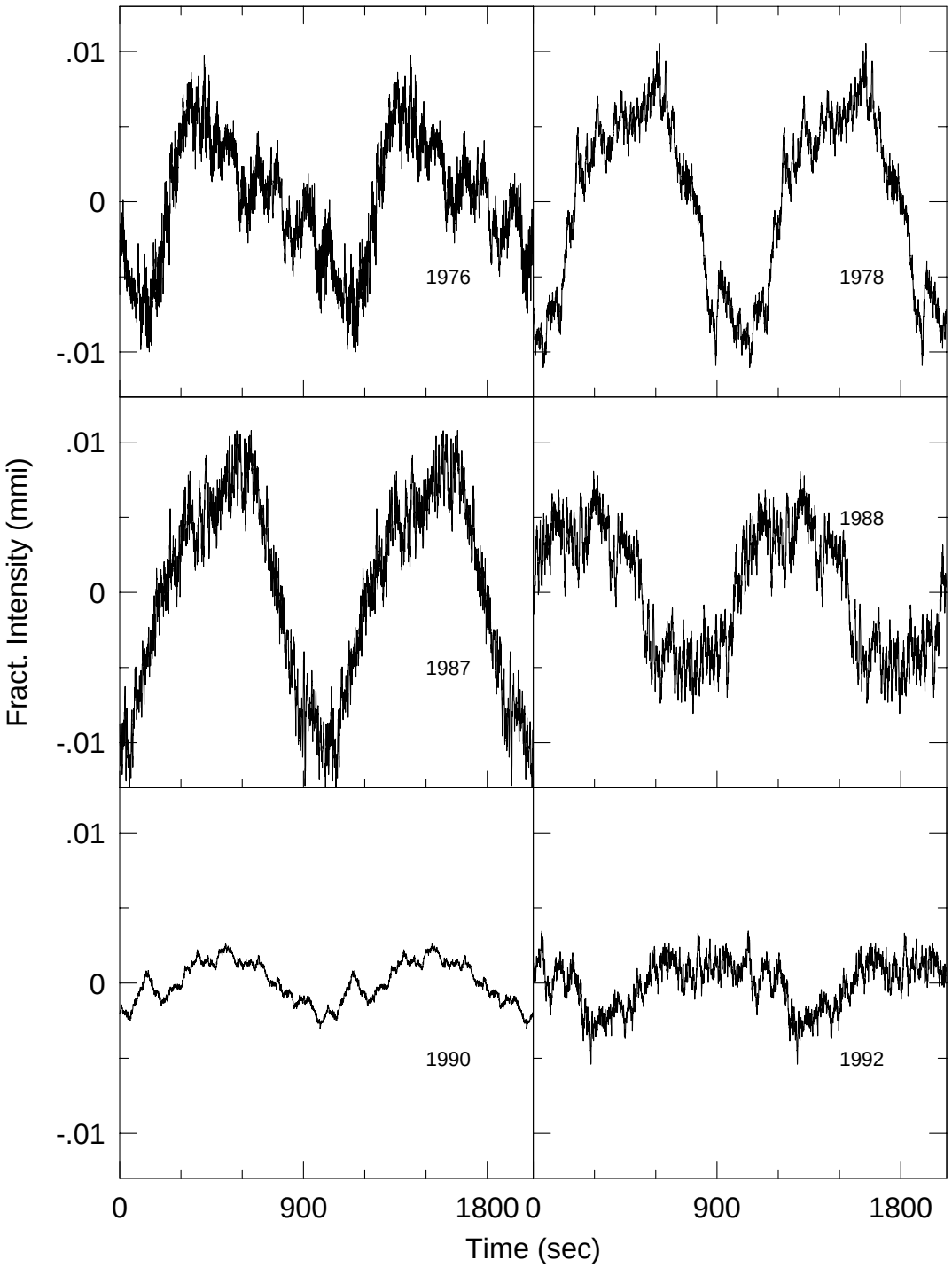

Figure 3.12: The seasonal pulse shapes of the 1011.4 second variation of AM CVn, created by folding each light curve at 1011.4 seconds. The amplitude and profile varies greatly, in contrast with the behaviour of the 525.6 second pulse

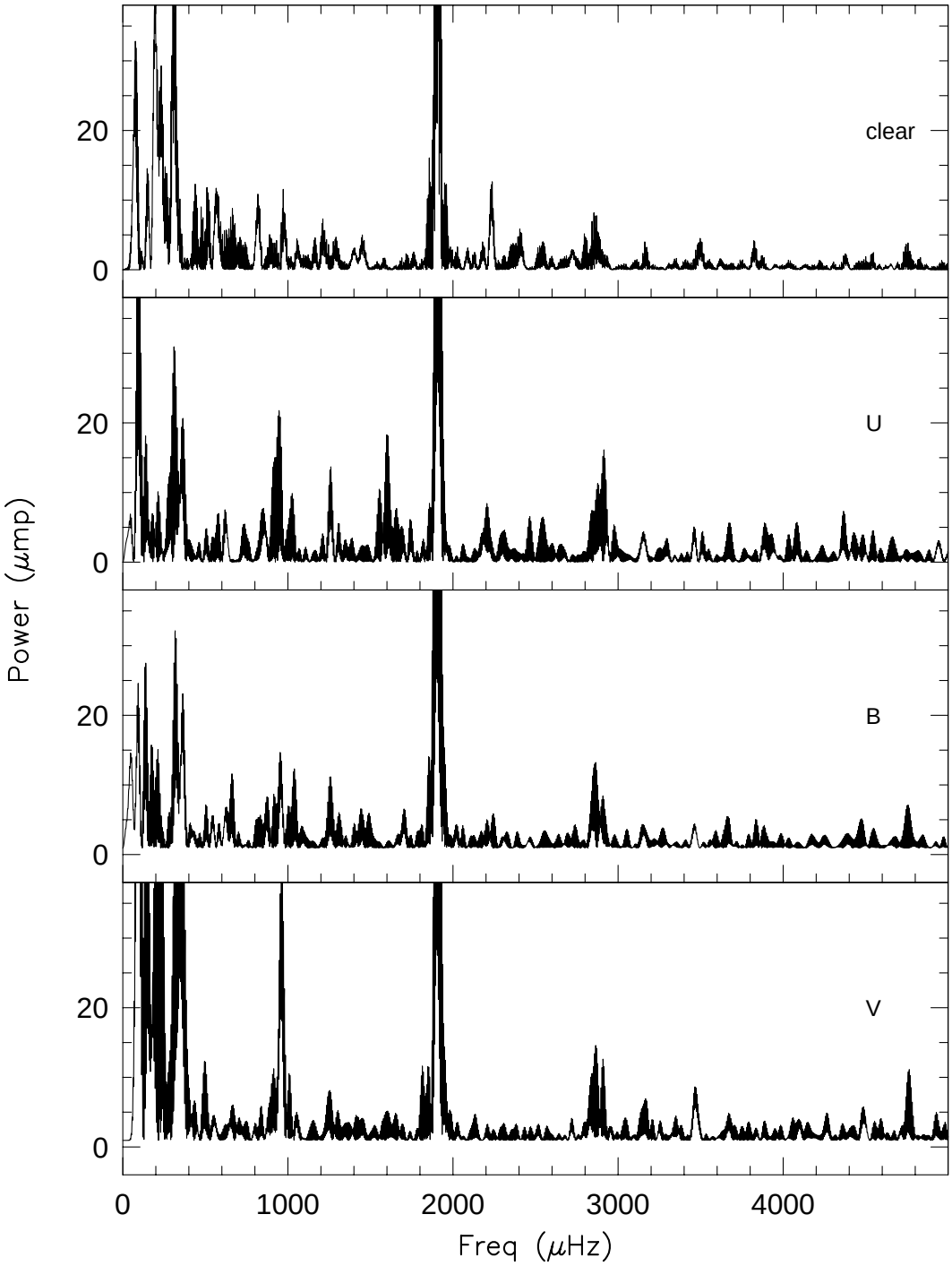

Figure 3.13: Multicolor UBVC photometry of AM CVn. Power peaking in different colors may be occurring in different temperature regions of the system.

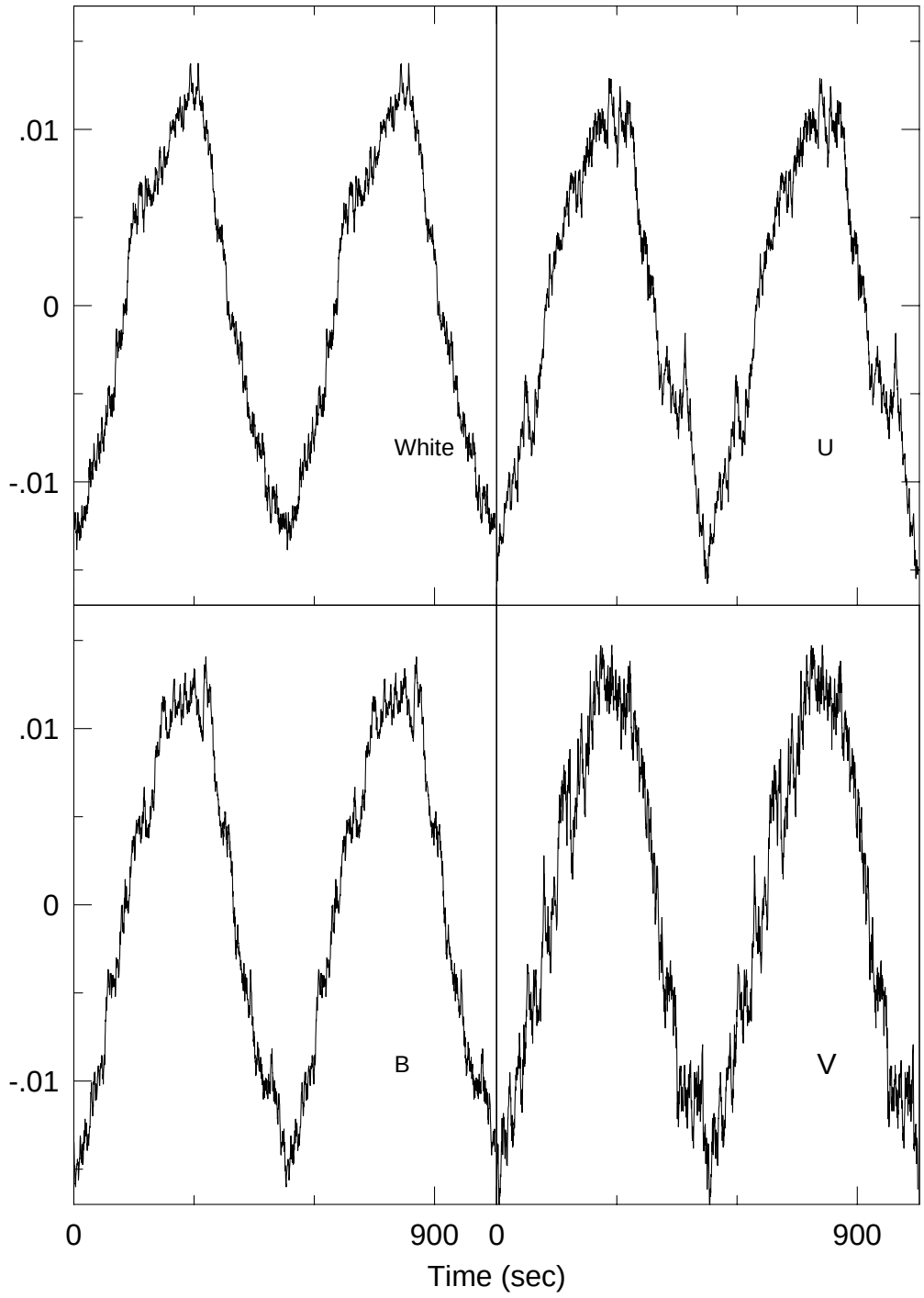

Figure 3.14: Average pulse shapes of the dominant 525.6 second variation in each color band. The amplitude and phase of the 525.6 second variation remains is independent of color.

of a difference in the U pulse shape must be explored with a larger telescope to reduce the noise level.

Further multicolor observations of AM CVn are extremely important. Variations arising from different regions in the system will have different temperatures, and hence will behave differently in each color. For example, the 1011.4 second period seems to have two components, hot (U) and cool (V). The 800 second power is also strongest in U, as is the unexplained power at 625 seconds, indicating origination in the hot region of the white dwarf accretor. Surprisingly, the 525 second pulse shape is color independent. This behaviour suggests we may be observing a temperature variation arising within a hot region. At high temperatures, the U, B, and V bands are out on the Rayleigh-Jeans tail of the spectrum. Since blackbody curves for different high temperatures are nearly parallel in this region, we would expect little amplitude change with color. We must also consider the second possibility that the 525.6 second variation may be an eclipse phenomenon. Extensive multicolor photometry will enable us to sort out the variations arising from the the cooler disk regions and those arising from the hot white dwarf.

3.5 Phase Stability

A controversy concerning the phase stability of AM CVn's dominant photometric period has been brewing since the object's discovery. Numerous authors have analyzed the phase and presented ephemerides (Patterson *et al.*, 1979, Solheim *et al.*, 1984, Patterson *et al.*, 1991), but a predictive ephemeris has never been achieved. The dominant period was claimed to be increasing

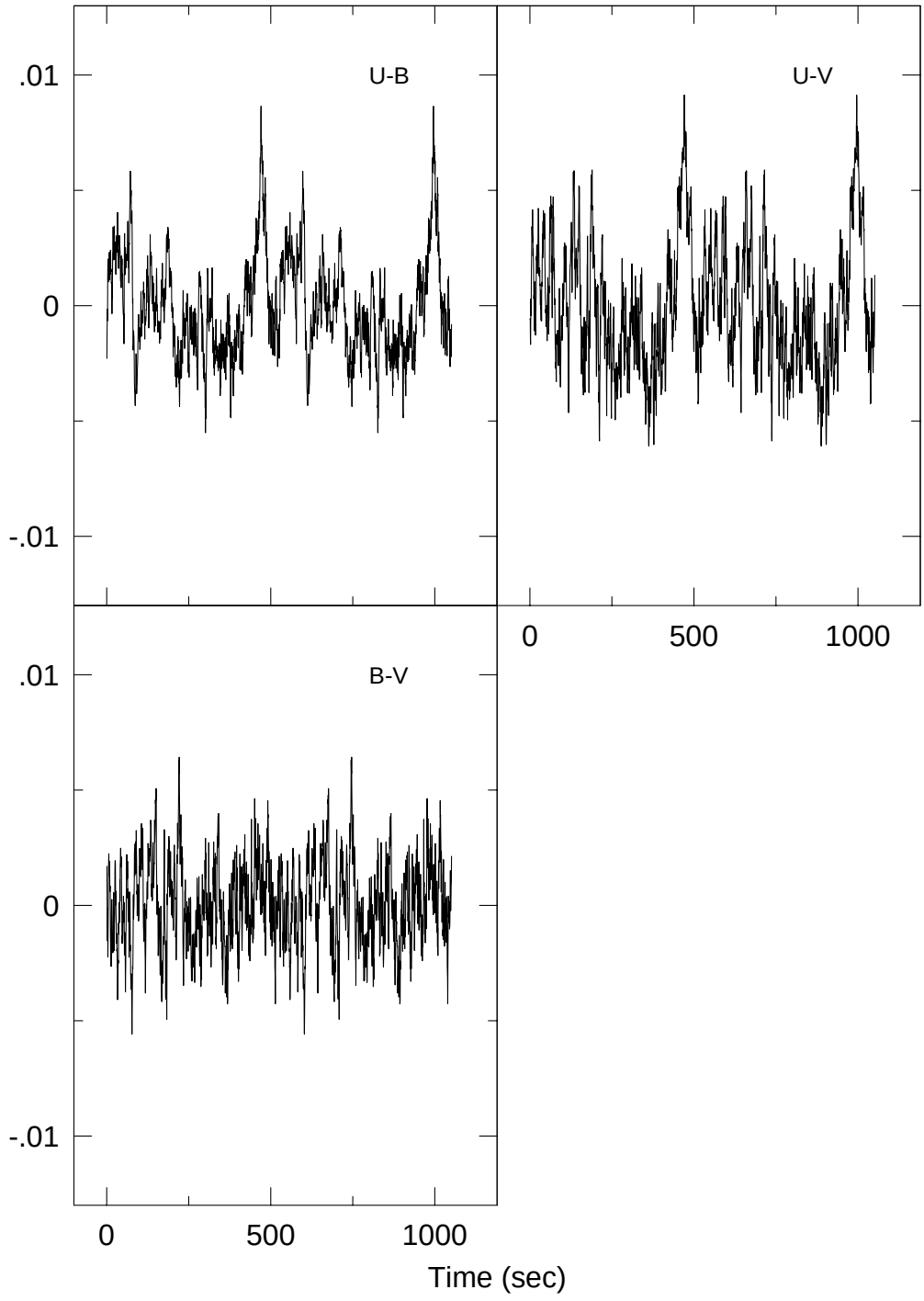

Figure 3.15: Each color 525.6 second pulse shape subtracted from another.

rapidly ($\dot{P} = 3.8 \times 10^{-10} ss^{-1}$, Patterson *et. al.*, 1979), to be decreasing ($\dot{P} = (-3.2 \pm 0.6) \times 10^{-12} ss^{-1}$, Solheim *et. al.*, 1984), and to be incoherent (Patterson, *et. al.*, 1992). AM CVn has also been reported to exhibit significant "phase jitter", in which the phase of the 525 second variation wanders by as much as a quarter of a cycle on timescales of days (Warner and Robinson, 1972).

The traditional method of phase analysis is the O-C diagram. Either by visual selection, or through least squares techniques, a time of maximum (or minimum) is obtained from a light curve. This observed quantity is compared with a calculated time predicted by an ephemeris. The difference (O-C) is then plotted as a function of time. The procedure is repeated for the next light curve, creating a series of O-C points characterizing the behaviour of the variation relative to that predicted by the ephemeris. An accurate model of a stable frequency will produce a series of O-C points that are best fit by a straight line with zero slope.

A problem with previous O-C calculations for AM CVn is the choice of period. Most previous O-C diagrams use 1051 seconds as their reference period, although power is never seen in the FT at 1051 seconds. The supposed 1051 second waveform is a double-humped structure, with one minimum slightly deeper than the next, and one maximum larger in amplitude and slightly wider than the next (Figure 3.16). This waveform is actually created by the interaction of the 525.6 and 350.4 second periods.

The earliest attempts at calculating AM CVn's O-C diagram involved visually identifying the "primary", or deepest, minima for each 1051 second cycle in an individual light curve and averaging them to obtain an observed timing

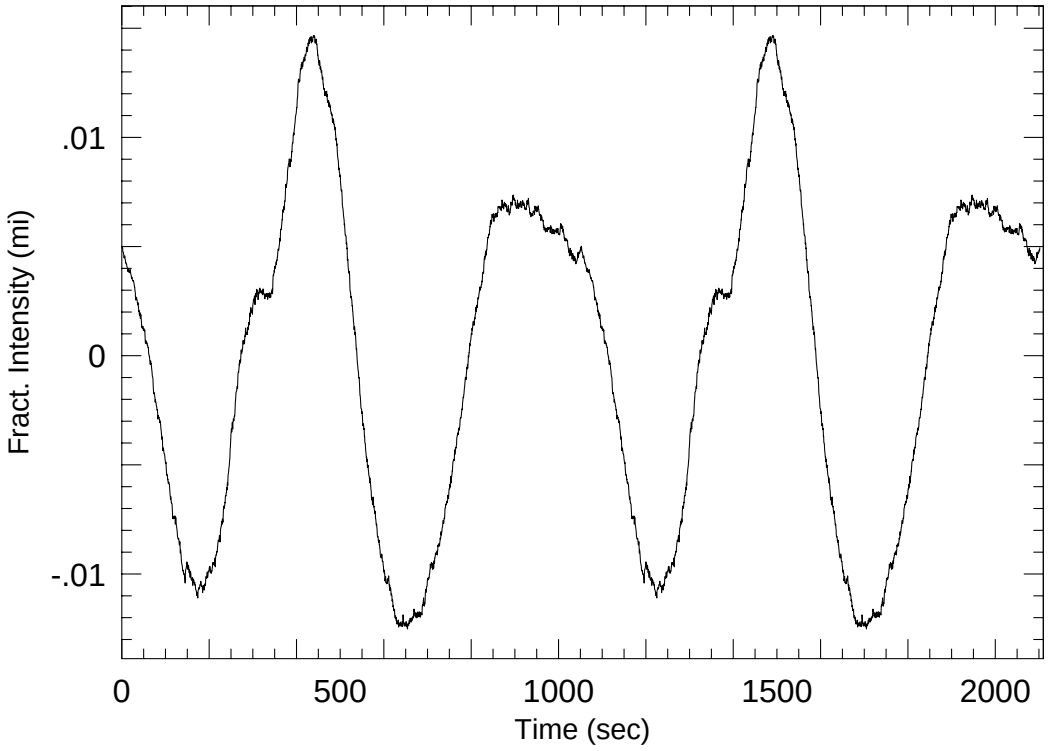

Figure 3.16: The 1990 data folded at 1051 seconds. There is a slight difference in the depths of the minima, but this would be indistinguishable in a single night of observation.

(Krzeminski, 1972). As Figure 3.16 clearly shows, the difference in the depth of minima in each cycle is subtle, and impossible to differentiate given the noise present in a single light curve. Because the minima cannot be unambiguously identified without a great deal of data, it is exceptionally easy to misidentify primary minima in different light curves, introducing half cycle errors. Finally, as the Fourier transforms of each year's data demonstrates, although there is no power at 1051 seconds itself, there are additional periodicities present, notably the 1011 second period and the complex structure associated with the 525 second variation. The position and depth of a single minimum in a given light curve will be modified by the interaction of the 525 second variation with these additional frequencies.

A second method frequently employed to calculate AM CVn's O-C diagram uses linear least squares techniques to fit a sinusoid with a constant period of 1051 seconds to individual light curves (Solheim *et al.*,1984). The times of first minima, or maxima, from each fit become the observed timings. We have clearly shown that there is no significant power ever present in any FT at 1051 seconds. Equivalently, the 1051 second waveform is not sinusoidal. Fitting a sinusoid with a 1051 second period to the data is not practical as the sinusoid will be fit to the small difference between the minima. This process effectively ignores most of the power present in the variation.

A more serious problem was recently unveiled by the Whole Earth Telescope in 1990 (Solheim *et al.*, in preparation). This data set for the first time clearly resolved the 525 into a doublet, with a frequency splitting of 20.7 μHz. These two frequencies require 13.2 hours to resolve, so a single night's data will not resolve the doublet and therefore a timing from an individual

night is not accurate. This introduces the additional problems posed by the alias patterns created by combining different nights of data. In the case of AM CVn, even two nights of data is not necessarily satisfactory; the FT must contain sufficient data to resolve the web of aliases. For example, the 1987 FT contains 11 nights of data spanning two months. Although this season contains enough data to adequately resolve the overlapping alias patterns, the alias pattern from the small component of the doublet is still at significant amplitude in the region of the 525 peak. If the resolution of the FT were reduced slightly, the alias patterns would not be separated and the aliases from the small component would contribute significantly to the power in the dominant peak. A timing obtained for the primary 525 second peak would be contaminated by the aliases of the smaller component of the doublet. The contributions from each component of the doublet *must* be resolved before an accurate timing can be obtained.

In our attempt to resolve the O-C dilemma, we will minimize these problems by using 525.6 seconds as our reference period, and by calculating seasonal timings for this period. Before we can perform this analysis at all, however, there are several stringent criteria that must be met. The 525.6 second peak must clearly demonstrate stability in both frequency and amplitude. A stable amplitude is required to eliminate the possibility that the 525.6 second periodicity is unresolved, and is a combination of two or more closely spaced variations beating together. The failure to produce an accurate ephemeris for AM CVn may point to the inherent incoherence of the frequency. An O-C diagram of a periodicity that wanders in frequency has no physical meaning, as each observed timing samples a different frequency. The 525.6 second period

must exhibit the same frequency and amplitude, within measurement errors, in every adequately resolved FT available. Figure 3.4 demonstrates that this is the case. One peak is present in the FT of each year, at the same amplitude and frequency.

The next criterion is to determine the period of the variation to sufficient accuracy to avoid cycle count ambiguities over the unavoidable gaps the the data set. The best seasonal period is 525.61816 ± 0.0003 seconds, from the 1992 data set. The period is accurate enough to determine timings for a stable periodicity for over 3 years before losing 1/10th of a cycle, is consistent with the 1990 seasonal periods, and is therefore adequate to calculate timings for the 1990 data without cycle count ambiguities. We can then combine these two seasons to improve our knowledge of AM CVn's period still further. The best period for 1990-1992 is 525.621008 ± 0.00002, with an amplitude comparable to each individual season. Continuing in this manner, and making sure the amplitude remains stable, we end up with a best period for the entire data set of

$$P = 525.621470 \pm 0.000003 \text{ sec}$$

If the 525.6 second variation is strictly coherent, with no period change, we would expect the measured periods from each observing season (Table 3.4) to agree with the best period for the entire data set. The data set value is less than one sigma from the 1990 period, but is over five sigma from the 1978 period and 11 sigma from the 1992 period, demonstrating that a strictly periodic model is not adequate for AM CVn, and forces us to consider the next simplest model, incorporating a constantly changing period.

Table 3.4: Seasonal Periods for AM CVn

Year	Period (sec)	Error	Amp (mmg)	Error
1992	525.61816	0.0003	11.7	0.2
1990	525.6194	0.004	10.5	0.3
1988	525.5625	0.007	9.6	0.3
1987	525.6150	0.008	11.4	0.2
1982	525.610	0.01	11.3	0.5
1978	525.5814	0.008	11.4	0.3
$1990 + 1992$	525.621009	0.000019	11.1	0.18
$88 + 90 + 92$	525.620857	0.000012	10.61	0.14
$87 + 90 + 92$	525.621467	0.000007	11.18	0.14
$82 + 87 + 90 + 92$	525.621386	0.000006	10.4	0.14
$78 + rest$	525.621470	0.000003	10.5	0.11

In the past, the photometric variations in AM CVn's light curve have been reported to wander in phase, by as much as a quarter of a cycle (Solheim *et al.*, 1984, Patterson *et al.*, 1992). This controversy concerning the stability of the 525 second period warns us to proceed with caution, and begin by examining the stability of the 525.6 second variation over short timescales and attempt to place a limit on its rate of period change. The 1990 WET data set contains the most continuous coverage available, 144 hours of coverage spanning nearly two weeks, eliminating the alias problems plaguing other seasons. Figure 3.17 gives the O-C for the unambiguously determined best period of this data set, 525.6194 ± 0.003 seconds. The observed timings were obtained by fitting sinusoids of this period to chunks of the 1990 data set. The chunks were selected so as to contain sufficient data to resolve the 20.7 μHz structure. The scatter is about 15 seconds, consistent with timing errors. Throughout this run, observed points are fit very well with a straight line, corresponding to a strictly periodic variation, but is fit slightly better with a parabola. Although

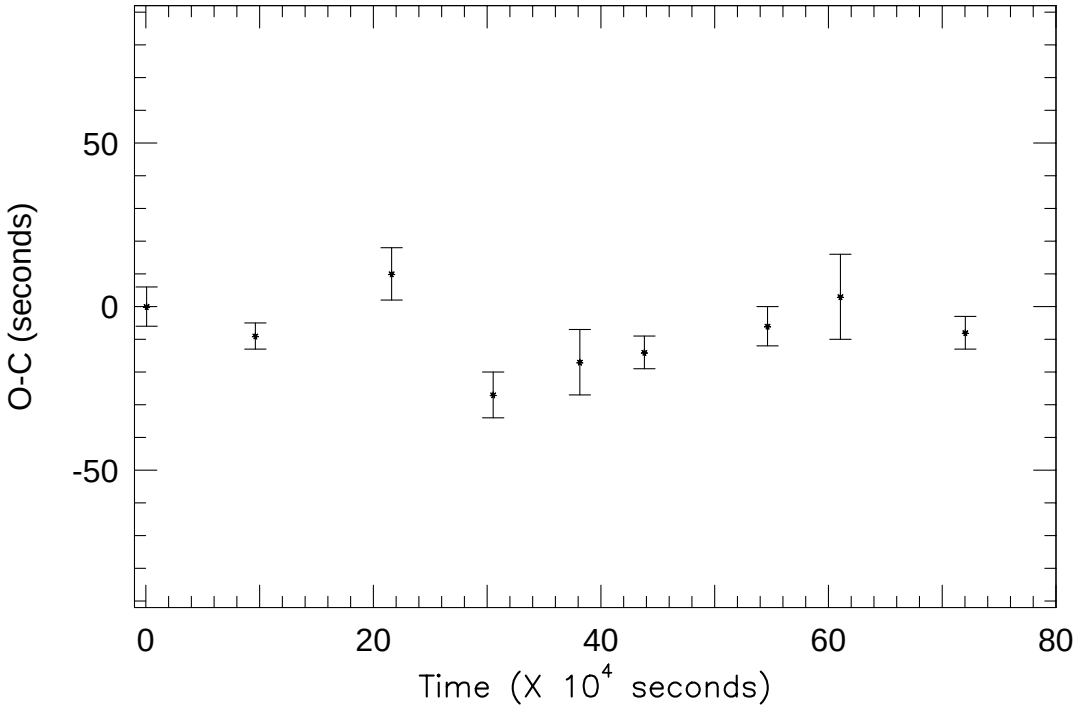

Figure 3.17: O-C diagram for the 1990 WET observing run.

this run is only 10 days long, we can place an upper limit on the period change of $2.3 \times 10^{-8} ss^{-1}$. We can also eliminate the possibility of any large, rapid random phase changes on timescales of days. There is no "phase jitter" in this data set.

The 1992 season spans several months, and can be employed to test the stability of the 525 variation over this period. Table 3.5 lists the O-C timings for April and June, and clearly demonstrates that the periodicity is stable over this timescale. The phase jitter reported by Solheim *et al.* (1979)

Table 3.5: O-C Timings

Date	Tmax (sec)	BJED RS	Offset	E	O-C (sec)
april 92	375 ± 2	8635.798648	6984620	0	0 ± 2
June 92	184 ± 2	8635.798648	11873060	9300.002	1 ± 2

is a result of beating with between the 525.6 second period and its companion $20.7 \mu Hz$ away. Previous attempts to calculate an ephemeris for AM CVn used timings obtained from a single nights data, which does not adequately resolve the 525.6 second peak and its nearby companion. An unresolved peak with an amplitude similar to that of the 525.6 second peak's doublet companion is capable of "pulling" the calculated time of maximum by as much as 20 seconds in either direction, or by nearly 10 percent of the period.

We have met our criteria for amplitude and frequency stability. Now, it is possible to improve our limit on the period change by examining the change in the best periods for each season (Table 3.4) and limiting the period change via $\dot{P} = \frac{\Delta P}{\Delta T}$. From the 1990 and 1992 periods, the period change of the 525 period must be less than $\dot{P} = |(2 \times 10^{-10})|\ s\ s^{-1}$, otherwise we would see a greater change in the seasonal periods. This figure is comfortably below our earlier limit.

We are now ready to begin the final step and calculate an O-C diagram. Each observing season, except the unresolved 1976 data set, was placed on a time base employing a time of zero corresponding to the beginning of the 1978 data. A sinusoid with a period of 525.6217470 seconds was fit to each observing season's data. Because the 1992 data set spans the longest timebase, the time of first maximum for this season was used as T_{zero}, and given an O-C

value of 0 seconds. All other O-C points were referenced to this initial timing. Figure 3.18 gives the O-C diagram for seasonal timings spanning 1978 to 1992.

The next step is the most difficult and painful of the whole timing analysis. Although we labored energetically to prove the basic stability of the 525 second variation and eliminate cycle count error due to insufficient knowledge of the period, we must allow for a nonzero, although constrained, value of $\dot{P}$. We can accumulate cycle count ambiguities during the data gaps because the variation is slowly changing its phase as the period changes. The largest gaps, during which the largest ambiguities accumulate, are between observing seasons, introducing a large quantity of cycle count aliases and greatly increasing the number of possible solutions to the O-C diagram. In order to prove we have measured a period change, all possible solutions except one must be eliminated to a high degree of confidence. We have shown that $\dot{P}$ must be less than $2 \times 10^{-10} ss^{-1}$. Therefore, from 1990 to 1992, we have the possibility of accumulating ± 1 cycles during that time. We can eliminate solutions that in 1990 pass through cycle count aliases greater than this. We can also apply similar limits to other data points, resulting in the fan-shaped plot given in Figure 3.18.

Values of constant $\dot{P}$ are calculated by fitting parabolas to the points in the O-C diagram. As a first attempt, we fit various parabolas to the possible values from 1992, 1990, 1987, and 1982. We then tested the predicting power of each fit by including the 1978 and 1988 points. In most cases, the values of the fit changed by at least 10 sigma when adding those two points, making it possible to eliminate those potential solutions. The only parabolic fit which changed by less than one sigma corresponded to $\dot{P} = 1.68(\pm 0.03) \times 10^{-11}$ s s^{-1}

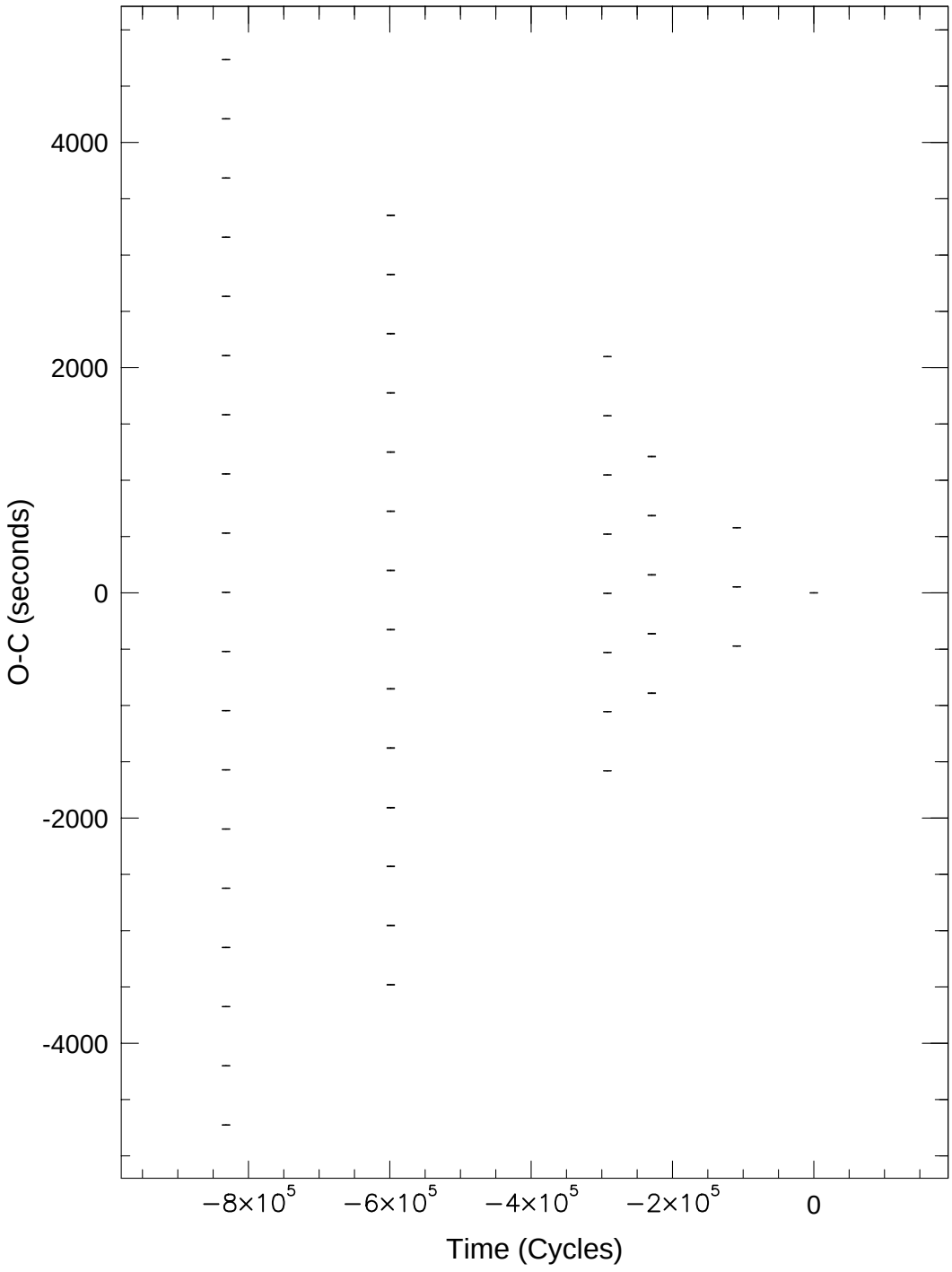

Figure 3.18: The O-C diagram for AM CVn's 525.6 second variation. These are all the possible timings. A solution must pass through one timing from each season.

Table 3.6: O-C P=525.621470

Cycle	O-C(sec)	Δ Fit(sec)	Error(sec)
0	0	-6.5	2
-108996	-472.6	6.2	2
-229337	-891	2.1	3
-292107	-1055.2	3.4	1.1
-598647	-1378	-9.4	3
-831743.991	-1046.2	4.2	2

(Figure 3.19). In this case, each individual point lies within 3 sigma of the fitted parabola (Table 3.6). The probability of obtaining 6 random points which lie on a parabola is one in 125000.

To confirm this value for the period change, we explored fitting a sinusoid with various values for $\dot{P}$ to the entire data set. The best value for the period change obtained via this method is $1.73 \pm 0.03 \times 10^{-11}$ s s^{-1}. This value is in good agreement with that obtained directly from the O-C diagram. Our measured period change for AM CVn is therefore $1.71(\pm 0.04) \times 10^{-11}$ s s^{-1}.

3.6 The Physical Nature of AM CVn

AM CVn is a complex, confusing object. Through carefule examination of this extensive data set, some indisputable facts have emerged that a satisfactory model of the object must account for. AM CVn is multiperiodic, with at least two independent variations, at 1011.4 and 525.6 seconds. The numerical relationship between 525.6 and 350.4 seconds, their stable amplitudes, and the presence of identical $20.7 \mu Hz$ splitting suggest that these two periodicities have a common physical origin. The unstable amplitude behaviour of

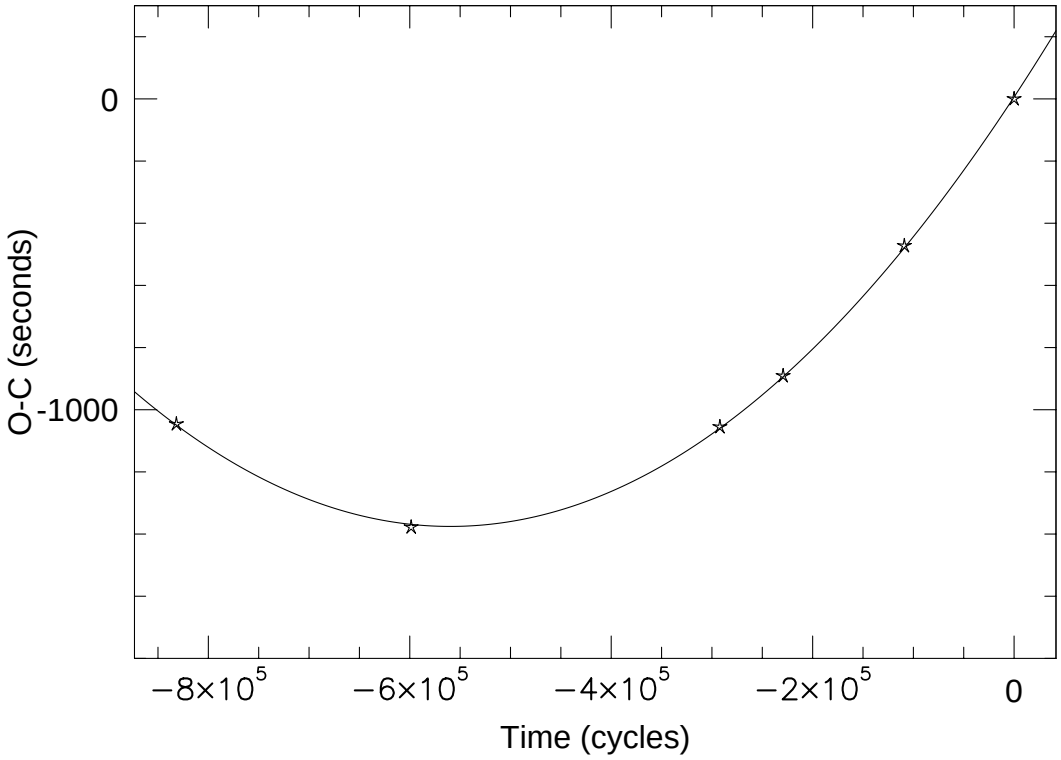

Figure 3.19: The best fit to the O-C points in Figure 3.18. The one sigma errors are the size of the points.

the 1011.4 second period argues that its physical mechanism differs from that of the 525.6 second period. The $20.7\mu Hz$ structure associated with the 525.6 and 350.4 second regions demonstrates that the actual periodicity in AM CVn cannot be 1051.2 seconds as previously reported, but must be 525.6 seconds. The pulse shape of the 525.6 second variation is nonsinusoidal and asymmetric. And finally, the measurement of $\dot{P} = 1.7 \times 10^{-11} ss^{-1}$ for the 525.6 second period is a strong confirmation of its long term stability. The mechanism responsible for the 525.6 second variation must explain this rate of period change.

$$\frac{P}{\dot{P}} \approx 1 \times 10^6 \text{ yrs}$$

Any model of AM CVn must also consider several other important factors. First, the object's spectrum is unusual. The optical spectrum contains broad, shallow absorption lines of neutral helium, with asymmetric and variable profiles (Patterson *et al.*, 1992). The IUE spectrum contains absorption lines of Si III, Si IV, C IV, He II, and N IV. (Patterson *et al.*, 1992). Secondly, AM CVn is not a strong x-ray source (Becker, 1981). Thirdly, the short-lived, non-repeating variations present in this data set could mimic the flickering reported by many authors (see Warner and Robinson, 1972). Flickering is generally a signature of mass transfer. Finally, AM CVn has a reported temperature of 25000K, placing it, on the H-R diagram, in the helium instability strip. At these temperatures, helium is partially ionized and provides an efficient mechanism with which to drive pulsations. Such pulsations may play a role in this system.

The bloody corpses of unburied models litter AM CVn's wake. In our quest to clear up the confusion, we will attempt to sift through the observational

facts in an unbiased manner to determine in which direction the data forces us to travel to explain the behaviour of AM CVn. We will begin with models incorporating single stars, the simplest possible starting position, and ask two questions: 1) what phenomena does this model predict, and 2) can this model explain the observed behaviour of AM CVn. If the answer to question 2 is no, the model will be modified and the questions repeated.

3.6.1 Single Star Models

One of the most rudimentary models to consider for AM CVn consists of a single hydrogen deficient, magnetic rapid rotator. To produce photometric variability, the magnetic poles must be either brighter or darker than the stellar photosphere. As the star rotates, the poles are carried through the line of sight, producing changes in brightness.

This model predicts the existence of a single physical period in the system, corresponding to the rotation period of the white dwarf. Since the pulse shape of the variation may be nonsinusoidal, harmonics of the periodicity may be present in the FT. Rapid rotation would also smear the spectroscopic lines, resulting in broad, shallow absorption lines.

The rapid rotator model does not account for several vital characteristics of AM CVn. First, a mechanism is required to produce the bright (or dark) magnetic poles. The most feasible possibility is accretion of matter onto the magnetic poles, but this requires the presence of a sufficient supply of accretable material, introducing a second star into the system. Secondly, this model establishes no mechanism to produce a second, nonrelated periodicity,

such as the 1011.4 second period observed in AM CVn. Thirdly, the presence of power at 350.4 seconds argues that if this model is correct, the rotation period of the star is 1051 seconds, and we are viewing two poles of unequal brightness, a form of amplitude modulation responsible for producing the 350.4 second peak. However, as discussed previously, the presence of the $20.7\mu Hz$ structure clearly demonstrates that the physical period in AM CVn cannot be 1051 seconds. The 525.6, 350.4, 262.8, 210.2 and 175.4 second peaks cannot be harmonics of 1051 seconds. Therefore, we cannot be viewing magnetic poles of unequal brightness. If the rotation period of the white dwarf is 525.6 seconds, than a complex source of amplitude modulation of pole brightness must be invoked to produce power at 350.4 seconds in the FT. Finally, although the rapid rotation may explain the widths and depths of the spectral lines, it can not explain the asymmetric and variable profiles. The ultraviolet continuum is similar to field DB white dwarfs (Liebert *et. al*,, 1986), but the detailed IUE spectra, containing absorption lines of highly ionized metals, is unlike that of any other known DB white dwarf (Liebert *et al.*, 1986), but is reminiscent of that observed in dwarf novae.

Our first attempt at modeling AM CVn as a single star has failed. However, the object has an effective temperature identical to known DB pulsators and we next consider a single DB nonradial pulsator as a possible model. The general features of DB pulsators, the lack of hydrogen, the range (from $\approx$ 1000s to 100s) of possible periods of pulsation, the large number of modes that can be simultaneously excited in an individual star, and the temperature (Unno *et al.*, 1989), agree well with the observed characteristics of AM CVn.

In many ways, the FT of AM CVn's light curve greatly resembles that

of PG1351, a well studied DB pulsator (Winget *et al.*, 1987). If we designate the 525.6 second variation as ν_o, AM CVn's FT has power at $\frac{2}{3}\nu_o, \frac{2}{2}\nu_o, \frac{3}{2}\nu_o, \frac{4}{2}\nu_o, \frac{5}{2}\nu_o$, and $\frac{6}{2}\nu_o$, similar to the pattern found in PG1351. There are differences in detail, however. Unlike AM CVn, for PG1351 the numerical relations with ν_o are not exact fractions, but are rather 1.47, 2.47, etc. The relative amplitudes of the various frequencies also differ. In PG1351's case, the $\frac{3}{2}\nu_o$ and the $\frac{5}{2}\nu_o$ peaks are much lower in amplitude than the integral harmonics. In AM CVn's case, the $\frac{3}{2}\nu_o$ frequency (350.4 seconds) has a much larger amplitude than the integral harmonics.

The presence of fine structure associated with each individual mode is also a characteristic of nonradial pulsators. Rotation destroys the spherical symmetry of the star, lifting the m degeneracy of each mode. Each mode then contains $2l + 1$ separate frequencies, where l is the spherical harmonic order. In the limit of slow rotation, the frequency difference between consecutive m's in an individual mode is a measure of the rotation frequency of the star (Unno, 1989).

$$\sigma_{klm} = \sigma_{kl} + m(1 - C_{kl})\Omega$$

$$C_{kl} \approx \frac{1}{l(l+1)}$$

The constant C_{kl} depends on the l value of the mode considered and on the equilibrium structure of the star. Observed frequency splittings range from $4.2\mu Hz$ for the DOV pulsator PG1159 (Winget, *et al.*, 1992) to $6.0\mu Hz$ for the DB pulsator GD358 (Winget, *et al.*, 1993). These frequency splittings correspond to rotation periods of 1.38 and 0.96 days, respectively. If AM CVn is a DB pulsator, and the 525.6 and 350.4 second peaks are l=1 modes, the

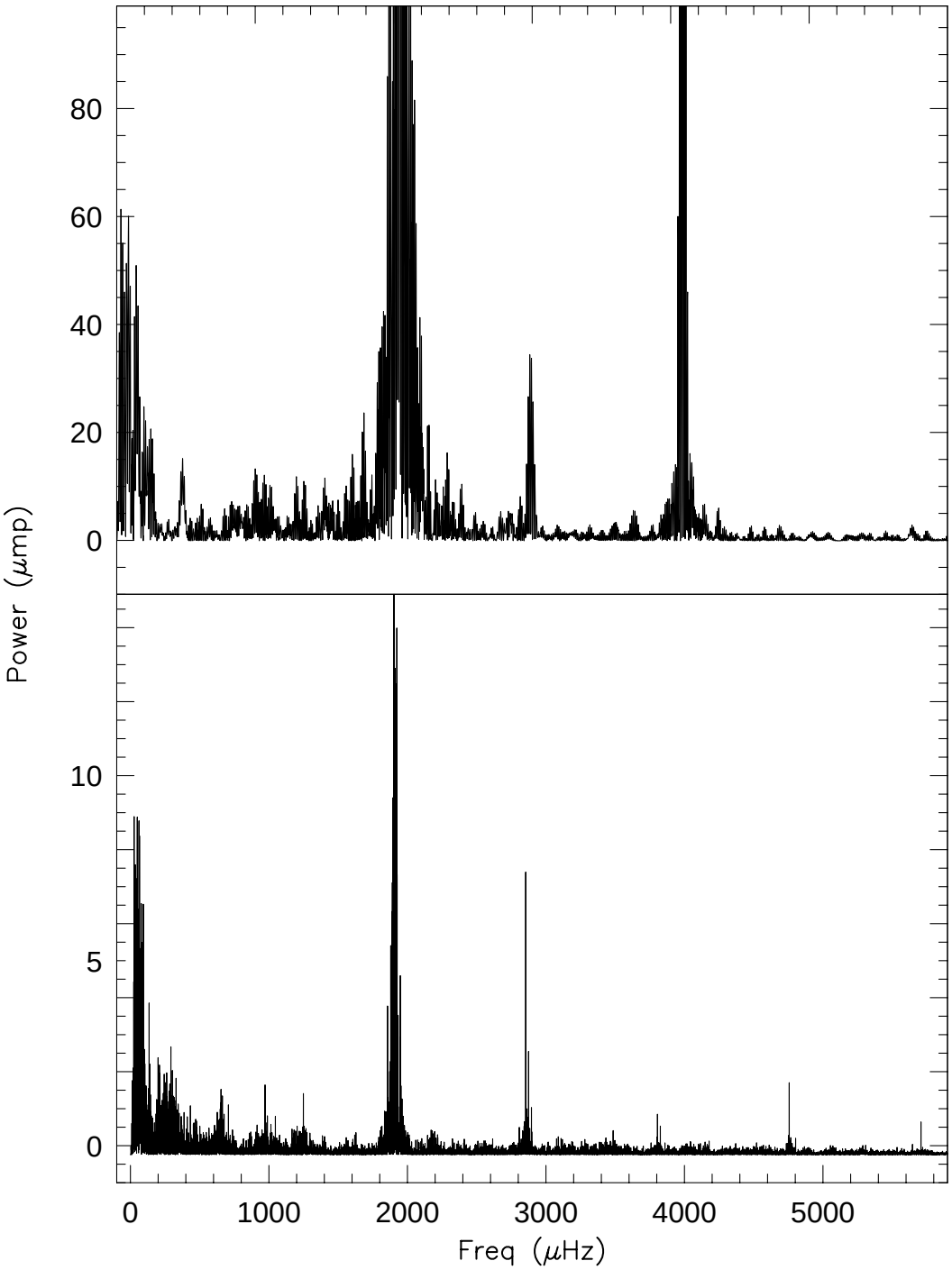

Figure 3.20: The FT of PG1351, a well studied DB pulsator. Note the similarity to the FT of AM CVn given in the second panel.

star's rotation period is 6.6 hours.

An additional fingerprint of a non-radial pulsator is the presence of sum and difference frequencies in the Fourier transform (Winget *et. al*, 1993). If the white dwarf is pulsating in a nonlinear manner, some power from the actual periods of variation will be redistributed into frequencies which are sums and differences of integer multiples of the excited modes. In the DB pulsator GD358, the sum and difference frequencies present in the FT outnumber the actual excited modes. These combination frequencies are have been shown to be consistent with pulse shape combinations due to the non-linear nature of the pulsation (Winget *et. al*, 1993).

The best data set to search for such combinations in AM CVn is the WET data from 1990 because of the lack of aliases and the fairly low noise level. There are several sum and difference frequencies present. A region of power centered on $654.0 \mu Hz$ corresponds to the frequency difference between 525.6 seconds and 800.8 seconds. A small peak $20.67 \mu Hz$ away from 262.8 seconds corresponds to the sum of 525.6 seconds and its doublet companion. It is impossible, given the limited timebase of this data set to distinguish between this sum and a possible $20.7 \mu Hz$ companion to the 262.8 second peak. The near unity of the amplitude ratios of the 262.8 second peak and this possible companion, so different from the amplitude ratios of the 525.6 and 350.4 second multiplets, argues that this 261.4 second peak is a combination frequency, not a doublet of the 262.8 second peak. A third peak at $972.0 \mu Hz$ corresponds to the frequency difference between 525.6 seconds and 347.88 seconds.

All of this is very exciting, but the DB pulsator model has several

serious flaws. As discussed for the magnetic rotating DB model, the spectrum of AM CVn is unlike any other DB white dwarf (Liebert, *et al.*, 1986). Although AM CVn displays only neutral helium absorption lines in its optical spectrum, similar to other field DB white dwarfs, the lines are unusually broad and shallow, and the profiles are asymmetric. The IUE spectrum from 1200 - 2800 angstroms contains absorption lines of silicon, carbon, and nitrogen. GD358, the prototype of the DB pulsators, displays no such spectral features in this range (Patterson, *et al.*, 1992).

Secondly, white dwarfs are not undergoing nuclear processes, and therefore do not have an internal nuclear furnace. These stars are cooling, radiating their thermal energy without replenishment. The cooling process can actually be observed in some DA and DB pulsators as the increase (or decrease, for the hot DO pulsators) of the pulsation period as the interior of the star cools and the driving region of partial ionization moves inward. The theoretically predicted value of $\dot{P}$ resulting from the cooling process, for a 25000K DB pulsating white dwarf is $\approx 5 \times 10^{-14} ss^{-1}$ (Bradley *et al.*, 1993). This is nearly 1000 times smaller than the $\dot{P}$ detected for the 525.6 second variation. If AM CVn is a DB pulsator, the period change of the 525.6 second variation is not an evolutionary change, and therefore cannot be a result of just the evolutionary cooling of the white dwarf.

A final, but secondary, problem is presented by the pulse shape of the 525 second variation. The pulse shapes of other white dwarf pulsators are nonsinusoidal, but not asymmetric in the manner of the 525.6 second pulse shape. The luminosity variations of pulsating white dwarfs are a manifestation of temperature changes on the stellar surface. It is difficult to imagine how a

temperature change could create a pulse shape as observed for the 525.6 second variation.

Both the DB pulsator model and the magnetic rotator model for AM CVn are incapable of describing all the behaviour of AM CVn. As a last attempt at a single star model, we will consider a magnetic DB pulsator, similar to the rapidly oscillating Ap stars (Kurtz, 1990). The oscillating Ap stars are non-radial pulsating A type stars, where the pulsation axis for at least one of the excited modes is aligned with the magnetic axis, rather than the rotational axis, of the star. This oblique pulsator model produces an observed short period variation that is modulated at the longer rotation period of the star. The phase of the pulsation will undergo a 180° phase change as the star passes through magnetic quadrature. Physically, the phase shift results from non-alignment of the pulsation and rotation axis. The pulsation is carried around the surface of the star as the star rotates, so the pulsation hemisphere being viewed changes with the rotation period. When the star has completed half a rotation cycle, the observer will view the opposing pulsation pole, resulting in a 180° phase change (Kurtz, 1992).

This model predicts that the short period variations observed in Am CVn are non-radial pulsations, at least one of which is aligned with the magnetic pole of the pulsator. The fine structure associated with the 525.6 and 350.4 second peaks is interpreted as a manifestation of amplitude modulation of the peaks at the rotation frequency of the star, indicating a rotation frequency of $20.7 \mu Hz$, corresponding to a period of 0.56 days, a similar magnitude to that observed in other pulsating white dwarfs (Winget, 1990). The power at 1011.4 seconds does not have fine structure associated with it, and therefore

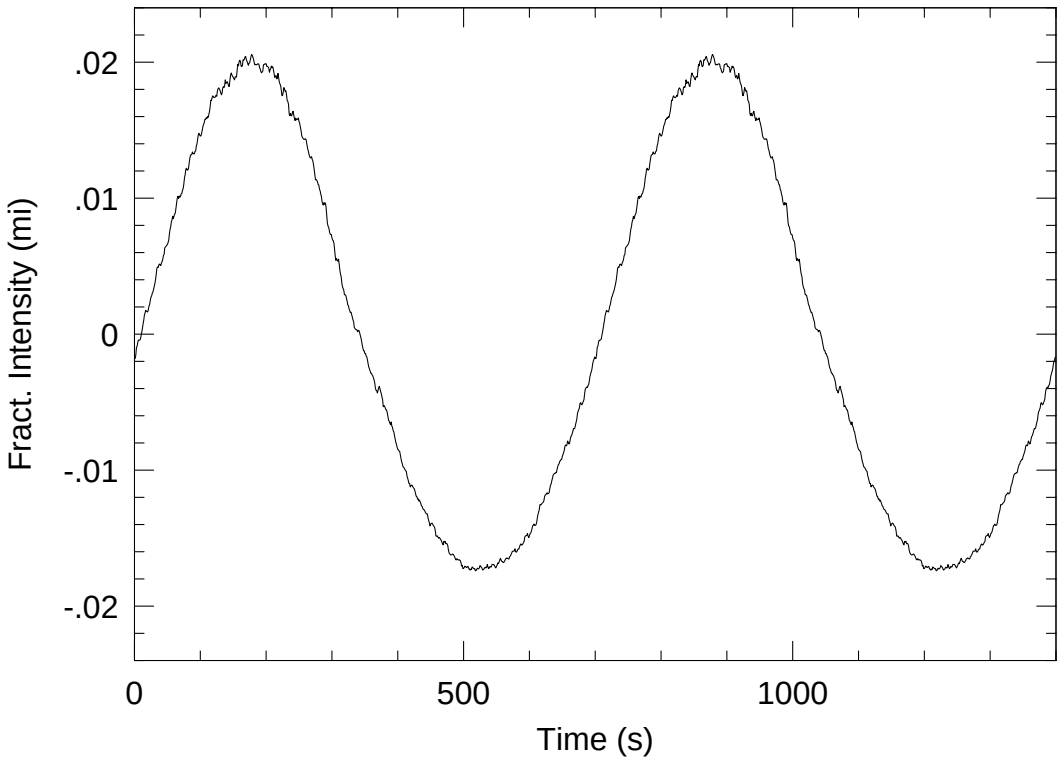

Figure 3.21: The pulse shape of the 700 second variation of the DBV white dwarf GD358. This pulse shape is a typical example of that arising from nonradial pulsations.

is a pulsation mode that is aligned with the rotation axis of the star. The amplitude changes of this variation could be explained as interactions between the material participating in the pulsation and the non-aligned magnetic field. The 1011.4 second variation would see a magnetic field of varying strength.

The downfall of this model occurs when examining the phase of the 525.6 second variation. If the oblique pulsator model is correct, it predicts a 180° phase change of the 525.6 second variation with the rotation frequency of the white dwarf. We have conclusively shown that such a phase change does not exist (Figure 3.17). Therefore, this model fails to explain behaviour observed in AM CVn.

3.6.2 Binary Systems

Although the DB pulsator model compares well with AM CVn in several important areas, it leaves key questions unexplained. The magnetic rotator model is even more unsatisfactory, compelling us to continue the search for an adequate model of AM CVn. The next step is to consider binary systems, as the reported flickering in AM CVn's light curve indicates ongoing mass transfer. Binary systems come in many colors and flavors and we would do well to begin by restricting the possible components of the binary. The complete absence of hydrogen in AM CVn's spectrum allows the immediate elimination of all types of binary models harboring a low mass, main sequence star. The only possibility is a binary containing two helium stars. The presence of a helium-burning main sequence star can also be dismissed, as such a star is luminous, and all evidence indicates that AM CVn is faint and relatively nearby

(Solheim, *et. al.*, 1984). Nondetection of radial velocity variations in the helium absorption lines, to a limit of approximately $30 kms^{-1}$ (Robinson, *et. al*, 1975) demonstrate that this hypothetical companion has a low mass. If we assume the photometric variations are representative of the orbital period, we are forced to a binary that must contain two helium white dwarfs. Indeed, if the orbital period corresponds to either 525.6 or 1011.4 seconds, and the mass of the accretor is assumed to be $1 M\odot$, the mass of the secondary must be between 0.02 and $0.04 M\odot$ (Faulkner, *et al.*, 1972), and the entire system would fit nicely inside Jupiter. The reported presence of flickering argues that the low mass degenerate secondary is filling its Roche Lobe and transferring material to its companion.

Within such systems, there are a multitude of possible sources and timescales of brightness variation: 1) orbital motion, 2) the rotation of either star, 3) the region(s) where the mass stream impacts the accretion disk or magnetic field, 4) the magnetic poles and 5) the dynamic timescales of any component of the binary. Many dwarf novae and related objects exhibit photometric variations that correspond to the rotational period of the white dwarf (Nather and Warner, 1969). In these systems, material is being accreted onto the magnetic poles of the white dwarf. Photometric variations arise as the bright (or dark) poles pass through the line of sight, carried as the star rotates. Other classes of cataclysmic variables demonstrate variations arising from their orbital periods, beating between the orbital period and rotation period of the accretor, reflection effects, asymmetries present in the accretion disk, rapid variations emanating from the hot spot, hot magnetic poles, and just about anything else you care to dream up.

It is always best to begin with the simplest model and increase complexity as needed. The first binary model we will consider is a simple interacting twin degenerate helium white dwarf system with no appreciable magnetic field. Material accretes onto the primary via an accretion disk. This model predicts variations resulting from the orbital period, from the region of impact of the matter stream and the disk (the hot spot), and also allows the possibility of some type of an eclipse. Spectroscopically, we expect to see most of the light emanating from the accretion disk. Therefore, the widths of the spectral lines should be consistent with Doppler broadening.

Let us designate 525.6 seconds to be the orbital period, as it is the only independent periodicity with the demonstrated long term stability expected for the orbital period. The measured rate of period change is 100 times larger than that due to gravitational radiation predicted by Faulkner *et al.*, (1972), but this apparent problem is easily overcome by assuming that mass is not conserved during the accretion process in AM CVn. Indeed, Solheim has reported that some absorption lines in the IUE spectra of the object are blue shifted, interpreted as a wind emanating from the mass accretor (Solheim *et al.*, 1989). If we assume that the period change is due entirely to mass loss, and the mass loss is spherically symmetric, then

$$\frac{dM}{dt} = -\frac{1}{2}\frac{M}{P}\dot{P}$$

(Nather, *et. al*, 1969). This gives a lower limit for the mass loss of

$$\frac{dM}{dt} = 3.2\times10^{-7} M \odot yr^{-1}$$

The variations which appear in individual nights of data and do not repeat could be the result of the flickering behaviour that is prevalent among

interacting binaries. The broad helium lines are consistent with those expected from a helium accretion disk (Smak, 1975). And finally, the absorption lines of Si III and IV, N V, C IV and He I and II, in AM CVn's IUE spectra are reminiscent of those observed in other interacting systems (Patterson, *et al.*, 1992).

This model leaves several unexplained facts. The presence of the 1011 second period is not accounted for. If 525 seconds is the orbital period, and no significant magnetic field is present to funnel accreting material onto the poles of the accretor, we are left with no mechanism to explain the 1011 second variation. Secondly, it is difficult to explain the $20.7\mu Hz$ structure associated with the 525.6 and 350.4 second periods. A precessing, elliptical disk has been suggested as a possible mechanism (Patterson *et al.*, 1993). The helium absorption lines have been shown to undergo profile variations with a frequency of $20.7\mu Hz$, interpreted as the precession period of an elliptical disk (Patterson *et al.*, 1993). If $20.7\mu Hz$ is the precession frequency of the elliptical disk, the light from the system should also be modulated by approximately 10 percent as the aspect angle of the disk changes with the precession period. A significant photometric variation should be detectable at the same frequency. We find no such periodicity present in any of our photometric data, within a limit of 3 mmi.

Hirose *et al.*, (1990) has calculated theoretical models of accretion disks within systems of extreme mass ratio. He finds that such disks will become unstable and precess, with beat periods between the orbital and precession periods similar to what we observe for the IBWDs. For AM CVn, he predicts (assuming $M_1 = 0.6M\odot$, a beat period of $20\mu Hz$, close to our

observed $20.7\mu Hz$ fine structure. There is no theoretical reason why the precession period should remain stable for more than the viscous timescale of the disk (Zhang it et al., 1991). In the SU UMa stars, eruptive variables believed to contain precessing elliptical disks during outburst, $\dot{P} \approx 5 \times 10^{-5}\mathrm{ss}^{-1}$, corresponding to a viscous timescale of a few weeks. The $20.7\mu Hz$ structure is detected over a timescale of years in AM CVn. Of course, the disk in AM CVn is composed of helium, as opposed to hydrogen in the SU UMa systems. It is unclear what effects the different composition will have on the magnitude of viscosity within the disk.

Finally, the 350.4 second period itself and its harmonics are unexplained. Its numerical relationship to 525.6 seconds and the presence of similar $20.7\mu Hz$ fine structure argue that its origin is related to the origin of the 525.6 second period. Simple orbital motion is unable to create an apparent variation like the 350.4 second period.

The basic interacting binary is inadequate to interpret the observed behaviour of AM CVn. The next logical step is to include a magnetic field in our binary model. Besides the possible sources of variation of a simple interacting binary, we may now also include the region where the magnetic pressure becomes equal to the ram pressure of the gas in the disk. At this location, the accretion disk is disrupted, and the material is forced to travel along the magnetic field lines (Frank *et al.*, 1985). An additional source of variation includes the magnetic poles, where incoming material strikes the white dwarf surface. The inclusion of a magnetic field provides a mechanism by which light from the system can be modulated at the rotation period of the white dwarf.

We must first consider the evidence for the presence of a magnetic field in AM CVn. The object is not a strong x-ray source (Becker, 1981), indicating that a great deal of matter is not funneling onto the poles, as would be expected if a strong magnetic field were present. There is also no evidence of circular polarization (Angel, 1970, Solheim, 1989). Current techniques can detect magnetic fields only down to about 10^6 Gauss, and then not with 100 percent accuracy. Although there is no compelling evidence arguing for the presence of a magnetic field in AM CVn, there is no argument against the presence of a field as great as 10^6 Gauss.

A magnetic field of $10^5 - 10^6$ G would have extremely interesting effects on the structure of AM CVn. If we assume the rotation period of the accreting white dwarf is shorter than the binary period, then we must designate 1011.4 seconds to be the orbital period of the system, and 525.6 seconds to be the rotational period of the white dwarf. Our current model consists of a binary undergoing mass transfer, therefore the secondary star is filling its Roche lobe. Assuming $M_1 = 1M\odot$ and $M_2 = 0.04M\odot$ (Faulkner *et al.*, 1972), from Kepler's law

$$P^2 = \frac{4\pi^2}{G(M_1 + M_2)}a^3$$

we get a separation of 1.5×10^{10} cm. To derive the sizes of the relevant Roche lobes in the case of extreme mass ratios, using (from Frank, *et al.*, 1985)

$$\frac{R_{L,2}}{a} = 0.462(1 + q)^{-\frac{1}{3}}$$

where $q = \frac{M_1}{M_2}$ we get

$$R_{L,2} = 0.16a = 2.4 \times 10^9 \text{cm}$$

$$R_{L,1} = 0.84a = 1.3 \times 10^{10}\text{cm}$$

The size of the accretion disk can be approximated by finding the distance of closest approach of the matter stream, or the circularization radius. Using (again from Frank, *et al.*, 1985)

$$\frac{R_{circ}}{a} = (1 + q^{-1})[0.500 - 0.227log(q^{-1})]^4$$

we get a lower limit of

$$R_{circ} = 7.0 \times 10^9 \text{ cm}$$

The magnetic radius of the accretor, the radius at which magnetic pressure equals the ram pressure of the accreting material, is dependent on the strength of the magnetic field, the mass of the accretor, and the accretion rate. We will assume a accretor mass of $1M\odot$, a magnetic field ranging from 10^5 to 10^6 Gauss, and an accretion rate of $1 \times 10^{-10} M \odot yr^{-1}$, (Solheim, 1984). Using (from Frank *et al.*, 1985) where μ_{30} is the magnetic moment of the accreting white dwarf in units of 10^{30} G cm^3, and $\dot{M}_{16}$ is the accretion rate in units of 1×10^{16} gm s^{-1},

$$R_{mag} = 5.1 \times 10^8 \dot{M}_{16}{}^{-\frac{2}{7}} M_1^{-\frac{1}{7}} \mu_{30}^{\frac{4}{7}}\text{cm}$$

we get

$$R_{mag} = 1.9 \times 10^9 \text{ to } 7.0 \times 10^9 \text{ cm}$$

The value of R_{mag} is only weakly dependent on mass and accretion rate, and does not change appreciably when these values are varied.

These values of R_{mag} lie within the circularization radius, but above the surface of the white dwarf ($R \approx 1 \times 10^9$) cm. The material in the accretion disk will impact the magnetic field before it strikes the white dwarf surface. If

the magnetic field were much smaller than $10^5 G$, the magnetic radius would be below the physical radius of the white dwarf. If the magnetic field were much larger than $\approx 10^6 G$, the magnetic radius would exceed the binary separation and no accretion disk could form. If a magnetic field of $10^5 - 10^6$ gauss is present in the system, AM CVn could be a helium version of an intermediate polar (King *et al.*, 1990).

In this intermediate polar model, the 1011.4 second period corresponds to the binary orbital period and the 525.6 second period is the rotation period of the magnetized white dwarf. We are then led to a simple explanation of the $20.7 \mu Hz$ structure associated with this periodicity. The material accreting onto the white dwarf via its magnetic poles must create a torque, forcing the white dwarf to precess. As the white dwarf precesses, we view the poles from a changing aspect angle. The $20.7 \mu Hz$ fine structure is the observational consequence of the precessing white dwarf. A second possibility is a modulation of the field lines themselves. As the accreting white dwarf rotates, it carries the magnetic field lines through space. If the field is unaligned with the rotation axis and hence the horizontal disk axis, the magnetic field is perturbed as material jolts the field lines. Since the field lines carry material to the poles of the white dwarf, the variations at the poles are would be modulated at the response frequency of the field lines.

We demonstrated previously (Figure 3.10) that the 525.6 second pulse shape may be modeled very closely as a convolution of two bright regions. If two luminous regions with the same period but differing phases, arising in different regions, exist in the system, the observed 525.6 second pulse shape could be created. A possible example could be the visible magnetic pole and the shock

region where the disk is disrupted by the magnetic field. Both would have be carried at the rotation period of the white dwarf, but may not necessarily have the same phase.

Finally, as pointed out for the simple interacting binary model, the IUE spectrum is reminiscent of that observed in other interacting binaries. The blue shifted IUE absorption features are explicable as a wind emanating from the system. If our hypothetical magnetic field is indeed unaligned with the rotation axis of the accreting white dwarf, the field could be acting as a wind mill , driving away as much or more material than is accreting along the field lines. The mass loss would explain the increasing $\dot{P}$ of the 525.6 second variation.

The precessing magnetic poles would have a subtle effect on the optical spectrum of AM CVn. The absorption features themselves originate in the accretion disk, but are partially filled with emission eminating from the hot poles. As the poles precess with a 13.4 hour period ($20.7\mu Hz$), the profiles vary, making the absorption profiles appear to modulate. The differences in the phase of the line profile variation in the core of the absorption lines and in the wing regions (Patterson, 1993) is then explained as reprocessing of the beam as it sweeps across the disk.

This magnetic accretor model, while it explains many phenomena observed in AM CVn, has several problems. First, the 525.6 second period is shown to be increasing. If 525.6 seconds is the rotational period of the accretor, the period should be decreasing as the white dwarf accumulates angular momentum from the accreting material. Evidence exists for a wind eminating

from the system, and therefore the assumption of mass conservation is probably wrong. Magnetic braking, or friction between the accretion disk and the magnetic field as it spins, could be the dominant mechanism of period change in AM CVn. Magnetic breaking would transfer momentum back outward into the disk, resulting in an increasing, rather than decreasing, rotation period. Our measure of $\dot{P}$ then is also a measure of the stability of the accretion rate and the value of $\dot{P}$ is a convolution of magnetic braking and changing accretion rate, indicating that $\frac{d\dot{M}}{dt}$ is constant over long timescales. Each timing used in the calculation of $\dot{P}$ is a seasonal timing, limiting the sensitivity of our measurement of $\dot{P}$ to fluctuations in accretion rate on timescales shorter than one year.

Second, the 350.4 second power and its harmonics are difficult to explain. The initial perception is to reason that we are viewing two magnetic poles of unequal brightness, but this would force the rotation period of the white dwarf accretor to be 1051 seconds, longer than the binary period. We have shown that 1051 seconds cannot be the physical period of the system, therefore this model has no straightforward explanation of the 350.4 second period and its fine structure. The $20.7\mu Hz$ structure associated with the 350.4 second period establishes the 350.4 second power's connection to the magnetic field, and it must somehow be related to the 525.6 second period.

Next, AM CVn is not a strong x-ray source, indicating that a large amount of material is not accreting onto the magnetic poles. If 525.6 seconds is the rotation period of the accretor, our measurement of a positive value for $\dot{P}$ confirms this fact, The white dwarf is not spinning up, but is increasing its rotation period. We calculated a lower limit to the mass loss required by

the measured $\dot{P}$, assuming spherical mass loss, for the basic interacting binary model. The magnetic poles may still be optically bright if the primary is accreting only a small fraction of the material, and the rest is being driven from the system. There are now 3 examples of intermediate polars with weak or absent x-rays: AE Aqr, DQ Her, and V795 Her (Zhang it et al., 1991).

And finally, as mentioned when discussing the single DB pulsator, there are sum and difference frequencies present in AM CVn's light curve. A similar phenomenon is observed in intermediate polars, where power is present in the FT at integer combinations of the orbital period and spin period of the white dwarf. However, in AM CVn, integer combinations of the orbital and spin periods are NOT observed. The sum and difference frequencies are combinations of 525.6 seconds and its $20.7\mu Hz$ companion, 525.6 seconds - 800.8 seconds, and 525.6 seconds plus one of the components of the 350.4 second triplet.

A final binary model to consider is a DB pulsating white dwarf embedded in an accretion disk, as a member of an interacting binary. As discussed for a solitary DB pulsator, the temperature of the system is commensurate with known DB pulsators, the periods of the variations are within the expected range, and the amplitudes are similar to those observed in solitary pulsators, especially when considering a DB pulsator viewed against the background of a bright accretion disk. Such an object should not be a strong x-ray source, and does not necessitate a strong magnetic field. Both the optical and IUE spectra are explained as a composite of white dwarf and disk characteristics.

In this model, the 800.8, 525.6, and 350.4 second variations would

be non-radial g-modes arising on the pulsating accretor. The fine structure associated with these frequencies measure the rotation period of the accreting white dwarf pulsator, at 6.6 hours. The 1011.4 second period, so different in behaviour from the other periodicities, is the orbital period.

The presence of sum and difference frequencies in the FT of AM CVn is a strong indicator of the presence of a pulsating DB. As discussed above, the sideband structure observed in other cataclysmic variables is not what is seen in AM CVn. Here, we see sums and differences of frequencies which are neither the orbital or rotational periods of the system.

There is one fatal flaw with the DB pulsating accretor model. The rotation period of 6.6 hours is far too slow, much slower than the orbital period of the binary. Other accreting white dwarfs in interacting binaries have been shown to be rotating on timescales of seconds, not hours (see Nather, 1969 for an example). In every case, the rotation period of the white dwarf is shorter than, or equal to, the orbital period. Of course, the $20.7 \mu Hz$ fine structure may not result from rotational splitting. The $20.7 \mu Hz$ structure could be interpreted as the precession of the pulsation axis, responding to the torque produced by the accreting material.

If the mass accretor in AM CVn is a DB pulsator, the interpretation of the measurement of $\dot{P}$ for the 525.6 second nonradial pulsation period is ambiguous. As discussed for a solitary pulsator model, the expected $\dot{P}$ due to secular evolution $\approx 1 \times 10^{-14}$ ss^{-1} and the $\dot{P}$ measured is 1.7×10^{-11} ss^{-1}. The theoretical $\dot{P}$ measures a cooling timescale, calculated for a solitary, nonaccreting pulsating DB white dwarf. The hypothetical white dwarf pulsator in AM

CVn is anything but a typical pulsator, and its outer layers of the accretor are certainly not cooling. The white dwarf is accreting material and its surface layers are being heated. The depth of the heating is dependent on the accretion timescale. The thermal structure of the accretor could be very bizarre, with a hot envelope surrounding a cooler core indicative of the original temperature of the primary when the current accretion episode began. Although little theoretical work has been done in this area, the rate of period change of an accreting pulsator should be dictated by the heating, and therefore the accretion, timescale.

In our discussion of binary models, we have neglected to mention one very important component of AM CVn: the mass losing secondary. This degenerate object is certainly a strange beast. Examination of the composition of the accretion disk is a probe of the composition of the secondary, and by extension, the composition of the core of what was once a main sequence star. It is surprising that the secondary seems to be composed solely of helium, with a smattering of other heavy metals. At $0.04 M\odot$, we should be well into the carbon core if this star followed a normal evolutionary track. A main sequence star without enough mass to burn helium to carbon has not had sufficient time to evolve to a white dwarf. It is fair to argue that the secondary has been deprived of a normal main sequence lifetime because of its membership in the binary. It is also interesting to note that the dynamical timescale of such a star

$$\tau_{ff} = \sqrt{\rho G}$$

is several hundred seconds. This is the timescale of the variations seen in AM CVn. If the secondary could be excited as a radial pulsator, it could modulate

mass transfer at these rates.

3.7 Conclusions

We have extensively analyzed the most comprehensive data set available on AM CVn and found the FT to contain power at 1011.4, 800.8. 525.6, 350.4, 262.8, 210.2 and 175.4 seconds. These periodicities can be explained in terms of one completely independent periodicity, 3 numerically related but possibly independent periodicities, two harmonics and several linear combinations. Our most important results are 1) the demonstration that the physical period of repeatability can not be 1051 seconds as previously reported, but must be 525.6 seconds and 2) the stability of the 525.6 second periodicity, with a continuous period change of $\dot{P} = 1.7 \times 10^{-11}\mathrm{ss}^{-1}$.

Despite this onslaught of observational data, AM CVn continues to guard its secrets. Although we can not definitively say what AM CVn is, we have made some progress in discovering what it is not. The object cannot be a single magnetic rotator or pulsator, these models are not satisfactory. AM CVn must be a binary containing two helium white dwarfs but a simple interacting binary is not sufficient to explain the observed behaviour. The intermediate polar model resolves most of the key observational facts, but leaves the 350.4 second period and the measurement of $\dot{P}$ unexplained. A DB pulsator in an accreting binary also fits the observations well, but only if the $20.7\mu Hz$ structure is not due to rotation.

Much additional work needs to be pursued. Conclusive evidence of the orbital period must be pinned down. Intensive searches for radial velocity

variations have been completed for 1051 seconds, but not for 1011.4 or 525.6 seconds. Profile changes with 13.4 hour period have been detected, but cannot be orbital in origin. The stability of the 1011.4 second period must be studied. If this is the orbital period, it should maintain a stable phase. The 1011.4 seconds amplitude variations makes an ephemeris calculation nontrivial, but also not impossible, to obtain. We are hopeful because despite the large amplitude changes, the 1011.4 second variation appears to maintain the same frequency. The stability of the 350.4 second period must also be investigated. If it is related to the dominate 525.6 second power, it should be effected on the same timescale as the 525.6 second variation. Therefore, we predict $\frac{P}{\dot{P}} \approx 1 \times 10^6$ years and $\dot{P}_{350} \approx 1 \times 10^{-11}$ s s^{-1} A measurement of $\dot{P}$ for the 350.4 second period will indicate if it is related to the 525.6 second period or if it is an independent variation.

Chapter 4

The Eruptive Variable PG1346+082

The Palomar Green (PG) survey object PG1346+082 is the second member of the interacting binary white dwarf family. This intriguing object is both a spectroscopic and photometric variable, altering its luminosity and spectral features on a wide range of timescales (Wood, *et al.*, 1987). It is an eruptive variable, undergoing outbursts ranging from a low state (minimum light) magnitude of 17.2 (m_b) to a high state (maximum brightness) of 13.6 (m_b) on a quasiperiodic timescale of days. Superimposed on these large scale variations are short period oscillations, centered on 1470 seconds, the characteristics of which are correlated with the overall magnitude of the object (Wood, *et al.*, 1987). Flickering, the classic signature of mass transfer observed in other predominantly hydrogen cataclysmic variables, has been reported in PG1346+082 during minimum brightness (Wood, *et al.*, 1987).

The most significant characteristic of PG1346+082's spectrum is the complete lack of hydrogen. The spectrum is governed by neutral helium, but the features actually present at any given time are dependent on the overall magnitude of the system. In high state, PG1346+082's optical spectrum is dominated by He I absorption lines and is indistinguishable from the spectrum of AM CVn (Solheim, *et al.*, 1984). The widths of the absorption features are consistent with either pressure broadening in the atmosphere of a compact

object, or a combination of pressure broadening and Doppler broadening in a swiftly rotating accretion disk (Wood, *et al.*, 1987). The relative strengths of the helium lines present in both the high state spectrum of PG1346+082 and that of AM CVn are quite different from field DB white dwarfs. The absorption profiles are considerably shallower and asymmetric, and both objects are missing the usually strong He I line at $4713\mathring{A}$ (Patterson, *et al.*, 1992). PG1346+082's IUE spectrum in high state is also similar to AM CVn, both are reminiscent of that observed in dwarf novae.

PG1346+082's low state optical spectrum is significantly different from that observed at maximum brightness. There are no features present above noise, with the exception of a weak He I emission feature at $4471\mathring{A}$ (Wood, *et al.*, 1987). The magnitude-dependent behaviour of PG1346+082's spectra is identical to phenomena observed in hydrogen-dominated dwarf novae, in which absorption lines are seen during outburst, and emission features during minimum light (Wade, 1985).

The dwarf novae type outbursts observed from PG1346+082 argue persuasively in favor of its binary nature. Considered with the lack of hydrogen in its spectrum, PG1346+082's membership in the interacting binary white dwarf family is secure (Wood, *et al.*, 1987). Through its outbursts, this object allows us access to an alternate avenue to explore the IBWD systems. If the outbursts arise in an accretion disk, we can use them to examine the structure and importance of disks in the IBWDs. The differences in behaviour between the helium and hydrogen disks and contrasts between helium and hydrogen outbursts characteristics could be used as a valuable probe of the age-old problems of viscosity and outburst mechanisms in dwarf novae and related objects,

possibly leading to actual progress towards resolving these difficult questions. Also, PG1346+082's effective temperature hovers around 20000K (Wood, *et al.*, 1987). If the temperature climbs into the helium instability strip during outburst, it may be possible to use the object as a probe of the boundaries of the instability strip, and also to measure actual growth rates of pulsations.

This chapter concentrates on the behaviour of the short period variations of PG1346+082, with the particular objective of understanding the origin of the band of power at 1470 seconds. Questions to be explored include: is the reported power at 1470 seconds consistent with a single frequency or a multitude of closely space periodicities? If a horde of periodicities are present, what can we deduce concerning the mechanism responsible? If the 1470 second power is consistent with a single period of variation, and the lessons of the hydrogen dwarf novae can be transferred to helium interacting systems, the 1470 second period may be a manifestation of the orbital period of the system or the rotation period of either degenerate components. If this is the case, we would expect the 1470 second power to maintain a stable frequency and, perhaps, phase. We will examine the behaviour and stability of the power at 1470 seconds, as well as its related harmonics.

4.1 Observations and Reductions

Our observations of PG1346+082 consist of a total of over 278 hours of white light and Johnson U, B and V multicolor high speed photometry (see Ch 2. for a discussion of the technique). Over half the data were taken in 1988, when PG1346+082 was the prime target of the inaugural run of Whole Earth

Table 4.1: Journal of Observations 1984-1985

Run	Observatory	Date	Run Start (UT)	Length	Integration
r2900	Texas	3 April 84	5:03:19	5.74	10
r2908	Texas	4 April 84	4:04:48	6.50	10
r2919	Texas	8 April 84	4:57:18	5.66	10
r2925	Texas	9 April 84	4:14:18	6.22	10
r2930	Texas	1 May 84	4:18:48	5.39	10
r2937	Texas	2 May 84	7:53:58	2.81	10
r2940	Texas	3 May 84	3:55:18	3.48	5
r2949	Texas	4 May 84	4:01:58	4.54	10
r2952	Texas	5 May 84	3:58:58	5.44	10
r3003	Texas	19 Jan 85	10:52:30	1.44	10
r3021	Texas	23 Mar 85	6:29:00	2.48	10
r3042	Texas	19 Apr 85	3:13:20	6.57	10

Telescope (Nather *et al.*, 1990) (Tables 4.1, 4.2 and 4.3). The data was taken and reduced using the techniques described in Chapter 2.

4.2 Overall Magnitude Behaviour of PG1346+082

The large scale magnitude fluctuations of PG1346+082 (Figure 4.1) introduce difficulties into our examination of the system's short timescale behaviour that are not normally considered by our standard analysis techniques, which assume a constant mean magnitude for the variable star. Our first step is to understand and avoid the possible artifacts introduced into our analysis by the overall magnitude variations of PG1346+082.

Our analysis techniques employ the units of fractional intensity, or the amplitude of the variation relative to a supposedly constant mean magnitude. The mean flux level of PG1346+082 is continually changing as the system un-

Table 4.2: Low State WET 1988 Journal of Observations

Run	Observatory	Date	Run Start (UT)	Length (hr)	Int (s)
ren20	Texas	9 March	11:24:50	0.478	10
pg13a	France	10 March	22:57:06	5.173	6
pg13b	France	11 March	24:03:06	4.395	6
tol-0005	Chile	12 March	3:56:00	4.933	10
s4227	South Africa	12 March	23:08:20	4.067	10
pg13c	France	12 March	23:20:06	5.233	6
tol-0011	Chile	13 March	3:23:00	5.625	10
ren28	Texas	13 March	5:54:08	5.931	10
bph68	Hawaii	13 March	9:18:00	5.967	10
a11	Australia	13 March	13:49:00	4.772	10
pg13d	France	13 March	23:21:06	5.052	6
tol-0017	Chile	14 March	4:10:00	2.658	10
ren29	Texas	14 March	5:24:10	5.514	10
bph69	Hawaii	14 March	8:57:00	0.639	10
a14	Australia	14 March	14:43:01	3.614	10
tol-0022	Chile	15 March	3:16:00	2.375	10
ren31	Texas	15 March	5:23:30	6.289	10
bph70	Hawaii	15 March	8:54:00	6.367	10
a19	Australia	15 March	14:46:00	3.817	10
s4238	South Africa	17 March	22:21:40	4.917	10
ren35	Texas	18 March	5:18:30	6.361	10
bph71	Hawaii	18 March	8:42:00	6.567	10
a23	Australia	18 March	13:24:00	1.211	10
ren37	Texas	19 March	5:19:00	5.502	10
bph72	Hawaii	19 March	8:45:00	6.547	10
maw3	Texas	20 March	4:29:00	7.150	10
bph73	Hawaii	20 March	8:38:00	6.677	10
s4246	South Africa	20 March	22:27:20	4.800	10
maw5	Texas	21 March	4:33:52	7.086	10
bph74	Hawaii	21 March	8:41:00	6.483	10
bph75	Hawaii	22 March	8:40:00	6.425	10
maw10	Texas	23 March	4:16:00	7.333	10
bph76	Hawaii	23 March	8:28:00	2.347	10
s4253	South Africa	23 March	0:28:10	2.683	10
maw12	Texas	24 March	4:05:50	7.453	10
maw14	Texas	25 March	4:11:30	7.325	10
s4256	South Africa	25 March	23:40:50	3.367	10
maw16	Texas	26 March	7:37:20	3.892	10

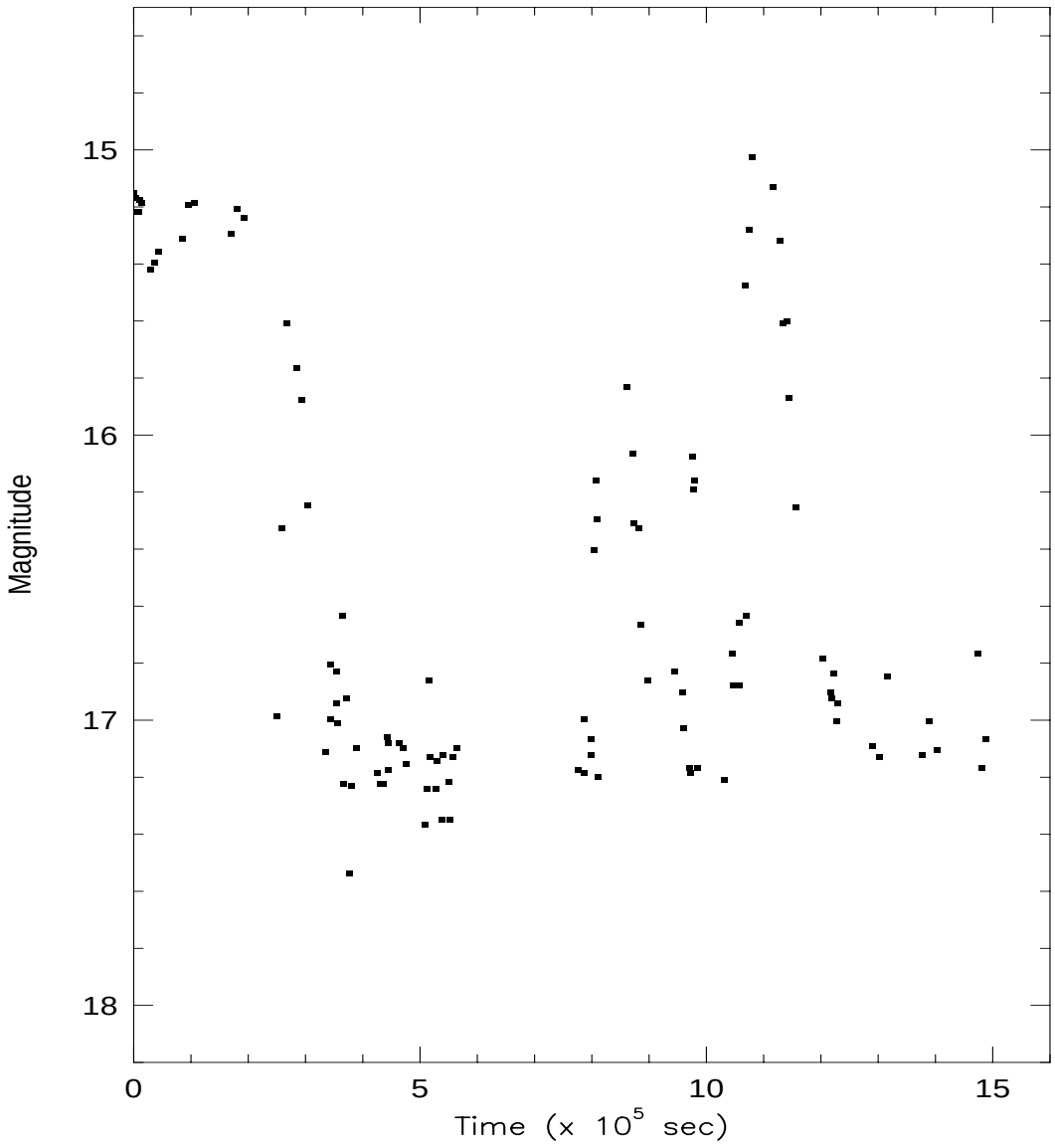

Figure 4.1: The overall magnitude of PG1346+082 during the March 1988 WET observing run.

Table 4.3: Hi State WET 1988 Journal of Observations

Run	Observatory	Date	Run Start (UT)	Length (hr)	Int (s)
ren18	Texas	9 March	6:28:20	1.772	10
ren19	Texas	9 March	8:39:20	1.867	10
ren22	Texas	10 March	6:13:20	5.603	10
ren24	Texas	11 March	5:47:00	6.067	10
ren26	Texas	12 March	5:36:10	4.283	10
bph67	Hawaii	12 March	10:57:00	4.333	10
a10	Australia	12 March	13:41:01	4.972	10
ren33	Texas	16 March	5;23:30	6.339	10
a26	Australia	20 March	13:15:02	0.689	10
a28	Australia	21 March	14:32:01	3.503	10
s4250	South Africa	21 March	22:54:20	4.550	10
maw7	Texas	22 March	4:17:00	6.558	10

dergoes large amplitude outbursts, introducing a form of amplitude modulation into the analysis. If any physical variation is present in the system at constant phase and amplitude, and does not partake of the processes resulting in the large scale outbursts, that periodicity will not appear as a single peak in an FT of PG1346+082's light curve because its relative amplitude will be modulated by the varying background. The FT will contain a forest of peaks, with separations in frequency characteristic of the amplitude modulation timescale.

If the large outbursts have any effects on the 1470 second power, we must compensate for any artifacts introduced by amplitude modulation. At first glance, it is not difficult to show that the fractional intensity of the short period variations is indeed dependent on the overall magnitude of the system (Figures 4.2, and 4.3).

To study the amplitude modulation in more detail, we measured the overall fractional intensity of the main band of power at 1470 seconds, as well

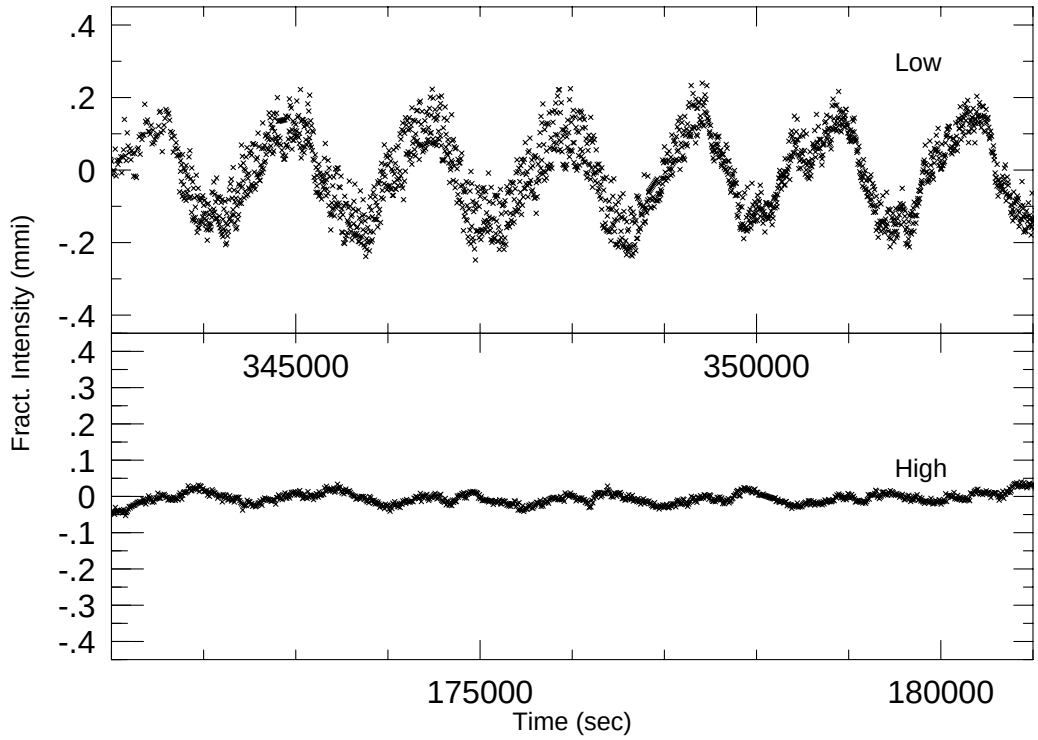

Figure 4.2: Portions of the WET 1988 light curve of PG1346+082 at differing magnitudes. The top panel is an example of PG1346 at low state, and the bottom panel a sample of the object at magnitude ≈ 15.5. Note the changes in vertical axis.

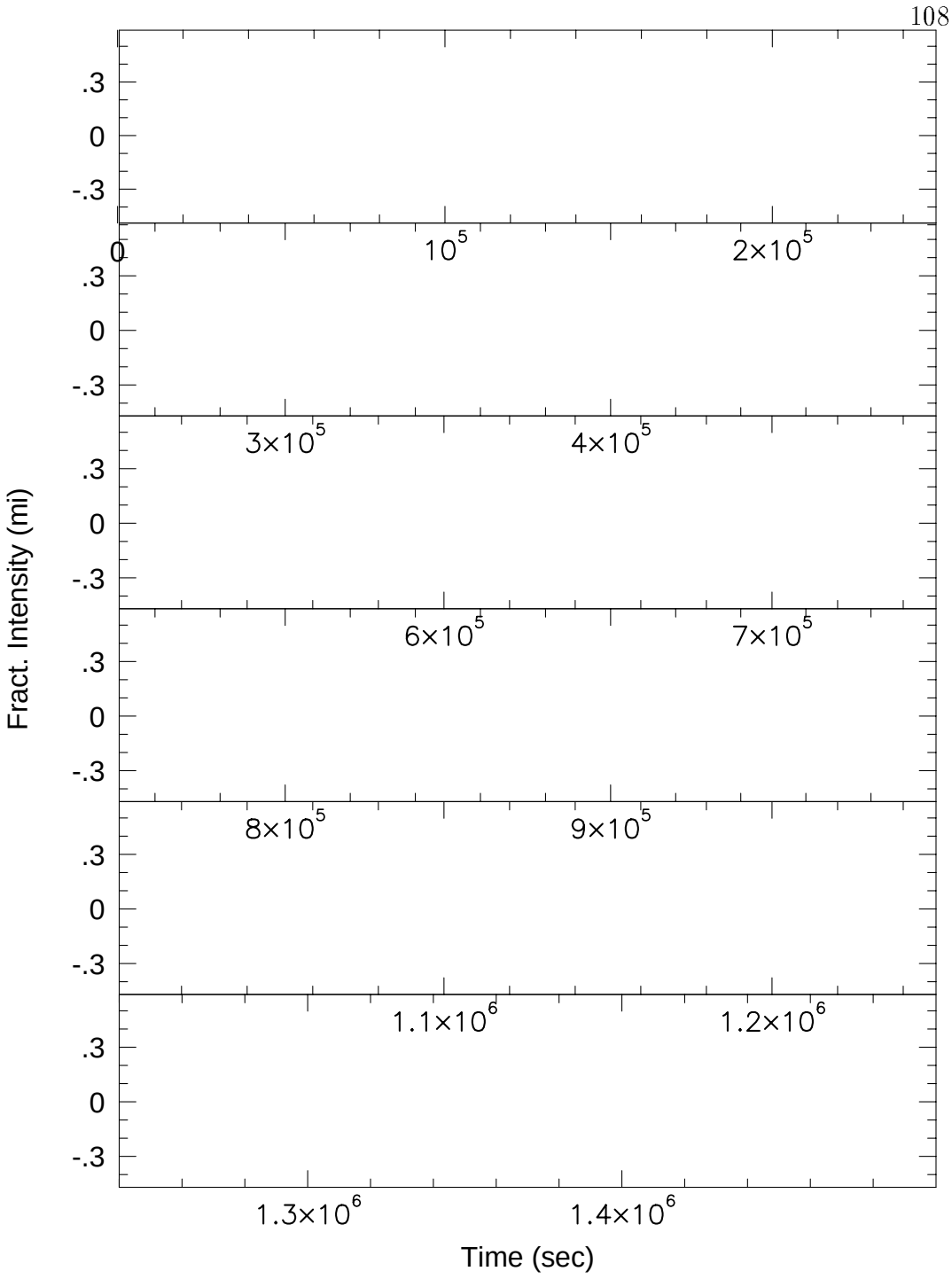

Figure 4.3: The entire light curve of PG1346+082 taken during XCOV I in March of 1988. All the large magnitude variations have been removed. The dominant 1470 second variation displays compelling amplitude changes.

as that of the first harmonic, as a function of time during the 1988 WET run (Figure 4.4). We chose the number of measured points to maximize both the resolution of the FTs used and the number of points required to adequately sample the distribution of fractional intensities. When compared to the magnitude fluctuations of PG1346+082 itself (Figure 4.1), both the 1470 second power and its first harmonic have their largest fractional intensities when the overall system is dim and their smallest fractional intensities when the system is bright. The behaviour of both the 1470 second band of power and the harmonic peak mirror the magnitude changes of PG1346+082, demonstrating that the fractional intensities of the 1470 second power is inversely dependent on the overall brightness of PG1346+082.

This inverse dependence of fractional intensities on overall magnitude suggests a constant source seen against a variable background. We see the source more clearly when the background illumination is dim, and with more difficulty when the background is bright. In other words, the contrast between the source of the 1470 second power and the background illumination is higher when the PG1346+082 is dim, and is reduced when the object is bright, resulting in the observed changes of fractional intensity. We can test this model by predicting the change of fractional intensity of the 1470 second power as a function of the changing magnitude of the system. During WET, PG1346+082 varied from ≈ 17.2 (m_b) to ≈ 15.0 (m_b). Using (Abell *et al.*, 1987)

$$m_2 - m_1 = 2.5log(\frac{f_1}{f_2})$$

the flux level at 15.0 m_b is 7.6 times that at magnitude 17.2 (m_b). The largest fractional intensity measured for the 1470 second variation is 89.7 mmi and the

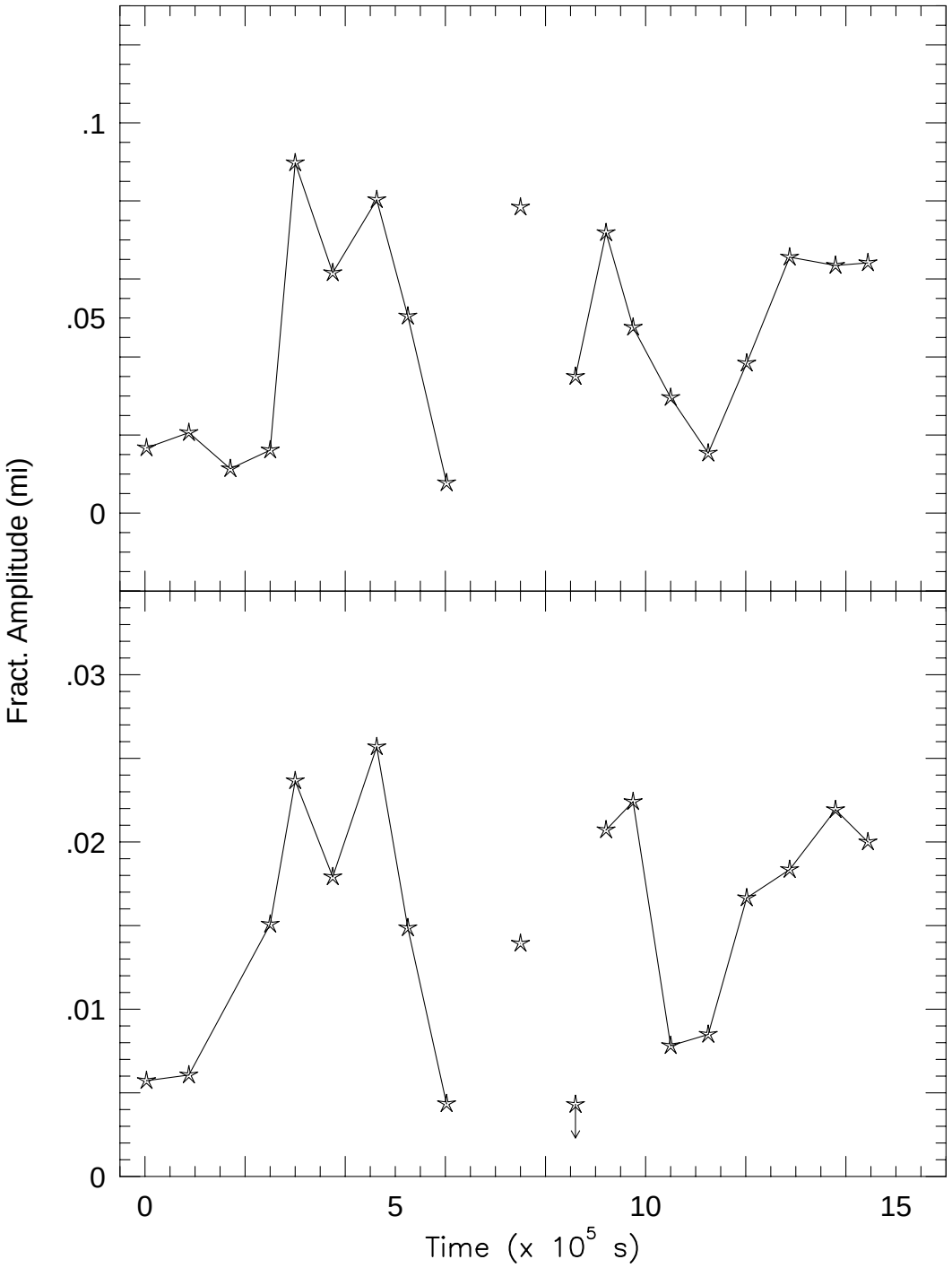

Figure 4.4: The amplitude of the 1470 second power as well as that of its harmonic at 735 seconds.

lowest is 11.3 mmi. This corresponds to a decrease in fractional intensity by a factor of 8, just what would be expected if the 1470 second periodicity were maintaining a steady amplitude viewed against an fluctuating background.

Our usual techniques of analysis assume the object in question is not changing its mean magnitude or variation characteristics over timescales shorter than the observing time. We have demonstrated that the large magnitude fluctuations of PG1346+082 give rise to the illusion of intensity changes in its short timescale variations, in a quasiperiodic manner on timescales of hours. Calculating a FT of a data set in which this form of amplitude modulation is present will introduce artifacts into the FT, manifested as a forest of peaks surrounding any physical periodicity. The FT of the entire WET PG1346+082 data set in the region of 1470 seconds is given in Figure 4.5, but it is impossible from just this FT to distinguish which of the multitude of peaks represent physical phenomena occurring in the system, or if the additional peaks are the result of amplitude modulation of the 1470 second power with system magnitude.

We must modify our techniques of analysis to minimize the effects of amplitude modulation on the FT, before applying them to PG1346+082. Our approach to the problem assumes PG1346+082 to behave in identical ways at similar magnitudes. That is, the object displays a certain behaviour in low state, and a certain behaviour in high state. Any time the system is in low state, its behaviour is identical to any previous low state, and any time PG1346+082 is bright, it is identical to any other bright state. Analyzing subsets of the PG1346+082 data in which the object is at similar magnitudes will reduce the effects of amplitude modulation of the 1470 second power. We therefore divided the 1988 WET data set into two subsets, high state and low

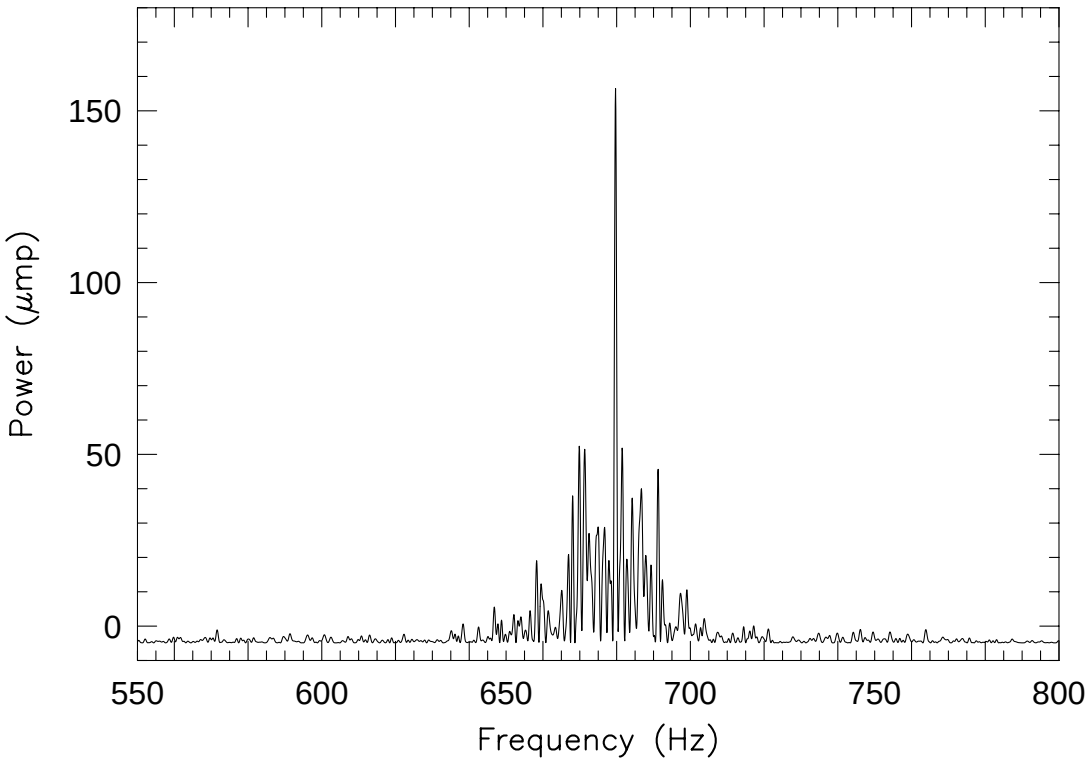

Figure 4.5: The FT of the entire WET observing run in the region of 1470 seconds.

state, by estimates of overall magnitude. In essence, we artificially chose and maintained a mean magnitude by including in the FT only light curves with the same mean magnitude.

4.3 The Fourier Transforms of PG1346

4.3.1 The Low State Power Spectrum

In 1988, PG1346+082 was the primary target of the two week long inaugural Whole Earth Telescope observing run, during which was obtained an unprecedented amount of nearly continuous low state data on the object. Unfortunately, the system did not remain in low state throughout the entire run, but rose to a magnitude of ≈ 15.4 several times (Figure 4.1), introducing gaps into the low state data record, and further complicating analysis of the FT.

If our previous conclusion that the 1470 second power represents a constant source seen against a varying background is valid, this low state data set offers the best possibility for the examination of the 1470 second power. Low state also offers the best chance to examine the mass accreting white dwarf.

The 1988 low state power spectrum is given in Figure 4.6. The 1470 second power is resolved into a band of peaks, with the dominant peak at 1471.305 ± 0.096 seconds, with an amplitude of 55.4 ± 0.6 mmis. The only other large amplitude power is at 735.554 ± 0.076 seconds with an amplitude of 19.1 ± 0.6 mmis, corresponding to the first harmonic of 1471.35 seconds, within 1 σ.

The continued presence of multiple peaks in Figure 4.6 is concern-

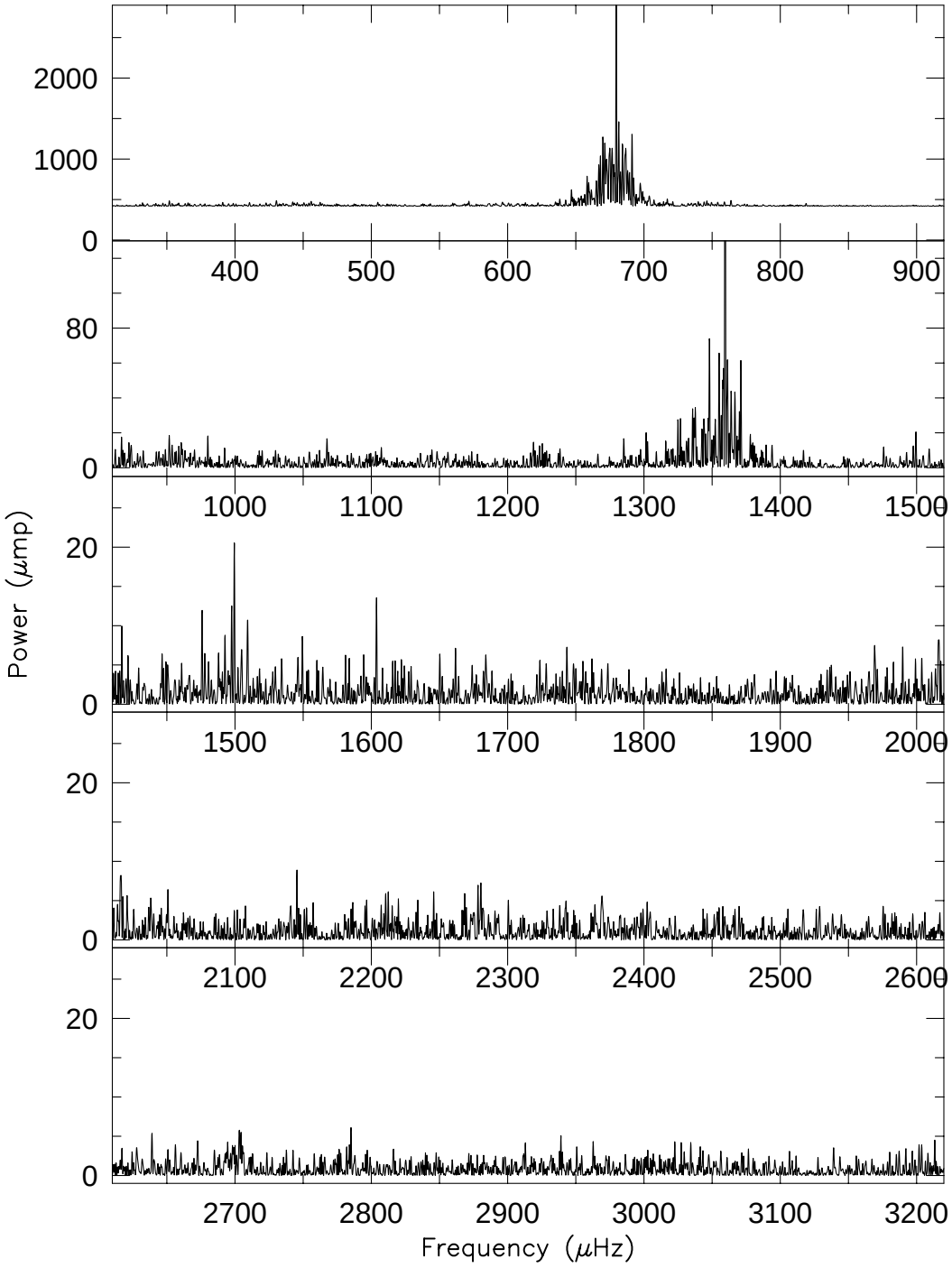

Figure 4.6: The low state power spectrum of PG1346 during the WET 1988 observing run.

ing. We are faced with three possibilities: the peaks may represent physical periodicities, we have not completely eliminated amplitude modulation, or our assumption of identical characteristics of the behaviour of different low states may be invalid. If the band of peaks is a manifestation of a continuing amplitude modulation, we can test this hypothesis by further subdividing the low state data into independent subsets and calculating an FT of each subset. A stable periodicity will appear with the same frequency and amplitude in each FT, while peaks due to quasiperiodic amplitude modulation will not, as each subset of the low state data samples the magnitude variations in a different manner.

To successfully separate possible amplitude modulation artifacts from actual power present in the system, we must also retain the ability to identify individual peaks in the FTs. The minimum timebase necessary to adequately resolve the FT of the 1470 second region requires approximately two thirds of the total time base of the low state data. We cannot just subdivide the low state data into completely independent portions to perform the necessary tests. As an alternative compromise, we calculated the FTs of the first two thirds, middle two thirds and last two thirds of the low state data (Figure 4.7). Although each FT contains data that is shared by the others, each also contains portions that are not included in the other two subsections. Artifacts should not appear in each FT, while coherent periodicities will be present with the same frequency and amplitude.

All three FTs in Figure 4.7 are consistent with the presence of multiple periodicities, but the FT of the first two thirds of the data contains a far larger number of peaks, demonstrating most of the additional power originates

in the first small portion of the data set not shared by the other two FTs. We re-examined this portion of the run and discovered it contained a significant fraction of data taken when PG1346+082 was at a magnitude slightly above minimum light, as the object was declining from a brighter phase at the beginning of the WET run.

The FT of the low state data, excluding the portion of the light curve we found to be producing artifacts, (Figure 4.8) confirms the continual presence of two frequencies at $679.67 \mu Hz$ (1471.3037 ± 0.0096) seconds at an amplitude of 55.43 ± 0.58 mmi and $669.89 \mu Hz$ (1492.7881 ± 0.0182) seconds at an amplitude of 31.92 ± 0.62 mmi.

The only other region of the low state FT containing significant power surrounds $1359 \mu Hz$ (Figure 4.9). The period of the dominant peak is 735.5541 ± 0.0076 seconds, corresponding to the first harmonic of 1471.3 seconds. The structure surrounding the 735.6 second peak is consistent with a single periodicity. Every additional feature can be accounted for as a window artifact, created by gaps in the data record. The FTs of each two thirds of the data (Fig 4.10) are also consistent with the presence of a single peak at 735.60 ± 0.03 seconds.

If the 1492.8 second periodicity produces a harmonic, or if additional, independent variations are present in this region of the low state FT, the amplitudes are low. As a final search for low amplitude power hidden among the 735.6 second window structure, we removed a sine curve with a period of 735.6 seconds from the 1988 low state data (Figure 4.11). No additional power is detected to a limit of approximately 2 mmi. The 1492.8 second periodicity

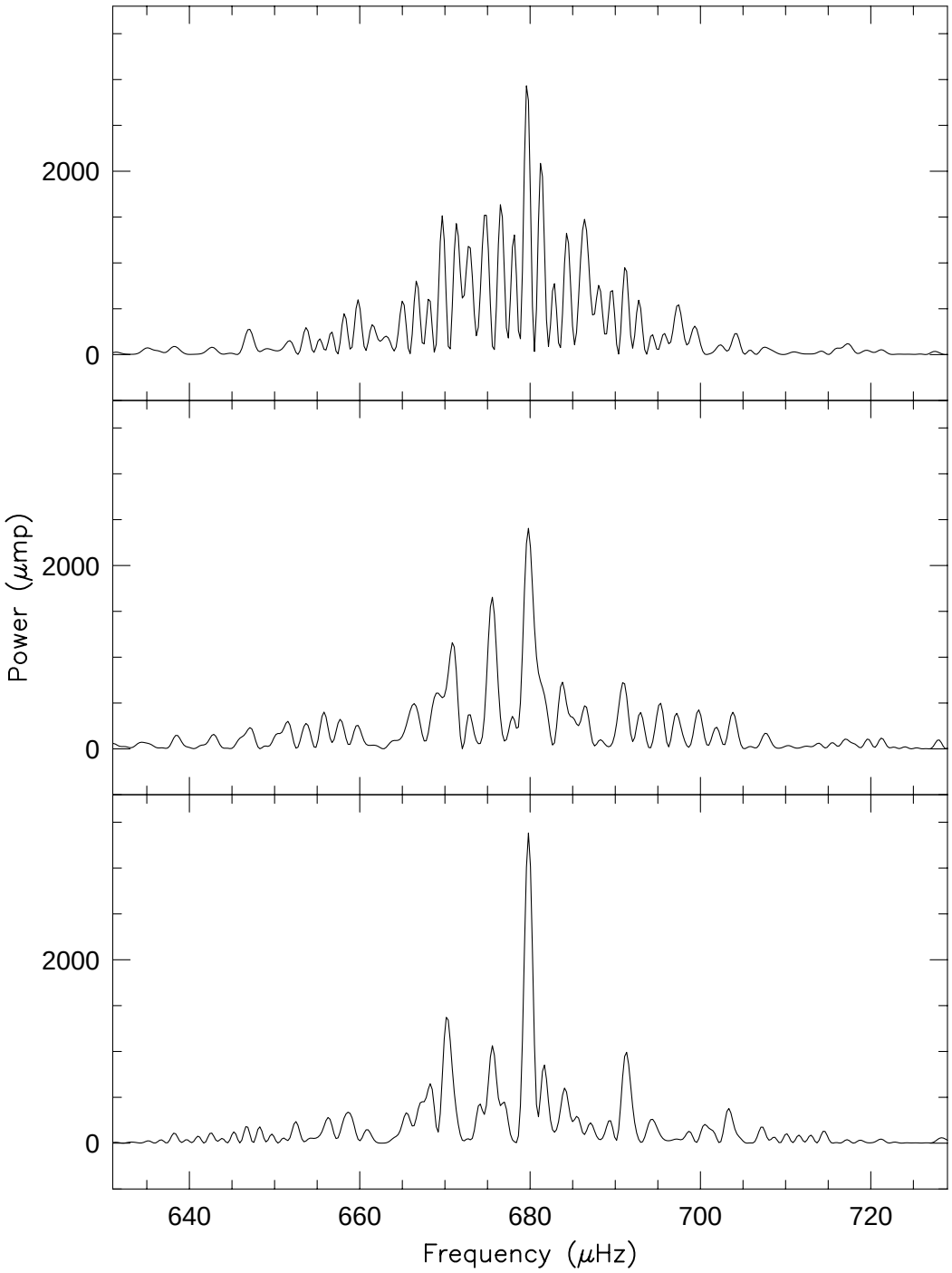

Figure 4.7: The FTs of the first two thirds, middle two thirds and last two thirds of the low state data set of PG136+082.

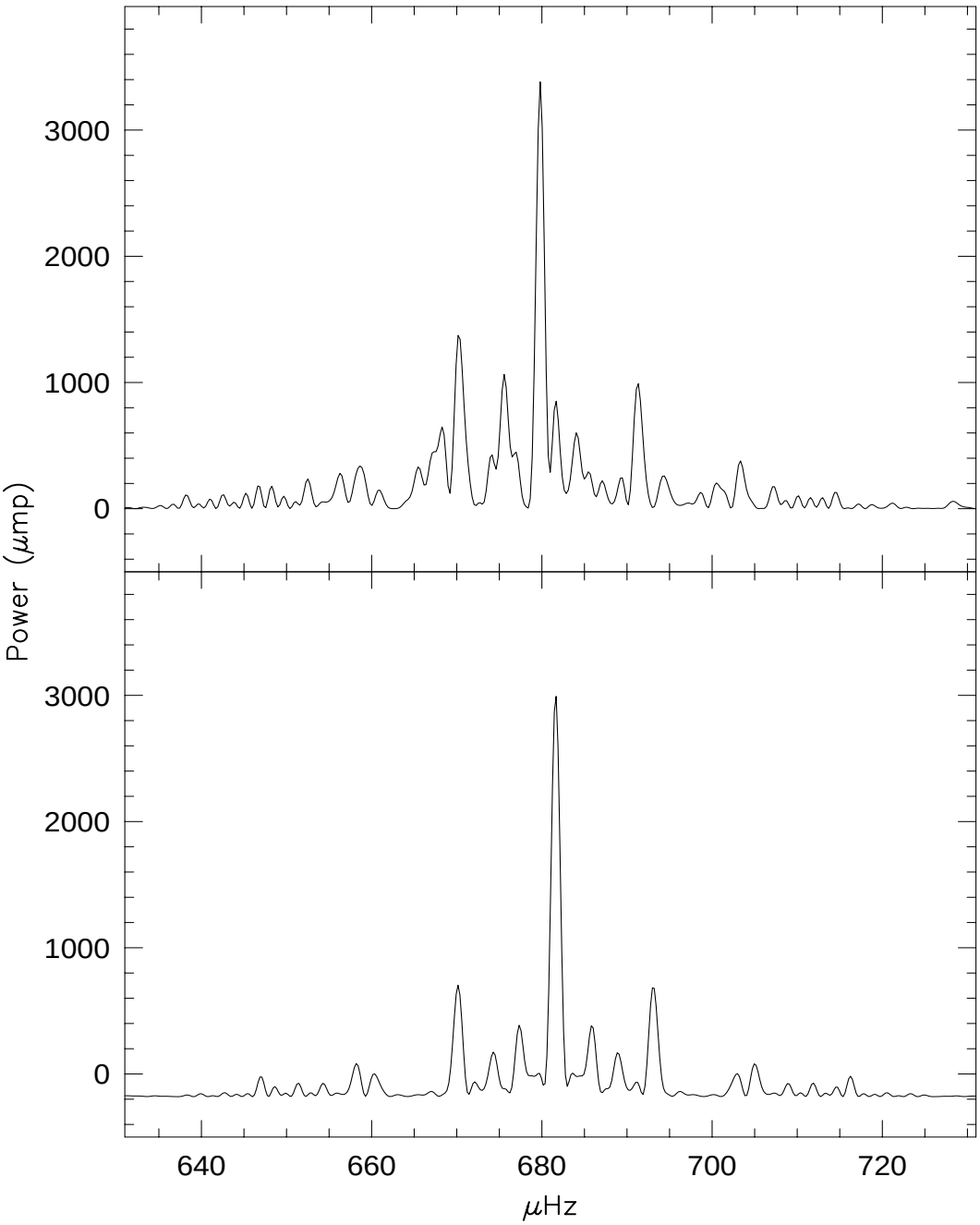

Figure 4.8: The Fourier transform of the low state data excluding the portion of the light curve creating amplitude modulation artifacts. The FT is consistent with the presence of two frequencies, at 1471.3 and 1493.0 seconds. The spectral window is displayed in the lower panel.

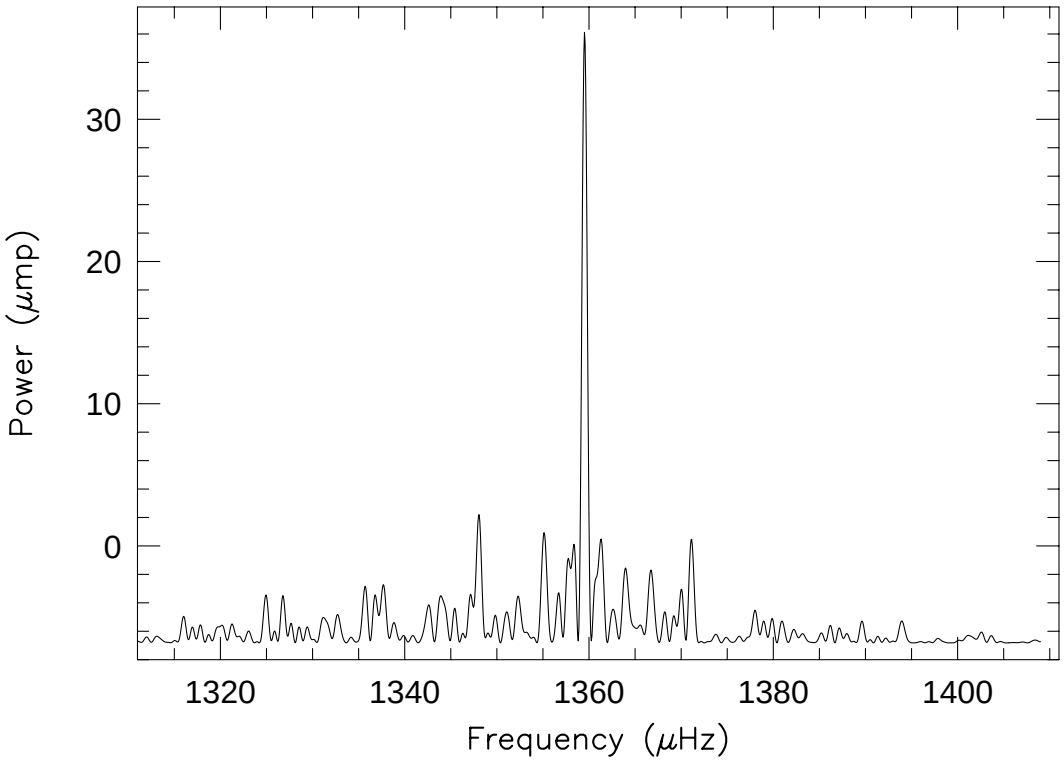

Figure 4.9: FT of the low state data in the region of 735.6 seconds, excluding the portion of the light curve found to be producing amplitude modulations.

does not produce a detectable coherent harmonic, indicating that the average variation is nearly sinusoidal.

In 1984, PG1346 was observed in low state on three nonconsecutive nights. While this is not a sufficient timebase to obtain a completely resolved FT in the 1470 second region, or for a detailed analysis, we can determine some general characteristics of the light curve. Our most surprising result is the change in the relative intensities of the 1471 second power and its first

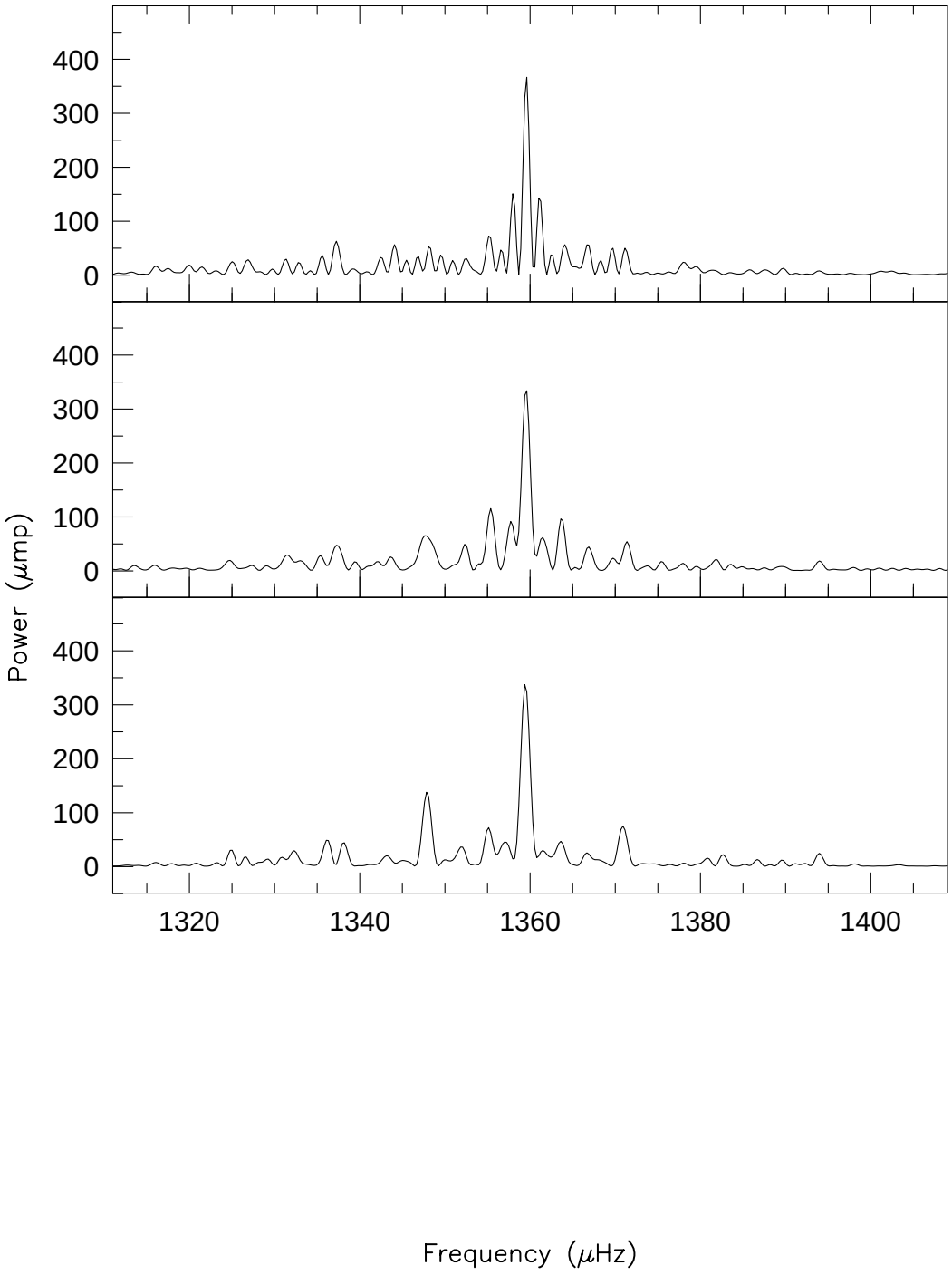

Figure 4.10: FTs of each two thirds of low state data in the region of 735 seconds. Each panel is consistent with the presence of a single peak (Compare to spectral windows given in Figures 4.8 and 4.9).

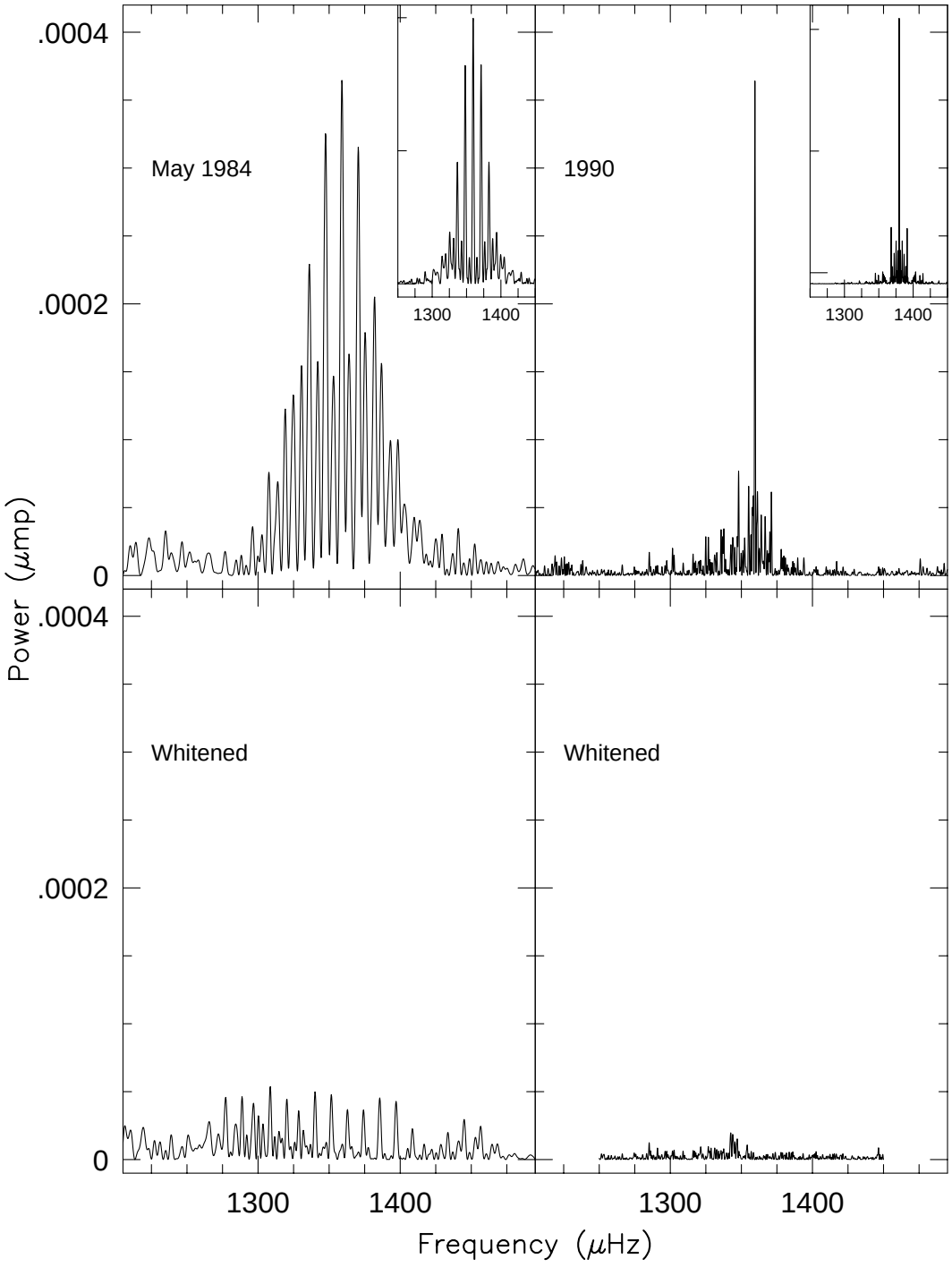

Figure 4.11: Low state data of PG1346+082 whitened by 735.6 seconds.

harmonic (Figure 4.12). During 1988, the harmonic consistently maintained an fractional intensity of $\approx$ 19 mmis, significantly lower than the fundamental at $\approx$ 55 mmis. In the 1984 data set, the 735 second peak has an fractional intensity of $\approx$ 26 mmis, but the 1470 second power has an fractional intensity only $\approx$ 16 mmi. Such change in relative intensities could be produced by a convolution of sampling characteristics and beating between two closely spaced periodicities such as the 1471.3 and 1492.8 second peaks detected in the 1988 low state data set. If the beat cycle between the two is not adequately sampled, it is possible to observe the object while both frequencies are out of phase with each other, resulting in an artificially low observed fractional intensity. However, this can not be the case in this instance. The beat frequency between 1471.3 and 1492.8 seconds is 9.79×10^{-6} s^{-1}, corresponding to 1.18 days. The 1984 data, while it consists of only three runs, spans four days, over three times the beat period. The change in relative intensities can not be the result of insufficient sampling of the beat between the 1471.3 and 1493.0 second peaks.

While we cannot resolve the FT of the 1470 second region, the 1984 data set is long enough to resolve the first harmonic. The power at 735 seconds is consistent with the presence of a single, isolated peak with a period of 735.949 ± 0.04 seconds, 10σ from the period of 735.554 ± 0.008 seconds measured in 1988.

4.3.2 The Presence of Additional Power

The temperature of PG1346+082 hovers at $\approx$ 20000 K. At these temperatures, helium partial ionization provides an efficient mechanism for the

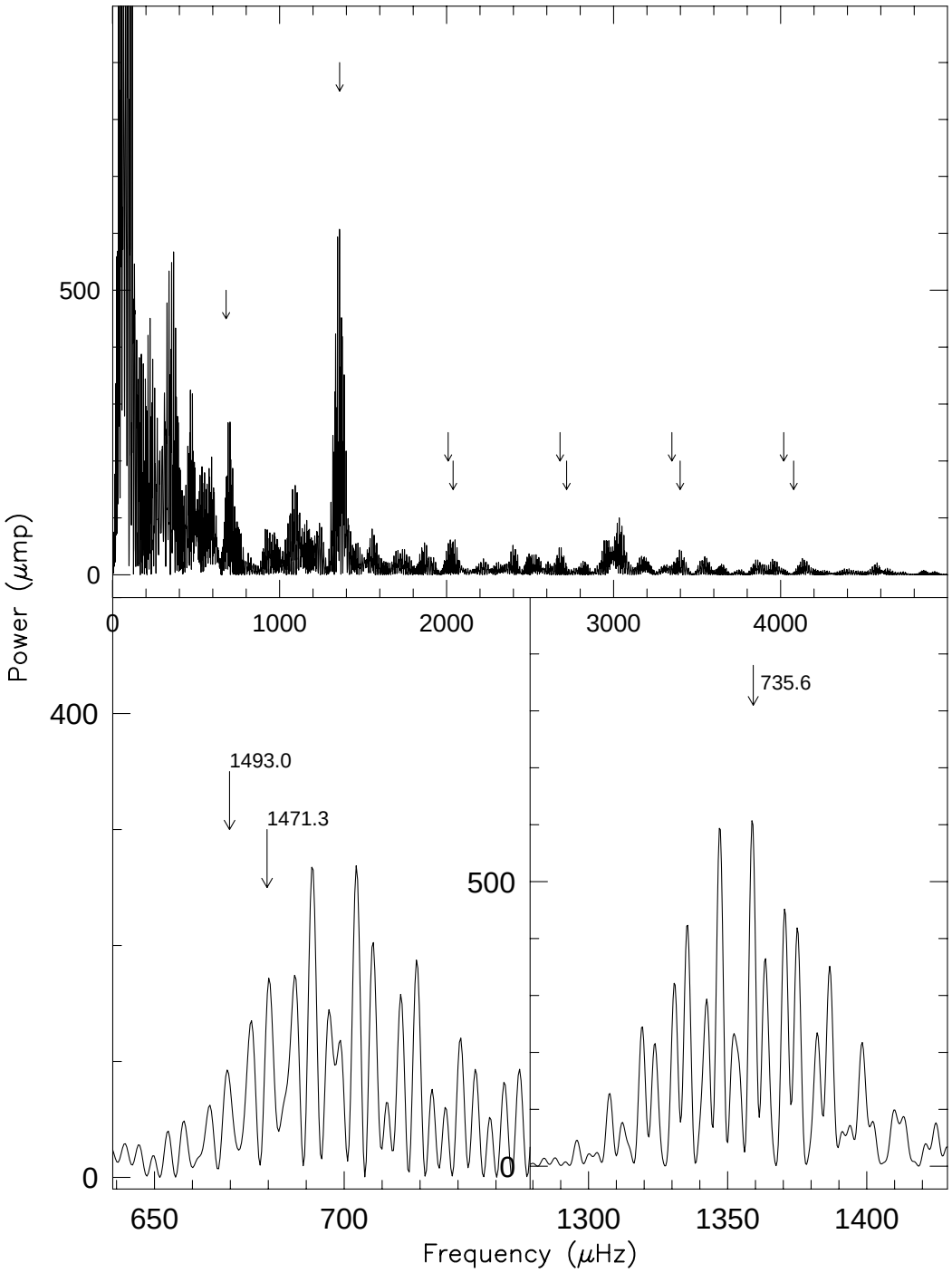

Figure 4.12: FT of the 1984 low state data. In the first panel, the lower arrows mark the location of the 1471.3 second period and its possible harmonics. The upper arrows are the location of possible 1493.0 second harmonics.

driving of pulsations. If stable pulsations arise on the mass accreting white dwarf or in the disk, they would produce additional power in the FT that could not be explained in terms of rotation or orbital motion. The low state data offers the only reasonable possibility of detecting any low amplitude oscillations.

Figure 4.6 displays a myriad of small peaks with amplitudes greater than the noise level of the Fourier transform. We can apply the same techniques we used in weeding out amplitude modulation artifacts to identify small amplitude stable periodicities. We divided the 1988 low state data into halves and compared the peaks present in each FT. No clear example of stable peaks exists in Figure 4.13 (the arrows mark positions of harmonics of 1471.3 seconds). The features at $\approx 1500 \mu Hz$ and $\approx 1605 \mu Hz$ are window artifacts from the 735.6 second peak. Suspicious, but not compelling, peaks to be investigated further are at $\approx 2783 and 3690\ \mu Hz$. However, our noise limit is only ≈ 2 mmi. Observations of PG1346+082 in low state with a large telescope such as the CFHT would greatly assist in the identification of additional power.

There are no clear examples of stable, low amplitude periodicities in PG1346+082's low state FT. We must, however, recall that PG1346+082 is an interacting binary and the best model for this object contains an accretion disk which may give rise to quasiperiodic variations with coherency times considerably shorter than the time base of the data set. Such a variation would not appear as a single, stable peak in an FT of the entire data set. Indeed, no power at all would be present if the run length is very much longer than the coherency time. If we sampled the data on a shorter timescale closer to the coherency times of the quasi-periodic variations, we would detect significant

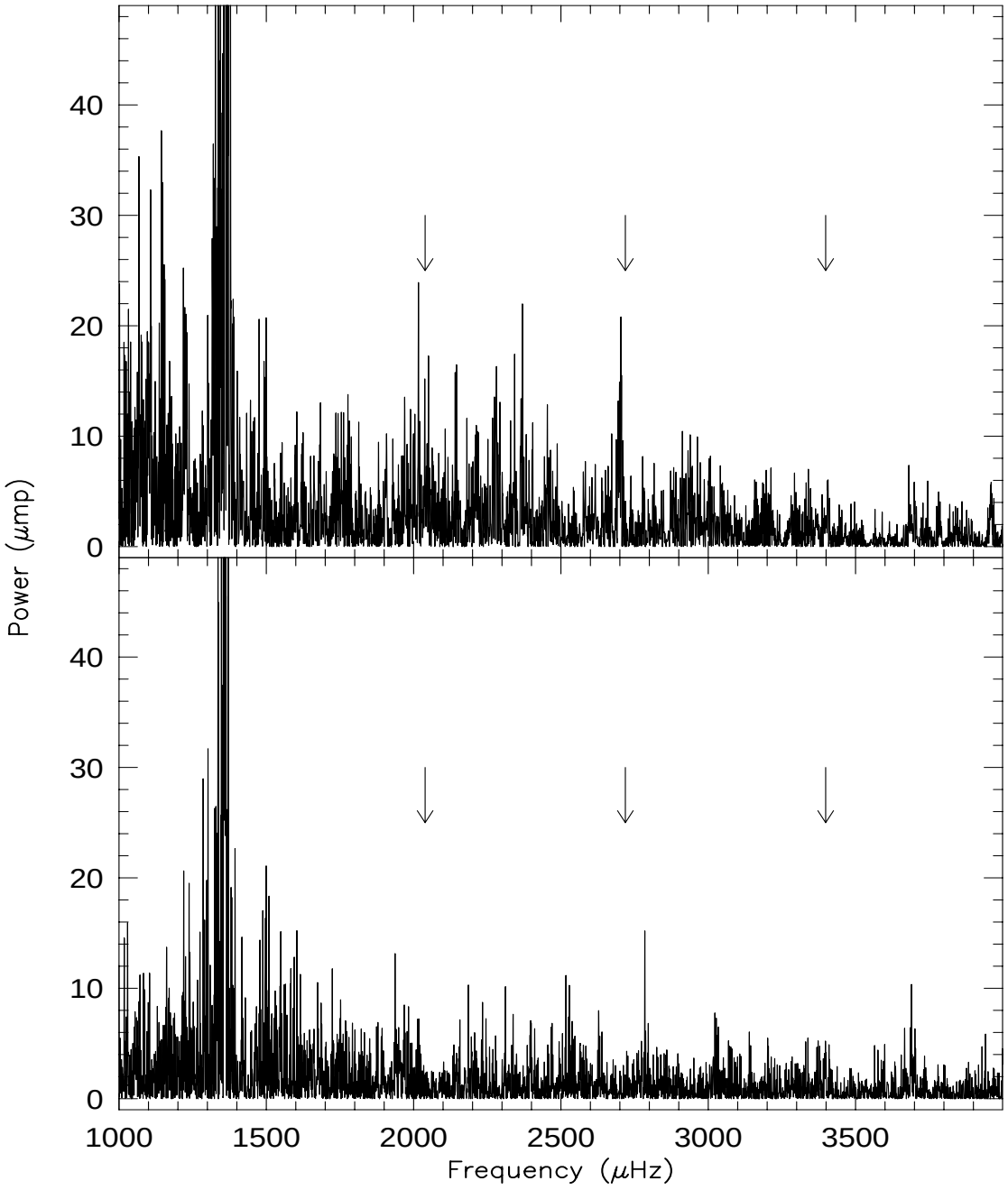

Figure 4.13: FTs of the two halves of the low state data of PG1346+082. The arrows indicate the locations of possible harmonics of 1471.3 seconds.

power, but the power would not repeat in the next observations. Power present in FTs of PG1346+082 on individual nights does change (Fig 4.14), suggesting that quasiperiodic variations are important in the context of PG1346+082. At present, we have no method to conclusively determine the origin of the changing power.

A signature of non-radial pulsations is the presence of a series of peaks equally split in frequency. We employed our template method (see Chapter 2) to search for equal frequency differences among the low amplitude peaks in Figure 4.6. The arrows mark the size of the one sigma deviations. No equal frequency splitting is observed in the FT of PG1346+082's low state light curve.

4.4 The High State Spectrum

The short timescale variations of PG1346+082 change as the magnitude of the system fluctuates. To better understand the physical process behind this observation and to explore the outburst mechanism, our next step is to examine the behaviour of PG1346 at high state and compare with the low state observations. We do not have the extensive coverage of PG1346+082 in high state enjoyed for the low state analysis, complicating our task by introducing more intricate alias structure. It will be difficult to disentangle the webs of aliases created by closely spaced periodicities, such as 1471.3 seconds and 1492.8 seconds identified in the low state 1988 data set.

In high state (Fig 4.16), the FT of PG1346+082's light curve is dominated by an unresolved band of power at $674\mu Hz$ and a series of harmonics not detected in the low state FT. The dominant power is similar to that observed

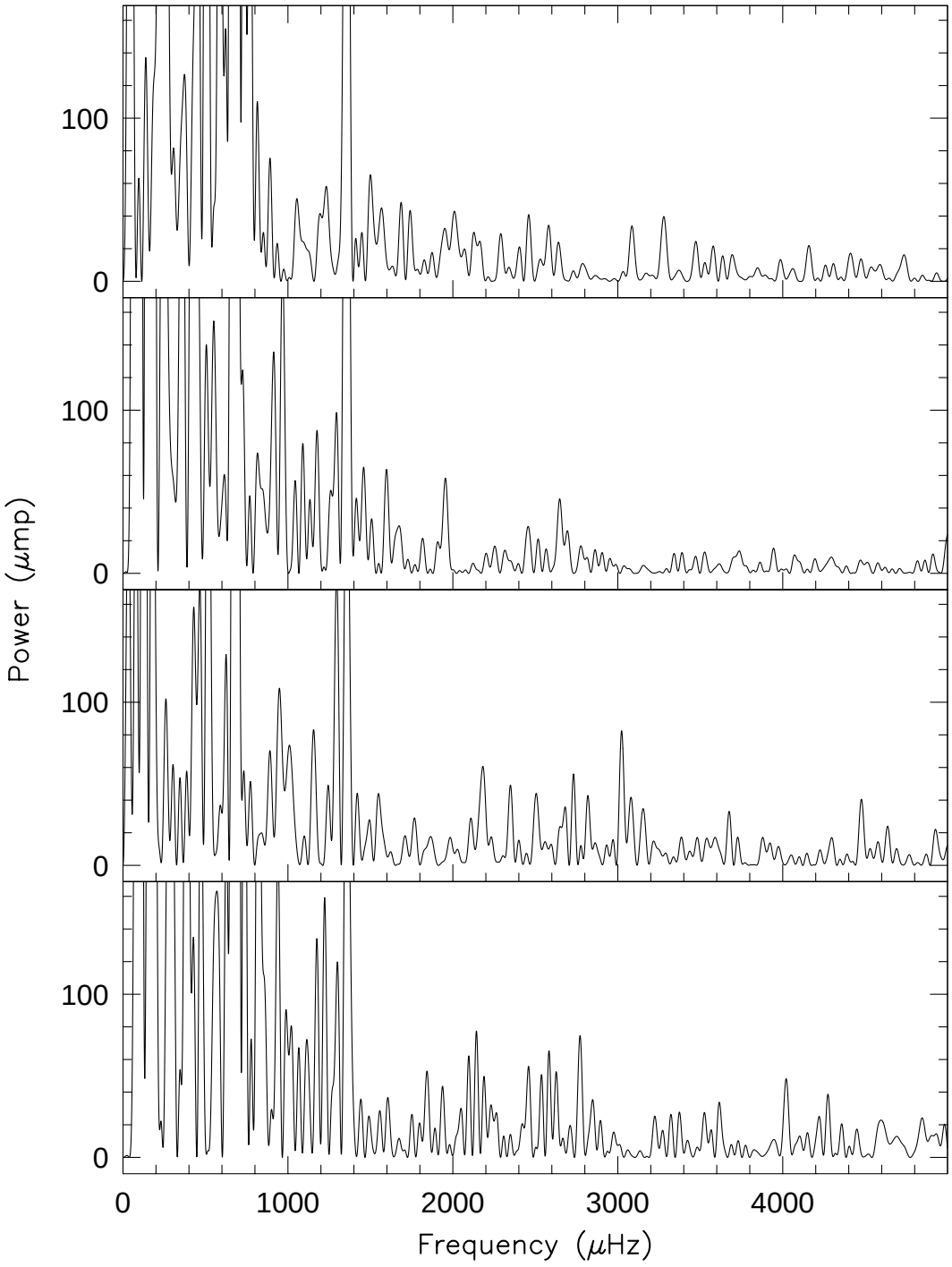

Figure 4.14: FTs of 4 consecutive nights of data of PG1346+082. Each run is of similar length, and taken with the same telescope and photometer.

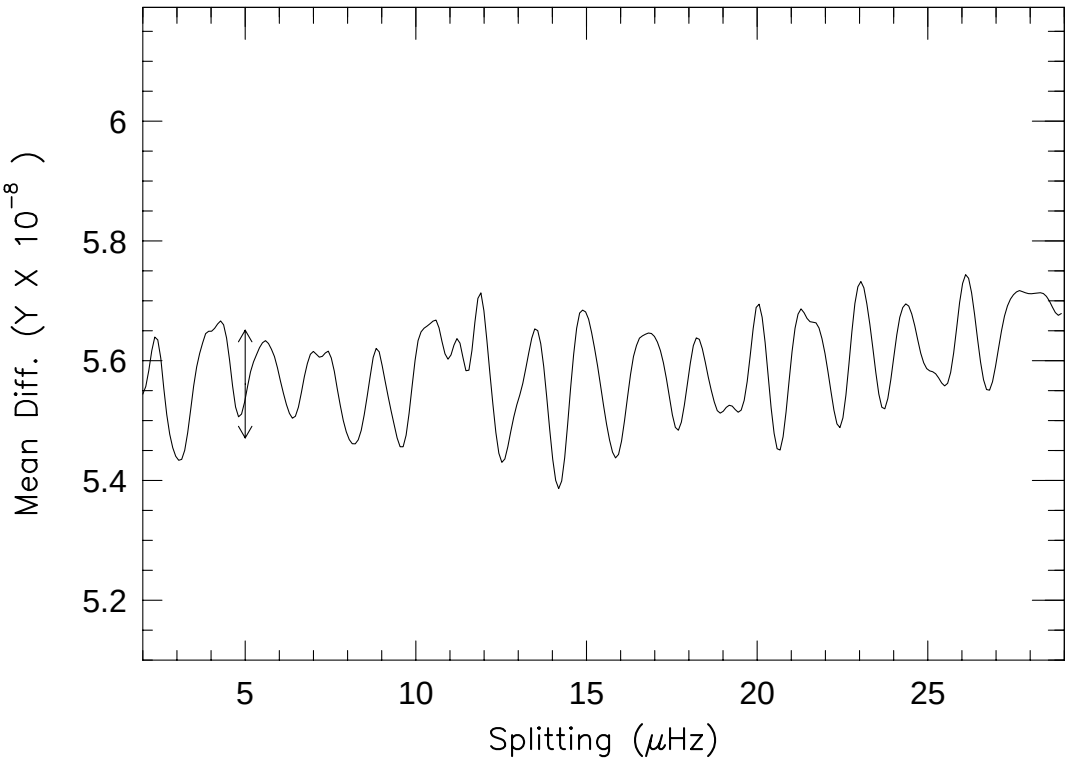

Figure 4.15: A search for equal frequency splittings in PG1346+082. Nothing significant is present in the FT.

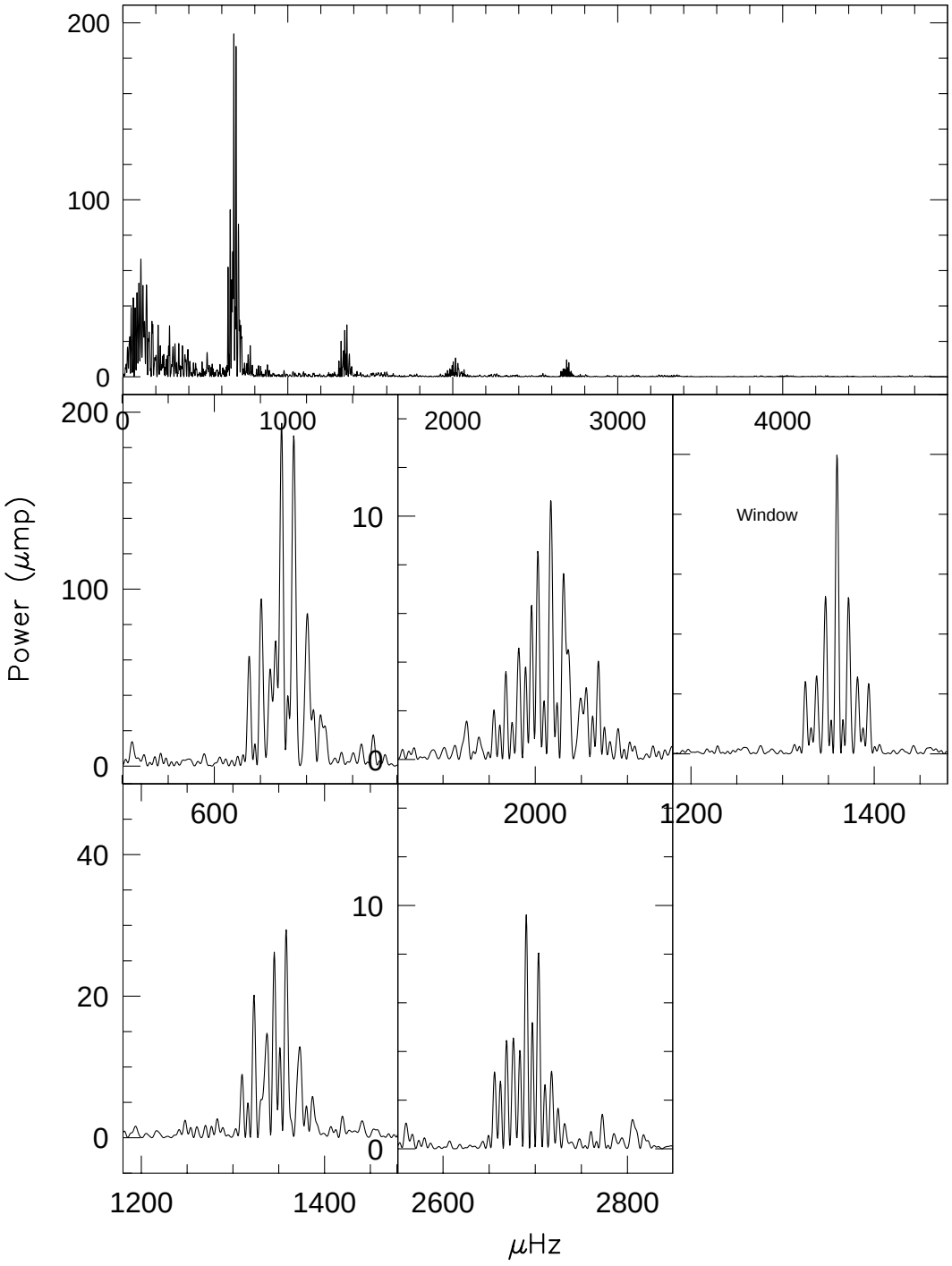

Figure 4.16: The Fourier spectrum of PG1346 during high state in 1988. The first panel contains the entire FT, the other panels are close ups of the regions of significant power. The arrows point to the location of the 1471.3 second peak and its harmonics. The panel on the right is the spectral window.

in the low state FT, but is not composed of identical frequencies (Figure 4.17). There are two large peaks, at $672.99\mu Hz$ (1485.89 ± 0.14 s) with a fractional intensity of 13.80 ± 0.34 mmis, and its one day alias at $685.99\mu Hz$ (1457.47 ± 0.14 s) at 13.70 ± 0.35 mmis. The low state power at $679.67\mu Hz$ (1471 s) is no longer the dominant frequency, although it may be present at low amplitude and blended with the unresolved peak at 1457.35 seconds. The 1485.89 second peak is also unresolved, perhaps blended with the 1492.8 second peak detected in the low state FT.

The complex series of harmonics we observe in the high state FT are a window into the physical processes occurring in PG1346+082 during outburst. If the harmonics result from pulse shape distortions, any model of the outburst mechanism must be able to reproduce this harmonics. If we assume that they are pulse shape distortions, we can use the harmonics to help identify the frequencies composing the unresolved 1480 second region of power.

The largest peak in the region of the first harmonic is $1358.07\mu Hz$ (736.34 ± 0.09 s), 7 sigma from the first harmonic of 1471.305 seconds. The second largest peak, at $1345.13\mu Hz$ (743.42 ± 0.10 s), is the possible harmonic of 1485.89 seconds. These two peaks are nearly one day aliases, therefore we cannot choose which contains the actual power, or if both do. The harmonic of 1457.35 seconds may also present, at $1373.01\mu Hz$ (728.327 ± 0.139 s).

The largest peaks in the region of the second, third and fourth harmonics are $2016.94\mu Hz$ (495.80 ± 0.071 s), $2690.05\mu Hz$ (371.714 ± 0.042 s) $3359.88\mu Hz$ (297.63 s), corresponding to the harmonics of ≈ 1486 s, not 1471.3 or 1492.8 s.

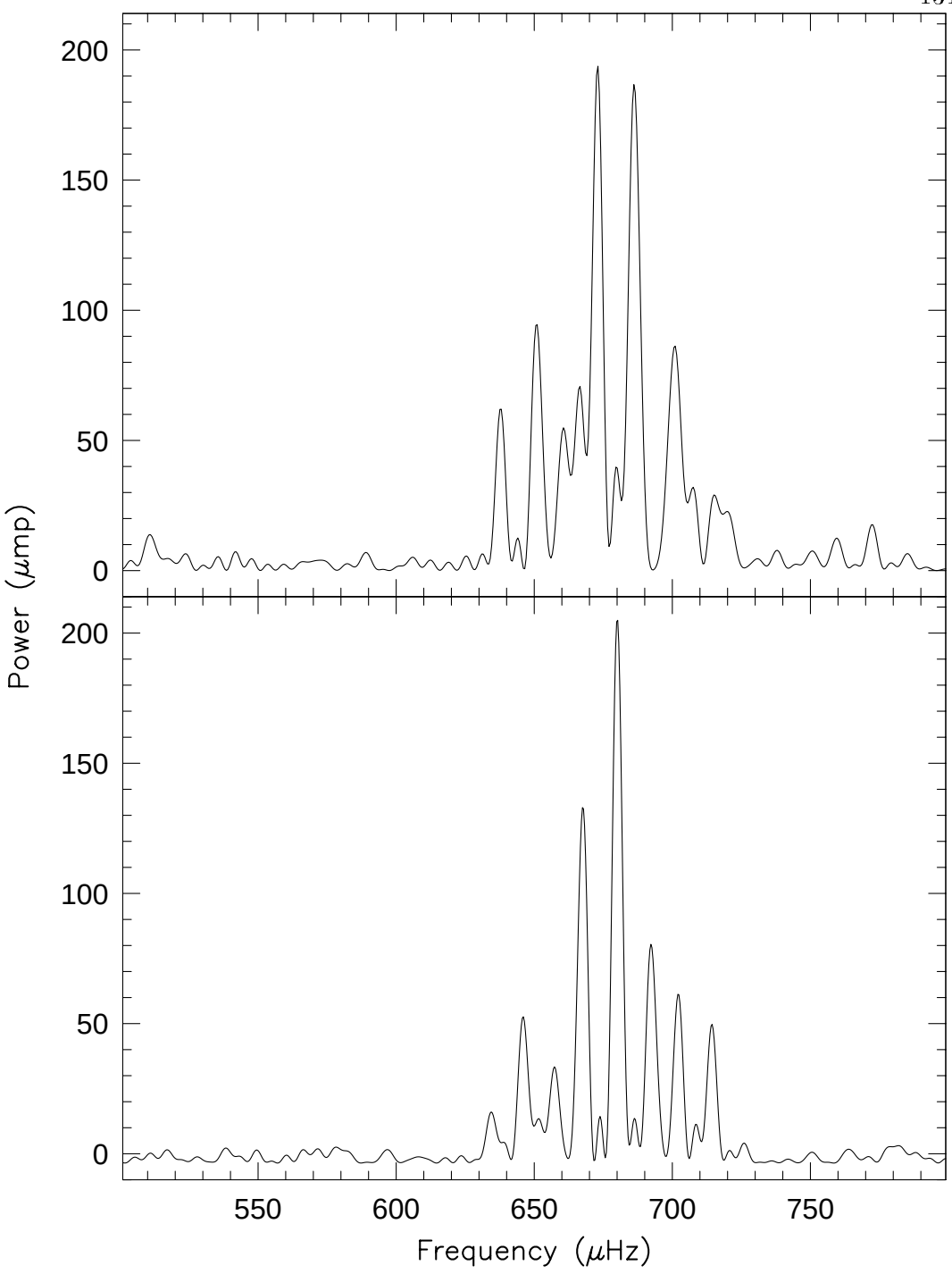

Figure 4.17: The 1988 high state FT and a simulation of the 1471.3 and 1493.0 second periods maintained the same frequency in hi state.

Table 4.4: Harmonics in PG1346+082 High State Data

Year	Harmonic Period	Fundamental
1988	736.34 ± 0.09	1472.68
	743.42 ± 0.10	1486.84
	728.36 ± 0.14	1456.72
	495.81 ± 0.07	1487.43
	371.71 ± 0.04	1486.86
	297.63 ± 0.08	1488.14
1985	741.07 ± 0.03	
	739.77 ± 0.03	
	746.09 ± 0.03	1492.18
	747.40 ± 0.03	1494.80
	734.86 ± 0.03	1469.72
	733.68 ± 0.04	
	499.80 ± 0.04	1499.4
	499.15 ± 0.04	1497.45
	496.968 ± 0.03	1490.9
	374.62 ± 0.04	1498.5
	373.03 ± 0.02	1492.12

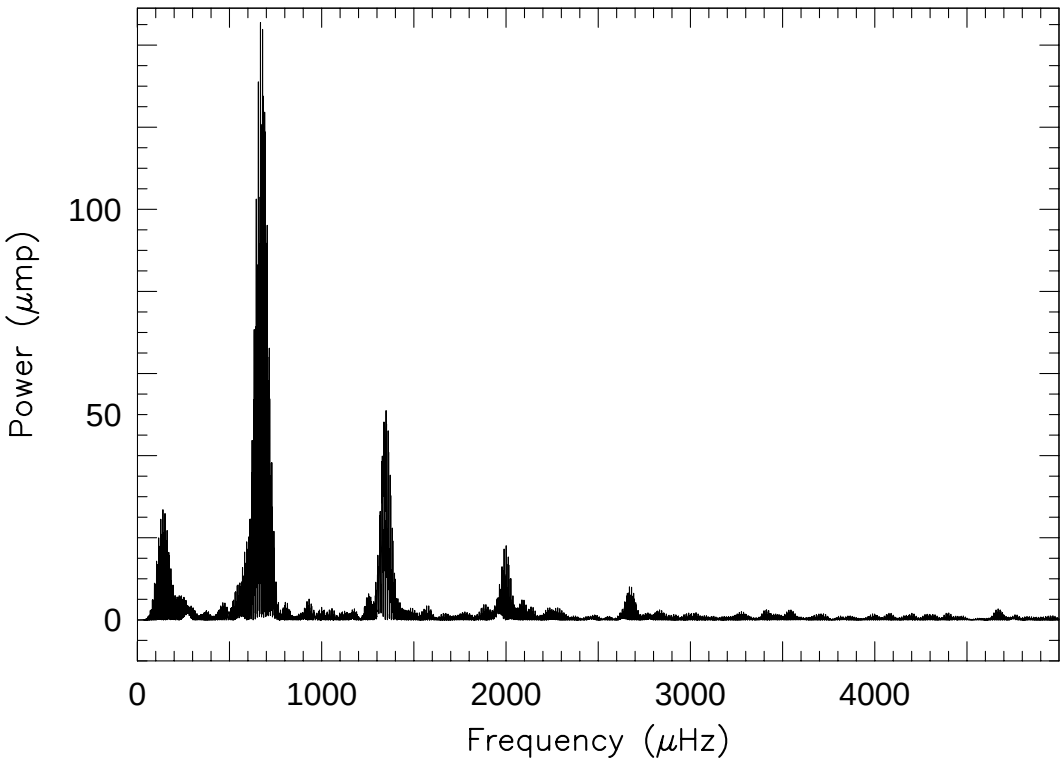

Figure 4.18: 1985 high state FT of PG1346+082

We have a small amount of high state data obtained in 1985 (Fig 4.18), in which we can examine the harmonic frequencies . Again, the harmonics in this data set are not consistent with a fundamental period of either 1471.305 seconds or 1492.8 seconds.

We demonstrated previously that the band of power at 1470 seconds varies in fractional intensity as a function of the magnitude of the entire system. We can now also conclude that the composition of the dominant band, including the harmonic structure, also shifts between hi state and low state.

4.5 Phase Stability of the 1471.3 Second Peak

One of our main objectives in our study of PG1346+082 is the identification of any stable variations, leading to the discovery of the orbital or rotational periods of the system. We expect periodicities arising from orbital or rotational motion to maintain predictable frequency and phase. Before we proceed, we must reexamine what the term "stable" entails in the context of PG1346+082. In Chapter 3, we defined several strict criteria that must be met before a peak present in an FT can be rigorously examined for phase stability. The peak must maintain a stable amplitude and frequency in every adequately resolved FT, to eliminate the possibility of beating between peaks closely spaced in frequency. Attempting to determine the phase stability of unresolved closely spaced variations will result in the detection of phase changes that have no physical origin within the object. Also, the frequency of the peak of interest must be determined accurately enough to avoid cycle count errors over gaps in the data. Period error is cumulative over the data gaps, so our usual criteria is to allow the accumulation of only one tenth of a cycle of possible uncertainty.

Because the frequency and amplitude of the band of power at 1470 seconds in PG1346+082 changes between low and high state, we cannot identify a single peak that maintains the same frequency and amplitude at all times, violating our criteria for examination of phase stability. Does this mean there is no stable periodicity in PG1346+082? The answer is no. In PG1346+082, the situation is exactly opposite of what we normally encounter in our studies of pulsating white dwarfs. Here, the variation appears to maintain a constant amplitude, while the background light changes. In many ways, it is our method

of measuring fractional intensity relative to an assumed constant mean magnitude that is responsible for the changes in amplitude of the 1471.3 second peak. Also, we do not understand the mechanism responsible for the frequency changes in the 1470 second power. It is possible that the power at present during high state is of a different physical origin than the power present at low state.

The question we must consider is not the continuous presence of a stable periodicity, but whether there exists an underlying stable clock within the system, hidden beneath the outbursts. Our best hope of identifying such a clock in PG1346+082 lies with the WET low state data set. The WET low state FT is consistent with the presence of two periodicities, at 1493.0 and 1471.3 seconds, plus the first harmonic of 1471.3 seconds. The 1471.3 second period is the dominant frequency, so we will begin by examining the stability of this period.

A standard O-C diagram (see Chapter 3 for details of the process) is impossible to calculate for the 1471.3 second period in PG1346+082. We require at least 1.2 days of continuous low state data to adequately resolve the 1471 and 1493 second periods, forcing us to split the low state data set into small chunks to obtain accurate timings. Subdividing the data set further complicates the alias structure associated with each frequency, increasing the timebase required to resolve overlapping alias patterns. The best compromise forces us to calculate timings for the first two thirds, second two thirds and third two thirds of the data, as we did when searching for amplitude modulation artifacts (Table 4.5).

Table 4.5: 1471.35 sec Period

Data Section	T(zero)	T-T(zero)	E	O-C
A	335669	-3.0	-2.0×10^{-3}	-3±9
B	774224	438552	298.06	90±9
C	774214	483542	298.05	80±9

Despite the limitations of a detailed O-C analysis, we can test the general phase stability of the 1471.3 second period by simply employing non-linear least squares techniques to obtain a best fit sinusoid for that period, and plotting this sinusoid over the light curve (Figure 4.19). The figure displays the identical fit plotted over the beginning and the end of the low state data set. The 1471.3 second variation is indeed coherent over the two week time span of the 1988 low state data set.

The frequency changes observed from high state to low state demonstrate that strict phase coherence is not maintained between states. The 1988 low state data set is not a continuous low state observation, but was interrupted by several excursion by PG1346+082 to a higher magnitude, after which the object returned to low state. After every outburst, the dominant 1471.3 second variation returned with its original phase.

The 735.6 second peak maintains a constant frequency and intensity in all low state FTs. If this harmonic is a result of a nonsinusoidal 1471 second pulse shape, its stable frequency and intensity demonstrates that the 1471 second pulse shape is stable. We can measure the harmonic's phase and extend that knowledge to reveal much about the phase of the fundamental 1471.3 second period. The O-C diagram of the 735.6 second period during 1988 is

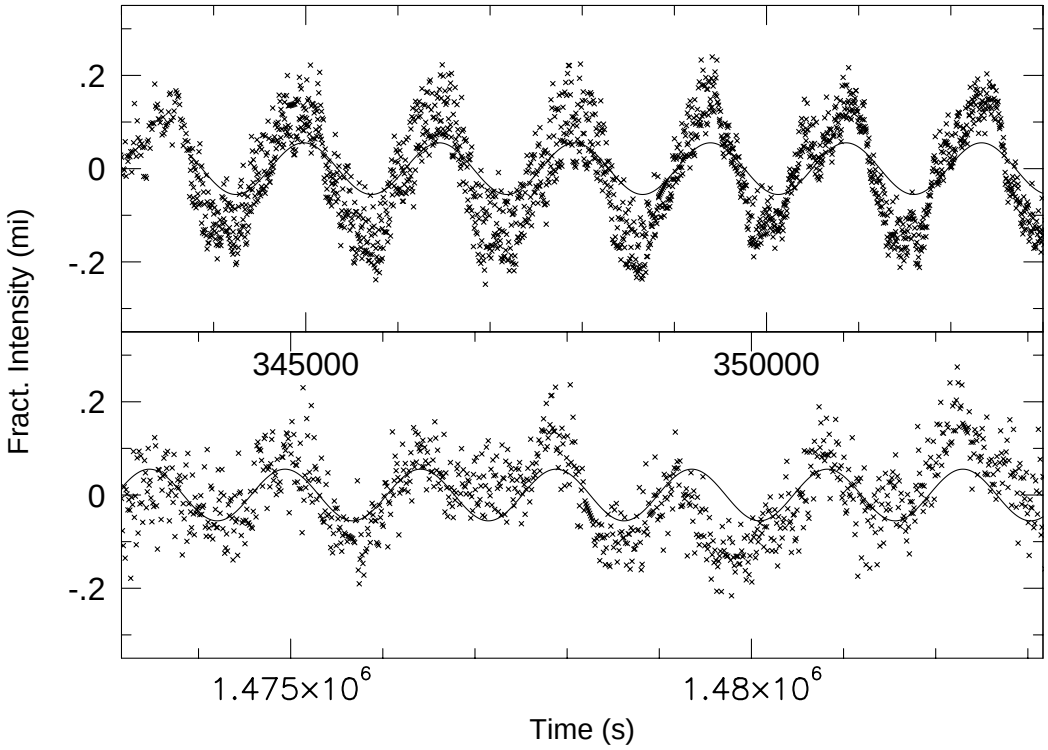

Figure 4.19: Phase of the 1471.35 second periodicity near the beginning and end of the 1988 WET run

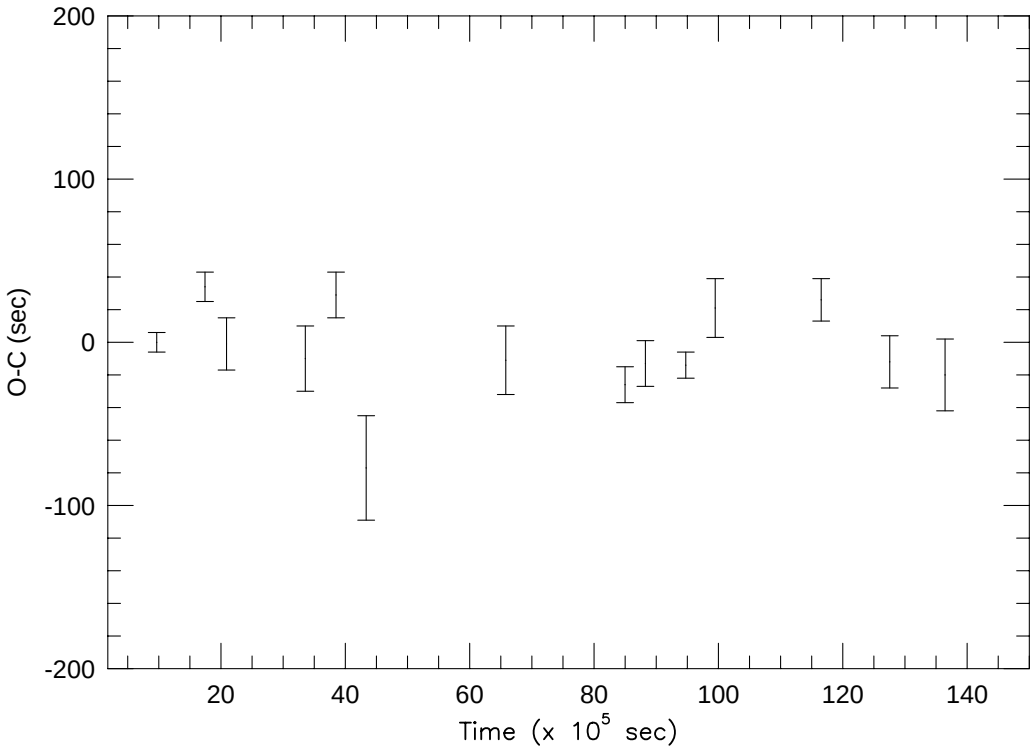

Figure 4.20: O-C diagram of 735 seconds during 1988 WET run

given in Figure 4.20. Throughout the 1988 WET low state data set, the 735.6 second period maintained a constant phase, further confirming the stability of 1471.3 second fundamental over the two week time span of the 1988 WET run.

4.6 Pulse Shapes and PG1346+082

The pulse shape (see Chapter 3 for details on the technique), provides an additional method to aid in the examination of the nature of the luminosity variations of PG1346+082. The average pulse shape of the 1471.3 second periodicity in PG1346+082 is given in Figure 4.21. The pulse shape is non-sinusoidal, with nearly flat bottoms between pulses. This pulse shape differs

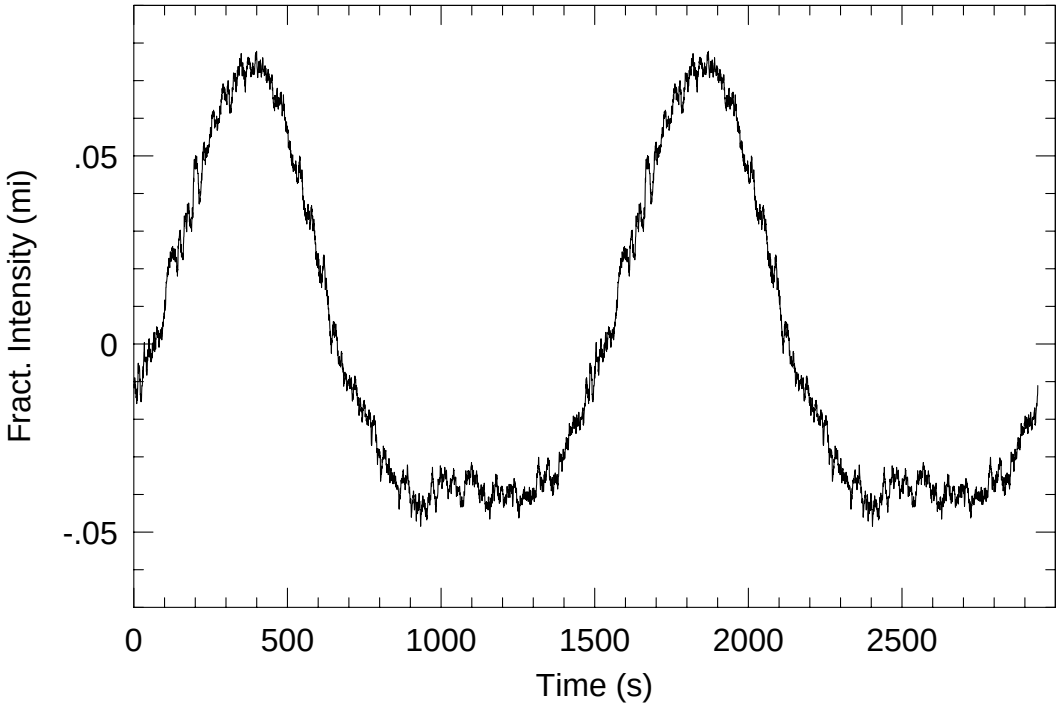

Figure 4.21: Low state pulse shape for P=1471.305 seconds

from that observed in AM CVn (Figure 3.8), as well as that of the DB pulsator GD358 (Figure 3.20). Clemens (1993) reports finding pulse shapes similar to the 1471.3 second pulse shape in some white dwarf pulsators, however. The 1471.3 second pulse is certainly not a pulse shape of an eclipse (see Zhang, 1986 for examples), but is more reminiscent of a bright region coming into view and then leaving view. If we assume the flat regions are times when the bright area is not visible, the bright region is visible for ≈ 0.70 of a cycle.

In earlier arguments, we assumed that the 735.6 second peak is a pulse shape harmonic of 1471.3 seconds, and not an independent variation in its own right. To justify this assumption, we examined the possibility of the 1471 second pulse shape giving rise to the harmonic at 735.5 seconds. We

subtracted a sinusoid from the 1471 second pulse shape to examine the residuals (Fig 4.22). The 735.6 second variation aligns with the maxima and minima of the 1471.3 second pulse shape. This is strong evidence that the 735.6 second variation is not a truly independent variation in its own right.

The average pulse shape of the 1492.79 second periodicity is given in Figure 4.24. As expected, this pulse shape is nearly sinusoidal, explaining the absence of harmonics of the 1492.79 second period.

4.7 The Physical Nature of PG1346+082

We have completed an exhaustive examination of PG1346+082's photometric behaviour. Our next step is to consider how our observations help to identify a unique model for the object. We will begin by reiterating the specific constraints our findings have on any model of PG1346+082. The object undergoes a 3-4 magnitude outburst on a timescale of a few days. The short timescale variations are consistent, in low state, with two periodicities, 1471.3 seconds and 1492.8 seconds, whose fractional intensities are inversely dependent on the overall brightness of the system. The change in fractional intensities observed is just that expected from a constant source seen against a variable background. The frequencies observed in the FT of PG1346+082's light curve in bright state are not consistent with periods of either 1471.3 or 1492.8 seconds, but both frequencies return when the system dims. The 1471.3 second variation returns with its original phase. The pulse shape of the dominant variation is clearly not that of an eclipse, but is more reminiscent of a bright region coming into and out of view. Any model we discuss must also consider the temperature of

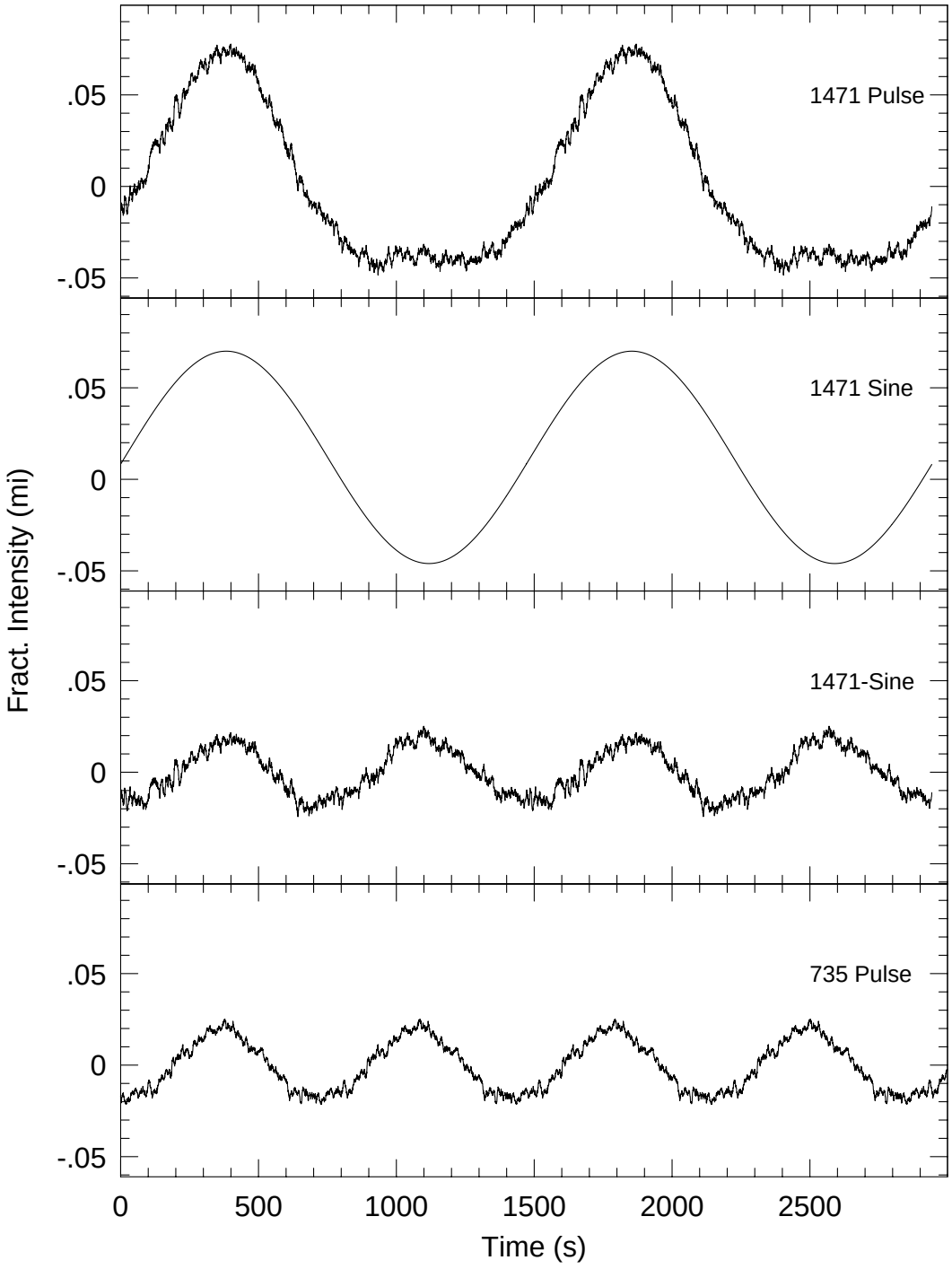

Figure 4.22: 1471 second pulse shape minus a sinusoid

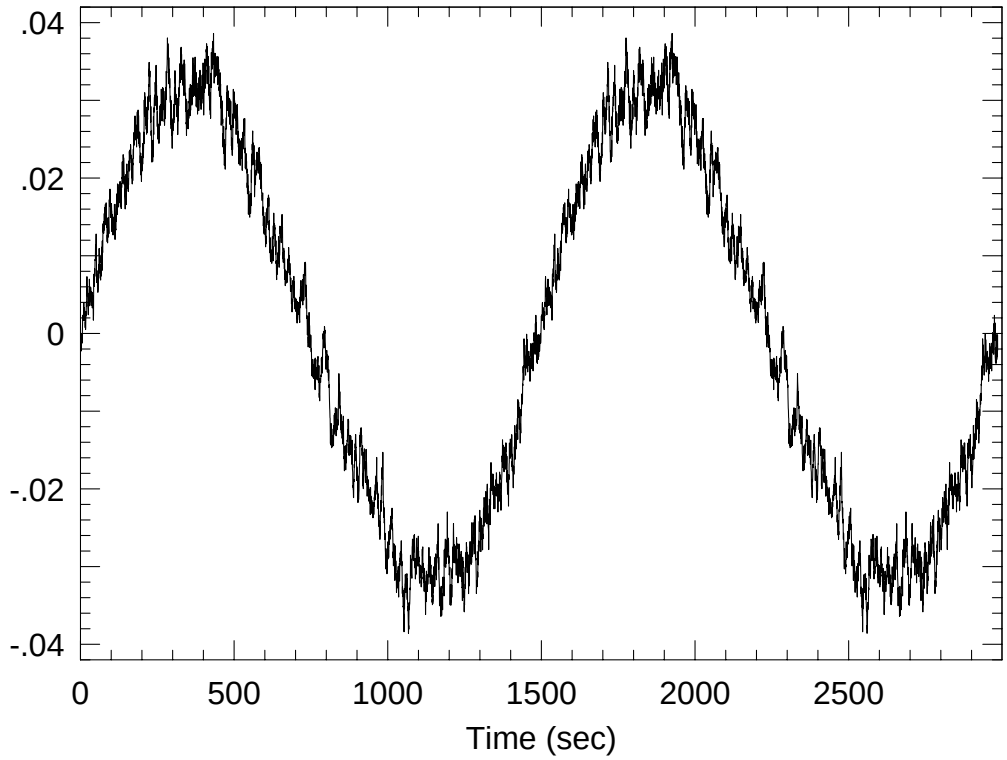

Figure 4.23: Low state pulse shape for P=1492.7881 seconds

PG1346+082 ($\approx 20,000$ K and the fact that the object is not a strong X-ray source.

The eruptive behaviour of PG1346+082 argues conclusively for its interacting binary nature and eliminates any single star models. Our task is to narrow down the possible components of the binary. As with AM CVn, the lack of hydrogen eliminates all low mass, main sequence companions. Employing arguments used for AM CVn, and discussed in Wood *et al.*, 1987, the secondary must be a degenerate helium star.

Following the path we laid out in our discussion of AM CVn, the first model we will consider for PG1346+082 is a simple interacting system in which the secondary is losing material to the primary via an accretion disk. In such an object, we would expect to observe brightness variations corresponding to the orbital period of the system, perhaps produced by a bright spot where the matter stream impacts the outer disk, or by an eclipse. Our simple model immediately fails, as it is unable to explain the presence of a second periodicity in the low state FT. We must include an additional mechanism to produce the second variation.

The simplest possible mechanism to explain the presence of the second periodicity in PG1346+082's low state FT is the rotational period of the mass accretor. The photometric variations arise as the bright, or dark, magnetic poles are carried through our line of sight as the white dwarf rotates. Can we choose which period (1471.3 or 1492.8 s), if either, is the orbital period of the system? While we possess no direct measurements, such as radial velocity observations, we can constrain the orbital period of the system. We have

shown that the 1471.3 second period maintains phase, despite excursions by PG1346+082 to brighter magnitudes. If the 1471.3 second variation were a manifestation of a hot spot on the edge of an accretion disk, it should not maintain strict phase coherence after outburst. Numerous studies of dwarf novae (Zhang, *et al.* 1986, Zhang, *et al.* 1987, Nather, *et al.* 1969) suggest that accretion disks do not remain the same size after an outburst as before, therefore the phase of the hot spot should be different before and after an outburst. If the 1471.3 second period is a manifestation of a hot spot on the edge of an accretion disk, it is telling us that the accretion disk remains the same size. If the edge of the disk in PG1346+082 does remain at constant radius, this system is the first example of such an object, and our model must include a unknown mechanism for producing outbursts in PG1346+082.

We must consider the possibility that the hot spot is not at the outer edge of the accretion disk, but further in the disk (Horne, 1991), allowing the disk to change size during outburst and the radial position of the hot spot to remain constant. 1471.3 seconds could then represent the orbital period of the system, leaving 1492.8 seconds as the rotation period of the accretor. PG1346+082 would then enjoy the dubious honor of representing the first example of an interacting binary in which the rotation period of the mass accretor is longer than the orbital period of the system.

If 1471.3 seconds is not the orbital period of PG1346, in our model it must represent the rotational period of the mass accretor. The rotation of the white dwarf should maintain phase whatever the magnitude of PG1346+082. This model naturally explains the change in relative intensities between the dominant 1470 second power and the first harmonic we observed in 1984 if we

are viewing both poles, each of which are capable of varying in relative brightness. The inverse dependence of the 1471.3 second period with the brightness of PG1346+082 suggests that the poles do not brighten during outburst. If luminous poles are responsible for the 1471.3 second variation during low state, most material accreted during outburst does not accrete via the magnetic field lines to impact at the poles.

If 1471.3 seconds is the rotational period of the accreting white dwarf, we are left with 1492.8 seconds as the orbital period of PG1346+082. Unfortunately, we do not possess a sufficient quantity of data to accurately measure the phase of this variation, so it is impossible confirm its stability. However, we have no evidence to indicate that the 1492.8 second period is incoherent.

Our interacting binary model, with an orbital period of 1492.8 seconds and a rotation period of the mass accretor of 1471.3 seconds, explains much of the behaviour of PG1346+082. We have one observation still to explain. During outbursts, the frequencies observed in FTs of PG1346+082's light curve are not consistent with either 1471.3 or 1492.8 seconds. A complex harmonic structure appears, consistent with a fundamental period of 1486 seconds. The outburst mechanism must be capable of reproducing this behaviour.

Many dwarf novae display quasi-periodic variations during outburst. The SU UMa stars demonstrate a phenomenon known as superhumps, periodic 20 to 30 percent enhancements of the object's light, with periods a few percent longer than the orbital period. The phenomenon is believed to be caused by an elliptical, precessing disk. While similar to the behaviour observed in PG1346+082, several key differences remain. If 1492.8 seconds is the orbital

period, then the frequencies observed in high state are shorter, not longer than the orbital period (Hirose *et al.*, 1990), suggesting that the elliptical disk is precessing in the retrograde direction. Secondly, superhumps occur only during especially bright outbursts in SU UMa stars. The frequencies present in PG1346+082's light curve change even if the system does not reach maximum brightness, and does not remain in high state for an extended period of time. It is interesting to note that 1471.3 seconds is $\approx 6.6 \mu Hz$ away from both 1457.5 and 1485.9 seconds.

We are unable, with our current data set, to explain the changes in frequency observed in PG1346+082. This is not a failure of our model, however, but a failure of our detailed understanding of the outburst mechanism and our lack of high state data. Future work on PG1346+082 must include high state observations. Unfortunately, obtaining this data is not left only to the persistence of the observer, but to the whim of PG1346+082 itself.

Our accreting binary model is fairly successful in explaining the behaviour of PG1346+082, but how unique is this model? The temperature of PG1346+082 dictates that we must consider the role played by nonradial pulsations in this system, substituting the luminous poles of the previous model for a luminous section of the accreting white dwarf, arising from a nonradial variation. Tidal forces provide a mechanism for aiding in driving, and for selection of a period oscillation. The 1471.3 second variation is driven because it is the normal mode of the accreting white dwarf closest in frequency to the orbital period (1492.8 seconds) of the system. If the accretor is pulsating, the pulsation would not take part in the outburst itself, resulting in the changes in fractional intensity we observe.

A nonradial pulsation might naturally shift frequencies during an outburst, when the white dwarf is accreting a larger than "normal" amount of material, affecting the driving region of partial ionization and leading to a slight change in period. We can estimate the change in mass required to produce the change in period observed using (Winget, 1981)

$$\tau_{th} = \frac{C_\nu T_n \Delta M}{L}$$

where τ_{th} is the pulsation timescale, C_ν is the heat capacity of the material, ΔM is the mass, and L is the luminosity. Substituting 1471.3 and 1486 for τ, 10^5 for C_ν, 10^6 for T, and 0.01 for L, we arrive at a change in mass of 10^{-12} $M\odot$. This number is not inconsistent with the mass transfer rates observed in other dwarf novae. It is not clear, however if a period increase or decrease would be expected from the accretion of material onto the white dwarf. The timescale for the period of oscillation to return to normal is also unclear, but is probably of order of timescale required for the white dwarf to cool. The nonradial pulsation may be capable of remembering its previous phase if tidal forcing, which would remember phase, is part of the driving mechanism.

We have learned more about the details of PG1346+082's photometric behaviour, but we are still unable to produce a completely ambiguous model for the object. While the accreting binary model, including luminous magnetic poles of the accretor, is successful in explaining many details of PG1346+082, we cannot eliminate the possibility of a nonradial pulsator in an accreting binary. To continue our investigation, additional high state data is required to obtain a completely resolved FT of PG1346+082 to better examine the phase and period of the variations during high state. Also, multicolor observations

would be helpful in differentiating between luminous magnetic poles and pulsation of the 1471.3 second period. We do not understand the effects of accretion and outbursts on pulsating white dwarf stars, the nature of tidally driven pulsations, and the coupling of a pulsating white dwarf. More theoretical work is necessary to examine whether such pulsations can even exist in the environment of PG1346+082.

Chapter 5

CP-Eri

CP Eri is the final member of the interacting binary white dwarf family we will discuss in this work. One of five faint blue variable stars at high galactic latitudes found by Luyten and Haro (Luyten, 1959), CP Eri qualifies as an interacting binary white dwarf system by demonstrating a complete lack of hydrogen in its spectrum. The object is both a spectroscopic and photometric variable (Abbott, 1992). In the manner of V803 Cen and PG1346+082, CP Eri undergoes large magnitude outbursts, from $\approx 19.7 to \approx 16.5 m_b$, on a timescale of about one day (Skzody, 1989), although our knowledge of the object's outburst behaviour is not as comprehensive as for PG1346+082 or V803 Cen. Short period variations at $\approx 1724 \pm 4.0$ seconds are superimposed upon the large magnitude outbursts (Howell, 1991, and Abbott, 1992). The 1724 second period is reported to lack strict coherence, and significant changes in the variations pulse shape from night to night have been observed (Abbott 1992). However, published FTs of CP Eri spanning several days are unresolved, arguing that an individual night's light curve is also unresolved. We have shown (see the more detailed discussion on pulse shapes in Ch. 3) that an accurate pulse shape can be obtained only if the parent light curve has a sufficient time base to completely resolve the period of interest from any other variations present in the object. If this criteria is not met, the pulse shape must be contaminated by the blended power, and we would expect the pulse shape of unresolved data

to change from night to night (see chapter 3 for a more detailed discussion of pulse shapes). So, the question concerning the long term coherence of the 1724 second period is still open.

The features of neutral helium detected in the spectrum vary from emission to absorption depending on the magnitude of the system. Absorption features are seen during high state, and emission features in low state, exactly as observed for PG1346+082 and V803 Cen. The spectral features are broad and shallow, characteristic of Doppler broadening in an accretion disk or a combination of Doppler broadening and pressure broadening in the atmosphere of a compact object. As with all members of the interacting binary family, no hydrogen is detected (Abbott 1992).

Our goal in CP Eri's case is a more accurate identification of any physical periodicities present in the light curve. The incoherent behaviour reported for the dominant 1700 second periodicity screams reminders of early observations of PG1346+082 (Wood, 1987). If the short period variations of CP Eri behave as in PG1346+082, the band of peaks at 1700 seconds is a manifestation of amplitude modulation of one or two physical periodicities, resulting in apparent incoherence. We will examine the FTs of CP Eri's light curve to test this hypothesis.

5.1 Observations and Reductions

Because of its faintness, CP Eri is a difficult object to observe with a standard photometer employing a photomultiplier tube. Our CP Eri data were obtained using a CCD as a detector and employing the CHRONOS software

package (Abbott and Opal, 1988), designed specifically for the collection of time-series data with a CCD as opposed to the traditional use of photomultiplier tube. With CHRONOS, it is possible to reduce the data in real time, resulting in a light curve for the observer to examine throughout the run.

The reduction techniques we employed are very similar to those of traditional time-series data reduction . We chose a sky annulus for each star (multiple comparison stars are possible with CCD photometry) to sample sky contribution, and an aperture size to recover stellar brightness from each integration. We used the same size aperture for all stars. Effects of extinction were removed by dividing each light curve by the light curve of a brighter comparison star produced by the same size aperture. A more detailed account of reduction techniques can be found in Abbott (1992).

The data consists of two groups of observations. We obtained several runs taken on Oct 12, 13 and 16, 1991 in white light with an integration time of 120 seconds. CP Eri was in bright state during the time of these observations. The second group of observations span November 1-5 1991, during which the object remained in low state. Again, we did not have a filter during the November observations, and we used an integration time of 180 seconds.

5.2 The Fourier Transform of CP Eri

5.2.1 The Bright Fourier Transform

An unresolved band of power at ≈ 1700 seconds dominates the bright state FT of CP Eri. The largest peak in this region is 1700.53 ± 0.26 seconds, with an amplitude of 15.8 ± 1.3 mmis. The alias pattern in this region, which

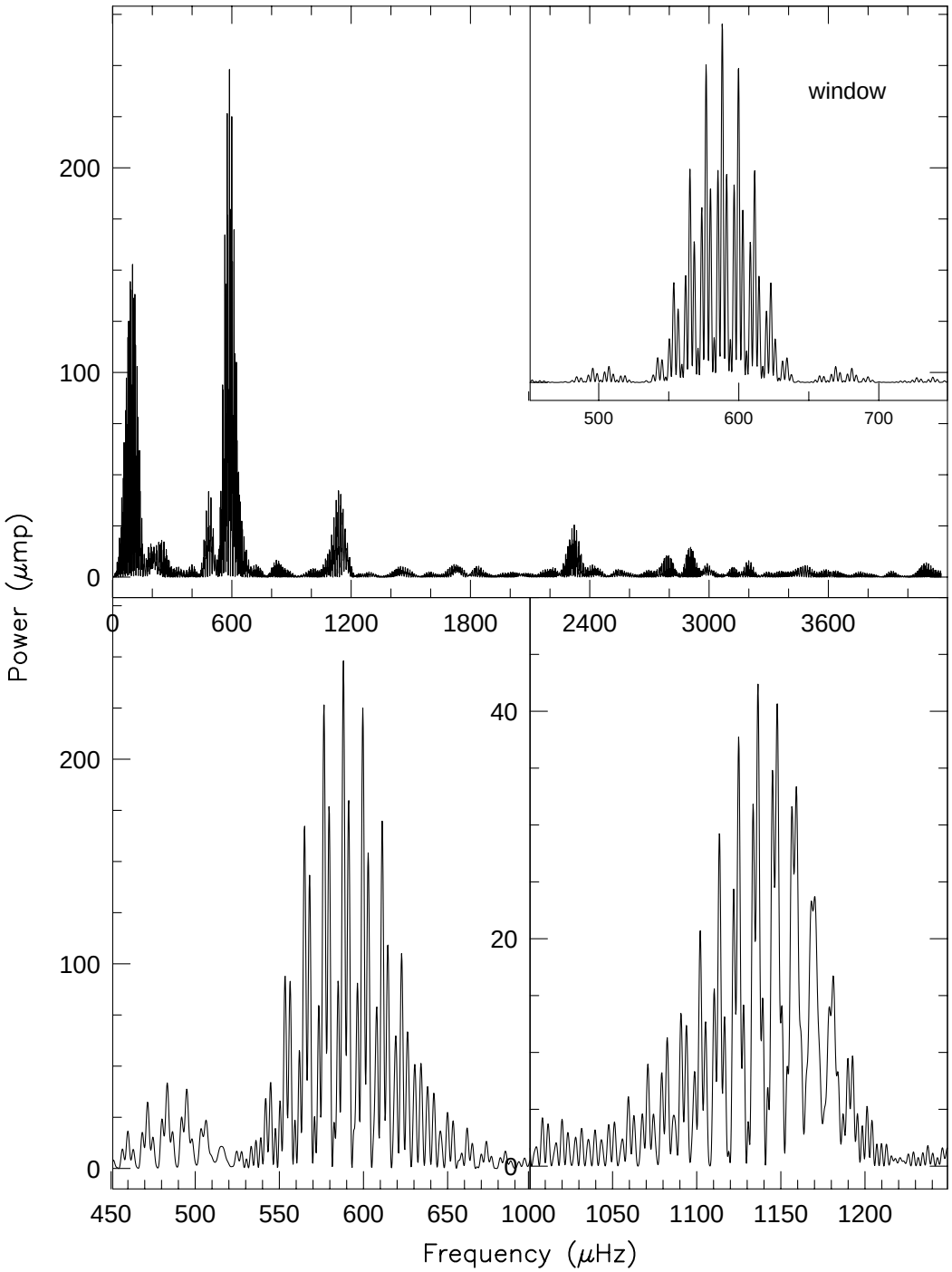

Figure 5.1: The Fourier transform of the bright CP Eri data set. The top panel is the entire FT down to the Nyquist frequency, the bottom panels show details of the dominant 1700 second band and its first harmonic. The inset is the alias pattern produced by a sine wave sampled as the data.

includes the feature at $\approx 500\mu Hz$, is roughly what we expect from a single variation, but we do see some excess power in a few alias peaks, a manifestation of unresolved alias structure. The excess is an positive indication of the presence of an additional periodicity hidden among the complex web of aliases. Unfortunately, because the FT is unresolved, we cannot positively identify any additional peak, and can only argue that at least two physical periods exist in this region of the FT. We must somehow reduce the amplitude of the alias forest before the actual additional peaks will emerge. The only existing consistent method of reducing aliases is continuous observation provided by the WET.

We find an extensive system of harmonics present in the FT (Table 6.1), with the first, third, fourth and seventh at significant amplitudes. The second and fifth are also detected at lower amplitude. The amplitudes of the harmonics are variable with time, as is apparent when we compare Figure 6.1 with the FT presented by Abbott (1992) in which the second harmonic, almost invisible in Figure 6.1, is the largest amplitude harmonic present.

We measure the amplitude of the dominant power in this data set as 15.8 ± 1.3 mmis. The amplitude reported by Abbott (1992) for the 1724 second period was ≈ 14 mmis, agreeing well with our measurement in bright state.

5.2.2 The Low State Fourier Transform

The low state FT is dominated by a band of power at ≈ 1700 seconds as well as power in the region of the first harmonic. The additional harmonics we detected in the October bright data are gone. The pattern in the region of 1700 seconds corresponds to the alias structure we expect from a single sinusoid

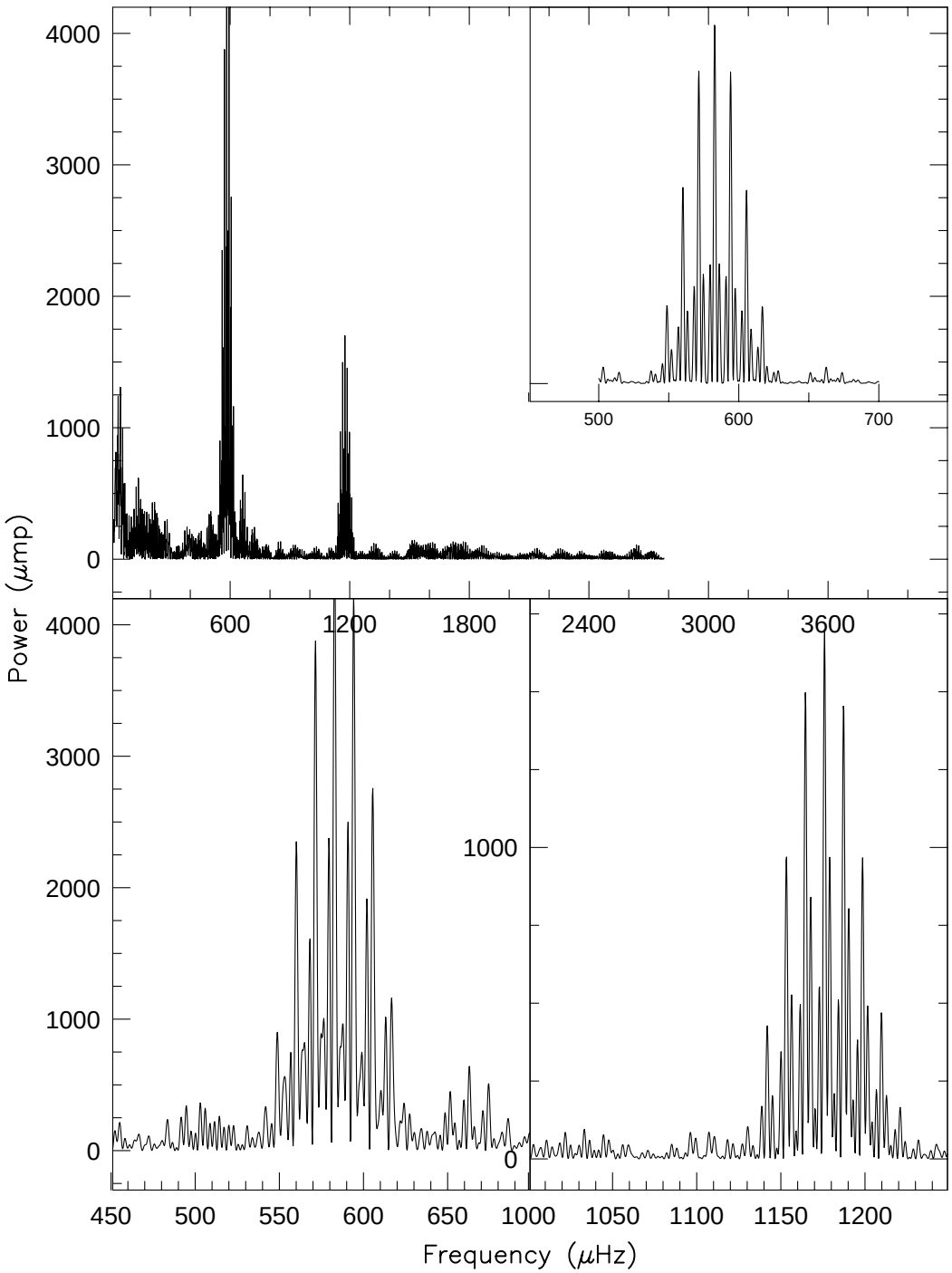

Figure 5.2: The low state FT of CP Eri. The dominant peak is at 1715 seconds.

Table 5.1: Photometric Periodicities of CP Eri

Frequency (μHz)	Period (sec)	Amp (mmg)	Fundamental (sec)	comments
588.05	1700.53 ± 0.26	15.9 ± 1.3		
576.49	1734.63 ± 0.29	15.0 ± 1.4		alias
1336.42	879.96 ± 0.19	6.5 ± 1.5	1759.92	
1147.84	871.20 ± 0.19	6.4 ± 1.5	1742.40	alias
2322.18	430.63 ± 0.05	5.0 ± 1.5	1722.53	
2310.54	432.80 ± 0.05	4.9 ± 1.5	1728.24	alias
2907.15	343.98 ± 0.05	3.9 ± 1.5	1719.89	blend
4092.66	244.34 ± 0.04	2.7 ± 1.5	1710.38	
4104.08	243.66 ± 0.04	2.6 ± 1.5	1705.62	alias
4077.97	245.22 ± 0.04	2.4 ± 1.5	1716.54	alias

with a period of 1715.854 ± 0.27 seconds and an amplitude of 68.8 ± 5.6 mmis. As we found in the high state data, a small amount of additional power is blended with some peaks in the 1715 second alias forest, again allowing us to argue for the existence of a second physical period. The severity of the blending eliminates all possibility of the positive identification of any actual period.

The pattern of peaks we find in the region of the first harmonic is consistent with the alias pattern created by a single variation with a period of 850.38 ± 0.13 seconds and an amplitude of 41.2 ± 6.3 mmis. Surprisingly this measured period differs by over 50σ from the period we expect for the first harmonic of 1715 seconds (857.5 seconds). The period instead corresponds, within one σ, to the first harmonic of 1700.53 seconds, the dominant period we found in the high state FT.

The frequency and amplitude behaviour of CP Eri mimic the behaviour we observe in PG1346+082. Different frequencies appear at different system magnitude states. The 1700.53 second period we found at high state is

absent in Figure 6.2, replaced by 1715.85 seconds, a change of $5.25\mu Hz$ or 15 seconds. We can watch while the entire first harmonic alias forest picks itself up by its skirts, shuffles over $60\mu Hz$ to higher frequency in the low state FT, and increases it's amplitude by nearly 7 times, now corresponding to a single peak with a period of 850.3 seconds. To confuse us utterly, the fundamental peak we observe in low state is no longer 1700.53 seconds. The fundamental has moved to lower frequency and increased its amplitude by over 4 times, to 1715 seconds. If CP Eri behaves as PG1346, we should find the amplitude changes in the fundamental and first harmonic to be inversely proportional to the magnitude of the system. Indeed, the amplitude change we observe in both the 850 and 1715 second power is of order that expected by the change in magnitude of the system.

We compared the pulse shape of the low state dominant periodicity 1715.854 with the pulse shapes of other IBWDs (Figure 6.3) The pulse shape in some ways resembles the 525.6 second pulse shape of AM CVn. The 1715 second pulse shape does not demonstrate the flat bottoms exhibited in the 1471 second pulse of PG1346+082.

5.3 What is CP Eri?

CP Eri displays many of the characteristics of PG1346+082 and the arguments employed in for PG1346+082 apply to CP Eri as well. We identified PG1346+082 as an interacting binary white dwarf system, with a possible orbital period of 1492.8 seconds and a rotation period of the mass accreting star of 1471.3 seconds. We are confident that the same basic model applies

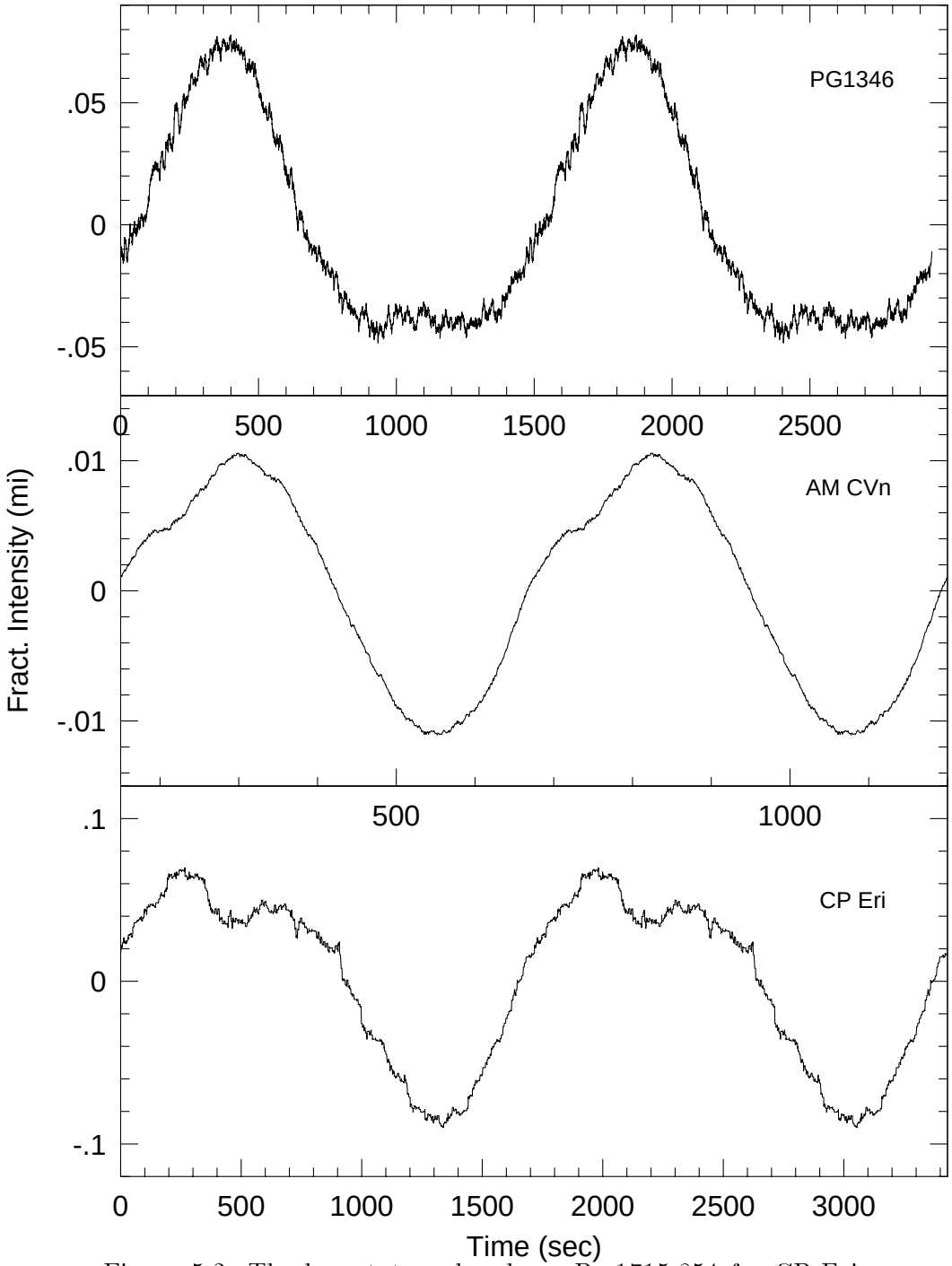

Figure 5.3: The low state pulse shape P=1715.854 for CP Eri.

to CP Eri. If PG1346+082 and CP Eri are two examples of basically the same beast, is the model flexible enough to stretch to explain the differences observed between the two systems? We believe the answer is yet, but further observations of CP Eri in high and low state are required to explain details such as the behaviour of the first harmonic in CP Eri's FTs.

Chapter 6

V803 Centaurus and G6129

The last two members of the interacting binary family we will discuss are V803 Cen and G6129. Although the differences in their behaviour are great, we have included both in this chapter because we lack a great deal of data on each.

6.1 V803 Cen

The variable star V803 Cen (AE-1) was first noted in 1975 by Elvius, but remained in relative obscurity until it was rediscovered during a literature search, conducted by E. L. Robinson, for blue objects similar to AM CVn and PG1346+082.

V803 Cen is both a spectroscopic and photometric variable, altering its luminosity over a substantial range of timescales. Its overall magnitude behaviour is identical to that of PG1346+082, undergoing 3-4 magnitude eruptions ($\approx 17.3 m_b$ to $\approx 13.6 m_b$) on a quasi- periodic timescale of a few days. In 1987, short timescale variations, at $\approx$ 1600 seconds, were found in V803 Cen's light curve (O'Donoghue *et al.*, 1989). This 1600 second variation displays characteristics similar to the behaviour first observed in the 1470 second variation of PG1346+082 (Wood *et al.*, 1987). The amplitude of the 1600 second period varies from night to night, and even disappears for several cycles (O'Donoghue

et al., 1990), indicative of beating between closely spaced, unresolved periodicities. A second variation at $\approx$ 175 seconds has been detected (O'Donoghue *et al.*, 1989) and short timescale incoherent flickering, the classic signature of mass transfer, has also been reported in V803 Cen's light curve (O'Donoghue *et al.*, 1990).

V803 Cen's optical spectrum is dominated by features of neutral helium. As is true for all other interacting binary white dwarfs, hydrogen is not detected. Paralleling PG1346+082, the features observed in the optical spectrum of V803 Cen at any given time depend upon the overall magnitude of the system. The optical spectrum contains broad, shallow asymmetric absorption lines of neutral helium during high state, and emission features when the system is dim (O'Donoghue *et al.*, 1989).

Our data set for V803 Cen is rather limited, severely curtailing what we can hope to accomplish in our analysis of this object. Our most important goal is to examine the amplitude of the 1600 second variation as a function of time. If we find a similar dependence on magnitude as observed for PG1346+082, we can constrain models for the short timescale variations in all IBWDs.

6.1.1 Observations

Our observations of V803 Cen consist of a total 47 hours of photometric data spanning nearly eight days in March of 1988 (Table 6.1). The data were taken, reduced and analyzed employing the techniques we discussed in Chapters 2, 3 and 4.

Table 6.1: Journal of Observations

Run	Location	Date	Run Start (UT)	Length (hr)	Int (s)	mag
s4224	SAAO	11 Mar 88	0:25:40	2.8	10.0	13.7
a9	MSSSO	12 Mar 88	12:07:52	0.6	10.0	17.0
s4226	SAAO	12 Mar 88	21:19:31	0.9	10.0	17.5
tol 16	CTIO	14 Mar 88	2:23:00	1.6	10.0	17.0
ra106	LNA	14 Mar 88	2:57:18	4.6	10.0439	
tol 18	CTIO	14 Mar 88	6:55:00	2.5	10.0	16.9
a13	MSSSO	14 Mar 88	11:54:00	1.4	10.0	16.9
s4229	SAAO	14 Mar 88	21:55:00	5.7	10.0	17.0
tol 21	CTIO	15 Mar 88	1:12:00	1.8	10.0	17.0
ra107	LNA	15 Mar 88	1:59:23	4.0	10.0454	
tol-23	CTIO	15 Mar 88	5:49:00	3.5	10.0	16.9
a18	MSSSO	15 Mar 88	11:30:00	2.8	10.0	17.0
s4232	SAAO	15 Mar 88	21:25:30	5.7	10.0	17.0-16.4
s4234	SAAO	16 Mar 88	21:33:10	1.2	10.0	17.3
a20	MSSSO	17 Mar 88	12:16:10	1.7	10.0	
s4237	SAAO	17 Mar 88	20:34:00	1.6	10.0	17.3
s4242	SAAO	19 Mar 88	20:50:40	1.1	10.0	17.3
s4245	SAAO	20 Mar 88	20:46:30	1.1	10.0	17.2
s4249	SAAO	21 Mar 88	20:57:20	1.4	10.0	16.9
s4252	SAAO	22 Mar 88	20:48:20	1.4	10.0	13.6

Our data set was obtained during the inaugural run of the Whole Earth Telescope. V803 Cen was the second priority target to PG1346+082, so unfortunately the coverage was not nearly as complete as that of PG1346+082. During WET, however, V803 Cen had the same disease as PG1346+082, and settled into low state for most of the run. This data set represents the most extensive available of V803 Cen in low state.

6.2 The Fourier Transform of V803 Cen

A complex, unresolved band of power centered at $670\mu Hz$ ($\approx$ 1500 s) dominates the FT of V803 Cen in low state. We also find power in the region of the first harmonic of the dominant 1600 second power, and at $\approx$ 1298 seconds. We do not detect the 175 second periodicity reported by O'Donoghue *et al.* (1989) (Figure 6.1, 6.2, 6.3).

The general description of V803 Cen is very similar to the northern hemisphere's PG1346. If the short period variations in each object result from an identical mechanism, we expect the variations of V803 Cen to exhibit the same intensity behaviour as PG1346+082. In low state, we measure a fractional intensity of $\approx$ 20 mmis for the 1600 second band of power. Although the object remained in low state for most of the run, in the very beginning and ending of the observing run, V803 Cen exploded into high state, climbing from magnitude 17.0 m_b to 13.6 m_b on a timescale of one day. We can place a upper limit of $\approx$ 2 mmis on the amplitude of the 1500 second power in high state. Following the procedure we laid down for PG136+082, this change in relative intensities is within a factor of two that expected from the change in flux observed. This behaviour suggests that, as in PG1346+082, the 1500 second power is a constant amplitude source viewed against the variable background of the V803 Cen system.

6.3 G61-29

The interacting binary G61-29 has a colorful history. The object was discovered via spectroscopy by Burbidge and Strittmatter in 1971, who found

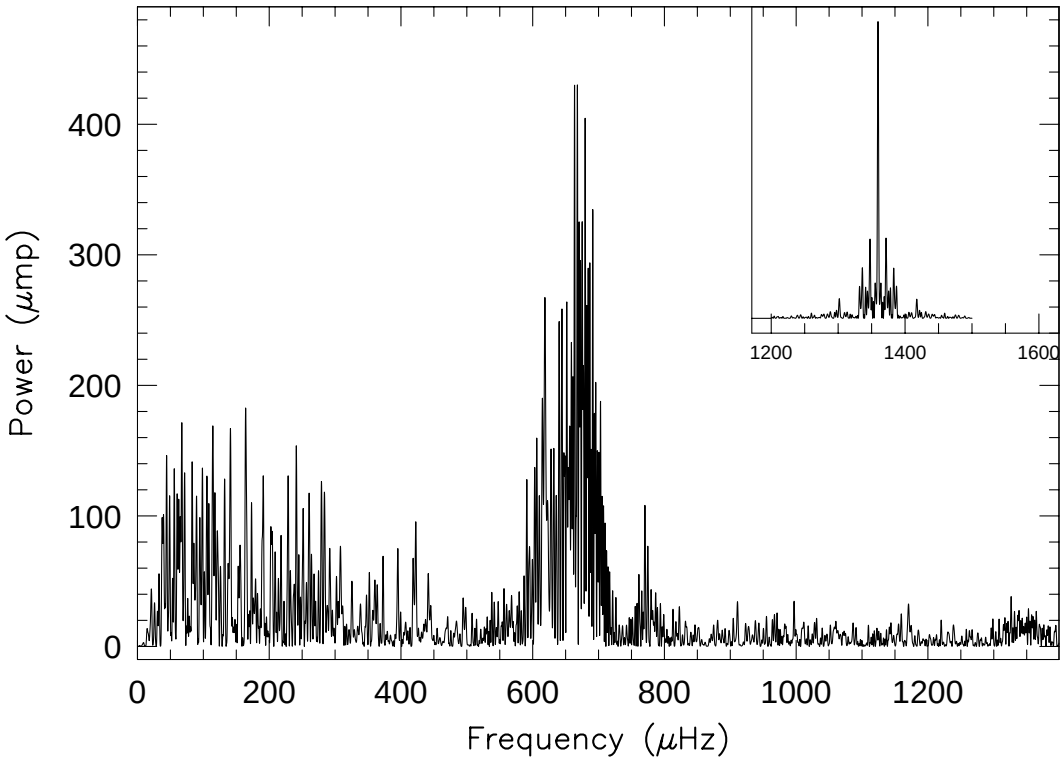

Figure 6.1: Low state FT of V803 Cen during March of 1988

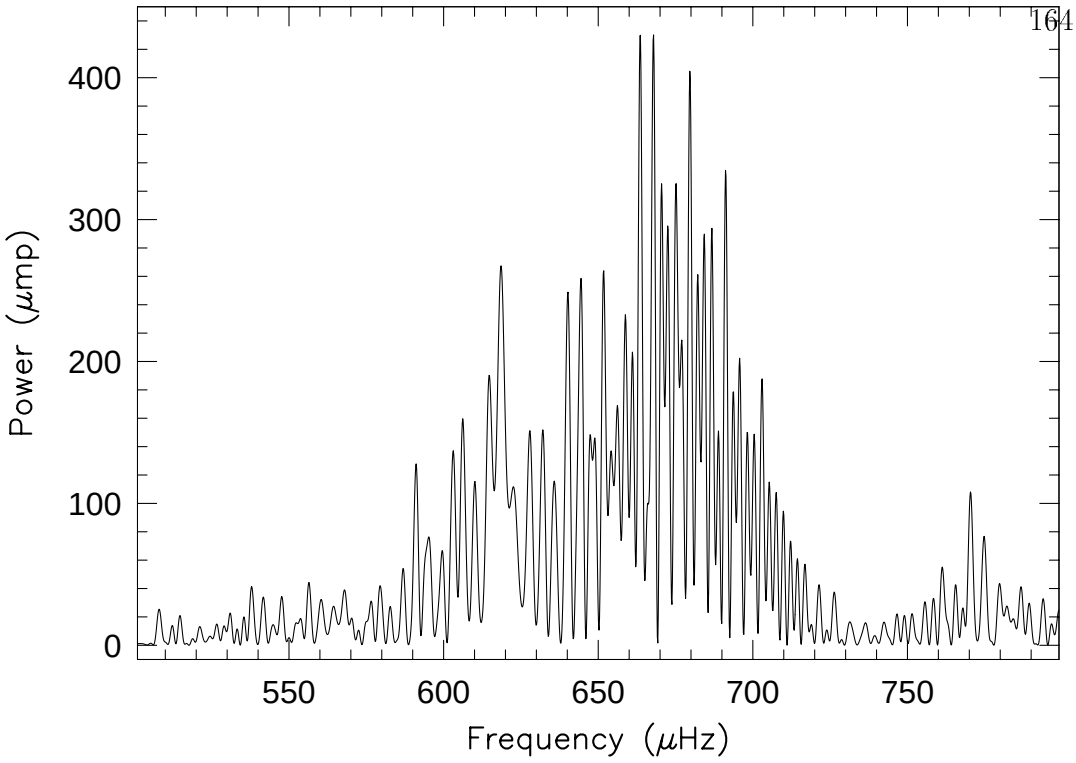

Figure 6.2: Low state FT of V803 Cen in the region of 1500 seconds

only broad He I emission lines, mentioned that the profiles seemed to be variable and noted the absence of hydrogen. In 1975, the emission lines were found to be an amalgam of two features, a broad, double peaked component, and a narrow, slightly red shifted central emission spike (Smak, 1975). The broad component is the classic, double peaked signature of rapidly rotating gases in an accretion disk. The origin of the central spike is unknown, but believed to arise from an expanding shell of material.

The question of variability in the emission profiles continued to plague G61- 29 as other observers also reported the phenomenon (Greenstein, 1977). In 1981, the problem was resolved when Nather *et al.*, (1981) closely examined the emission profile variations in the broad component arising in the accretion

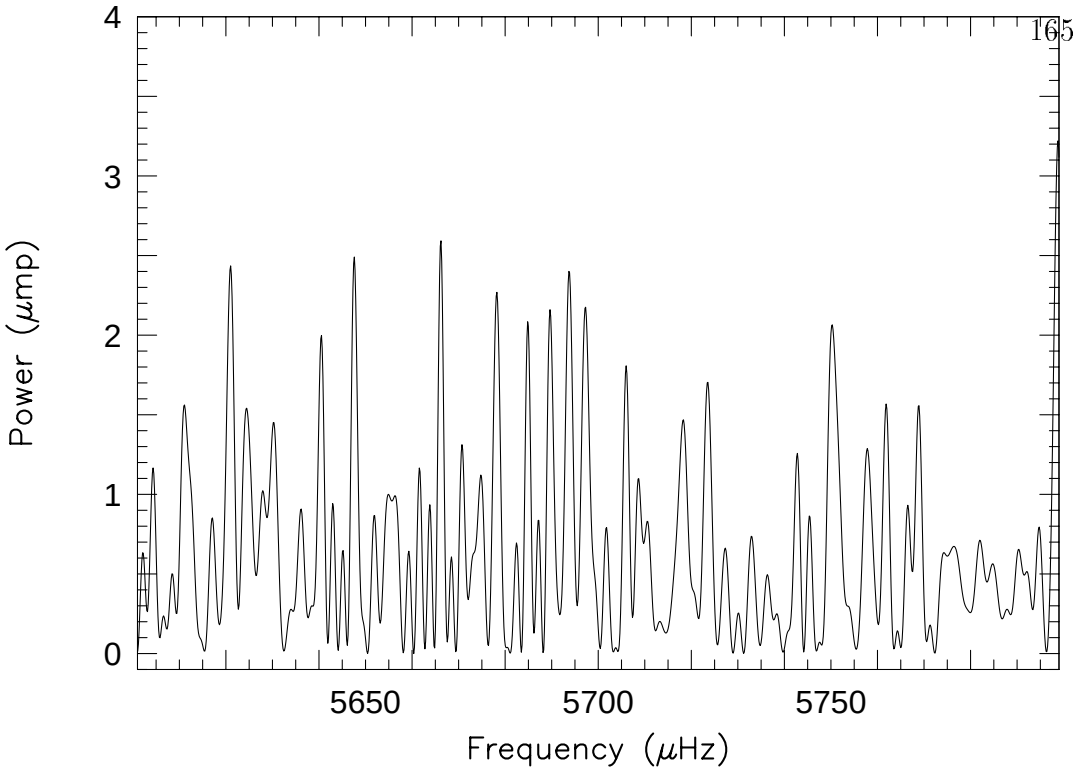

Figure 6.3: Low state FT of V803 Cen in the region of 175 seconds

disk and discovered a 46.5 minute periodicity, the famous "s" wave of G61-29. The authors attributed the periodic variation of the profiles to the orbital motion of a hot spot on the outer regions of the accretion disk. Since the hot spot is tied to the mass donor via the accretion stream, the time for the spot to complete one orbit is a good indicator of the orbital period of the system. G61-29 is therefore the only interacting binary white dwarf system with a demonstrably known orbital period.

G61-29 is also a photometric variable, first discovered by Warner in 1972, who reported the presence of violent flickering activity in G61-29's light curve and was the first to suggest a binary model in the context the object. He assigned a tentative orbital period of 6 hours, 16 minutes based on the similarity

of the light curve to the cataclysmic variable VV Pup. Later observers (Smak, 1975 and Nather *et al.*, 1981) reported much less photometric activity. Indeed, Nather *et al.* (1981) reported that at times no photometric variations were present at all. Warner's observations were later shown to be instrumental in origin (Nather, 1993).

We obtained a small amount of multicolor (Johnson UBVRI filters) data on G61-29 in March of 1990. Our goal is the identification of the photometric equivalent of the spectroscopic period, as well as an investigation of differing behaviour of G61-29 as a function of color.

6.4 Observations and Reductions

We obtained two nights of multicolor data on G61-29 using the Steining multicolor photometer. This photometer is essentially identical to the standard photometer described by Nather (1973) except for the addition of dicroics that split the variable star's light beam, as a function of color, into four individual photomultiplier tubes, allowing for truly simultaneous multicolor observation, with Johnson U, B, V, and R filters, of the target object.

We employed the data reduction techniques discussed in Chapter 2. Each observing run produced 4 separate light curves. We treated each light curve individually and reduced each separately.

6.4.1 The Light Curves and Fourier Transforms of G61-29

The light curves of G61-29, as a function of color are given in Figure (6.4). The figure displays two light curves in each color, spanning the two

nights of observations we obtained. Each curve displays quasiperiodic variations, resembling the flickering phenomenon observed in hydrogen cataclysmics (Robinson, *et al.*, 1987). On visual inspection of the light curves, we observe changes in the variations as a function of color. In particular, the V light curve undergoes rapid, semicoherent variations on a timescale of several hundred seconds during the second night of observations. If we assume that all of the photometric variations originate in the hot spot, the structure of the spot must be considerably more complex than a small, localized region of impact. If the variations were arising from a localized region, the spot would not have a large temperature profile, and the observed photometric variations would be dominant only in the color band characterizing the temperature of the spot. In G61-29, we find short period, incoherent variations in all color bands, and the character of the variation in each color is different. This behaviour reminds us of the multicolor observations of AM CVn, where some periodicities, particularly the 1011.4 second variation, exhibit differing amplitudes with color and regions of power present in the FT change as a function of color.

We calculated the FTs of the light curves given in Figure 6.4, as well as the FT of the light curve representing the sum of all the different colors (Fig 6.5). We formed the summed light curve by simply adding the photons observed at each photomultiplier tube during each integration, without attempting to correct for varying sensitivity of the individual tubes.

Our primary goal concerning G61-29 is the photometric identification of the 46.5 minute spectroscopic profile variation identified by Nather *et al.* (1981). The largest feature we find in each FT (with the exception of the R FT) is a low frequency band of peaks, probably arising from transparency vari-

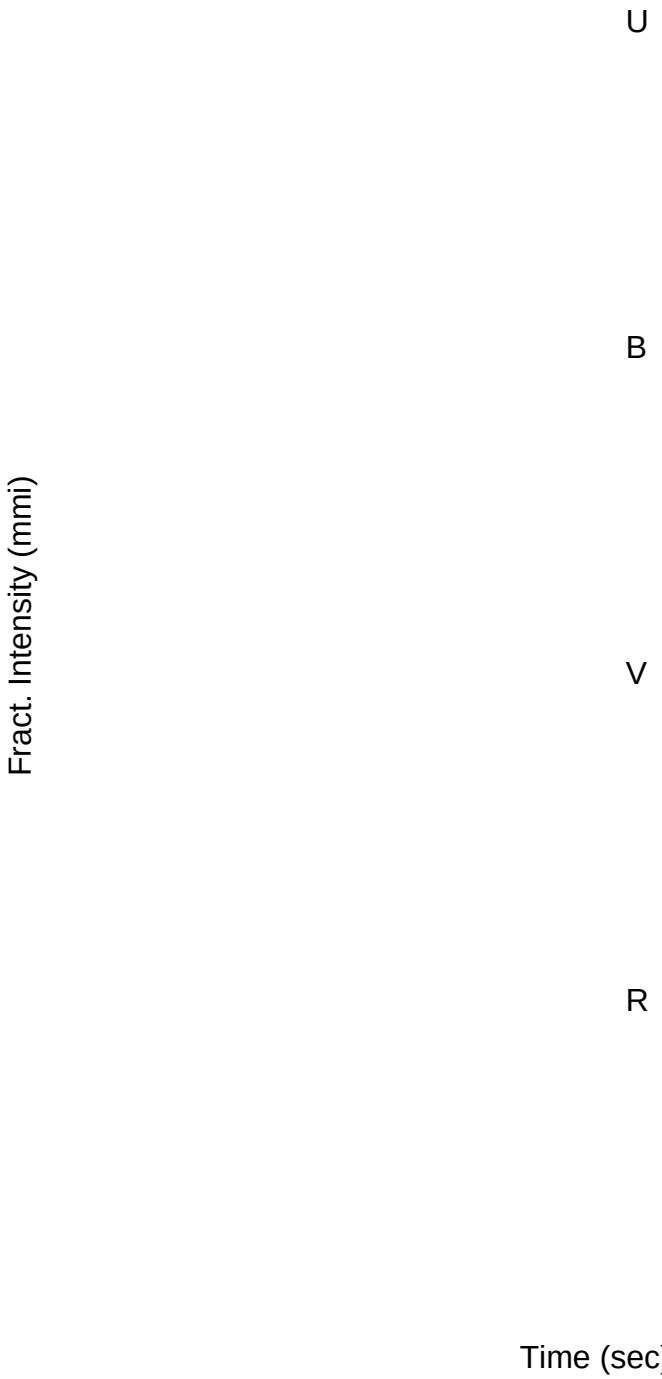

Figure 6.4: The light curves of G61-29 obtained with the Steining photometer

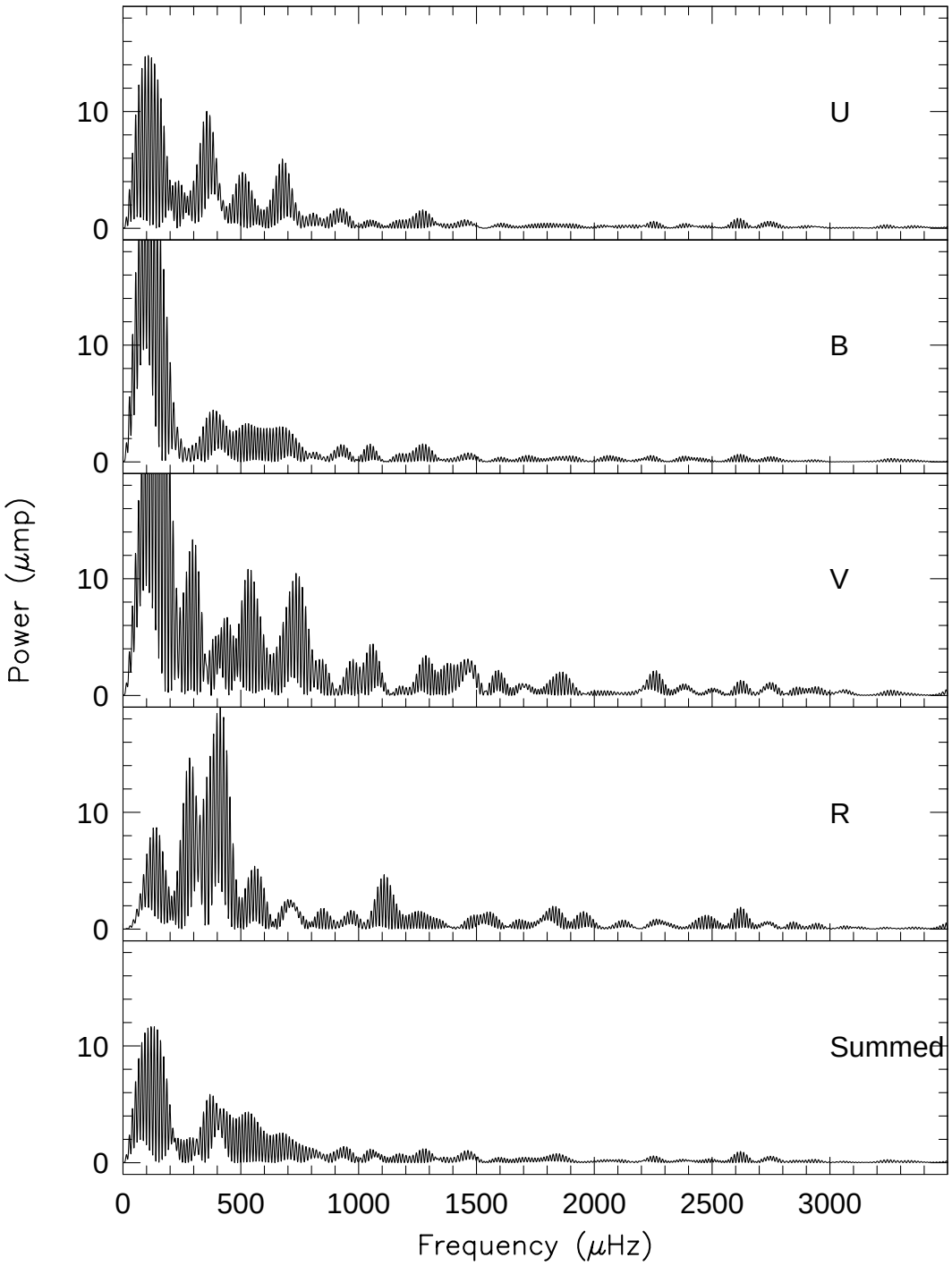

Figure 6.5: Fourier Transform of the light curve of G61-29. The top four panels are the FTs of each color band, the bottom panel is the FT of the summed light curves.

ations incompletely removed during the reduction process. All FTs in Figure 6.5 contain power near the region corresponding to a period of 2790 seconds, but the power is blended with nearby peaks and at low amplitude. Our best chance of distinguishing the 46.5 second period lies with the FT of the summed light curve, where we find a small region of power at the period of interest. Unfortunately, the signal is small, and, again, is not an isolated frequency, but an unresolved band of power. Our best guess of the periodicity responsible for the power is 2812.5 ± 2 seconds. While we cannot absolutely identify any periodicity present, we can state that this region of power is consistent with the period detected in the spectral line variations.

We list the significant periodicities we find in Figure 6.5 in Table 6.2. We are interested to note that each FT contains a peak at $\approx$ 379 seconds, with the R FT having the largest amplitude. The R and V FTs also contain significant power at $\approx$ 3400 seconds. The R FT contains power in the region of the first harmonic (1790 seconds) and the fourth harmonic (902 seconds) of 3400 seconds.

6.5 Discussion

The presence of power at 379 seconds in the R light curve raises an interesting possibility that we must speculate on. The characteristic stellar dynamical timescale is given by

$$\sigma^2 = \rho G$$

If we use Kepler's Law

$$P^2 \propto a^3$$

Table 6.2: Photometric Periodicities in G61-29

Color	Frequency (μHz)	Period (sec)	Amp (mmg)
R	282.55	3539.15 ± 2.5	38 ± 2
	412.56	2423.92 ± 1.0	43 ± 2
	558.66	1790.09 ± 1.1	23 ± 2
	355.88	2809.93 ± 1.6	37 ± 2
	1108.17	902.39 ± 0.4	22 ± 2
	2633.98	379.65 ± 0.9	13 ± 2
V	295.13	3388.29 ± 3	36 ± 2
	354.94	2817.39 ± 5	16 ± 2
	543.64	1839.44 ± 1	33 ± 2
	734.20	1362.01 ± 1	32 ± 2
	2607.30	383.54 ± 0.1	11 ± 2
B	354.31	2822.39 ± 3	20 ± 2
	263.40	379.66 ± 0.1	8 ± 2
U	355.11	2816.07 ± 2	32 ± 2
	506.58	1974.03 ± 1	22 ± 2
	676.67	1477.82 ± 1	24 ± 2
	2624.07	379.64 ± 0.1	8.3 ± 2
all	355.55	2812.53 ± 2	25 ± 1
	2607.52	383.51 ± 0.09	10 ± 1

to calculate the separation of the two components of G61-29 and (Frank, 1985)

$$\frac{R_2}{a} = 0.462(1+q)^{-\frac{1}{3}}$$

to calculate the size of the secondary's Roche lobe, assuming the secondary does indeed fill its lobe we find a radius for the secondary of $\approx 6 \times 10^9$ cm. Calculating a density from this information and assuming a mass of $\approx 0.04 M_\odot$ (Faulkner, *et al.*, 1972), we retrieve a timescale of ≈ 413 seconds for the secondary star. Although we emphasize the extremely speculative nature of this discussion, it is possible that the 379 second power is somehow coupled to the secondary white dwarf, perhaps as some sort of regulation of mass transfer.

Chapter 7

Summary, Conclusions and Discussion

7.1 Summary

We have covered a great deal of observational ground, and analyzed a large amount of data. But all of our effort is in vain if we have not discovered some insight into the interacting binary white dwarfs we did not know before. Summarized here are the principle results of this work:

1. AM CVn

   - We demonstrated the true period of variation in AM CVn to be 525.6 seconds, not 1051.2 seconds as previously accepted.
   - The 525.6 second period is coherent on timescales of decades, despite previous claims to the contrary.
   - We have measured a $\dot{P}$ of $1.68(\pm 0.03) \times 10^{-11}$ s s^{-1} for the 525.6 second variation.
   - We found linear combinations present in the FT that are not direct combinations of the supposed orbital and rotation period and which any improved model for the system must explain.
   - We show that the behaviour of the 1011.4 second period is qualitatively different from the other variations, suggesting

a different mechanism than the other periodicites. The variation may possibly represent the orbital period of AM CVn.

2. PG1346+082

   - We found the short period variations to consist of two separate frequencies, 1471.3 and 1492.8 seconds.
   - The 1471.3 second period is coherent, at least over a two week span, despite large changes in the magnitude of the system, and therefore could be either the rotational period of the mass accretor, or the orbital period of the system.
   - The amplitude of the short period variations is inversely proportional to the system's magnitude, suggesting a constant source seen against a variable background.
   - The frequency of the variations change by $\approx 7\mu Hz$ between high and low state. In high state, the complex harmonics correspond to 1486 seconds, while in low state, the only harmonic present is the first harmonic of 1471.3 seconds. Any model must reproduce this observation.

3. CP Eri

   - The short period variations show the same amplitude modulation details as PG1346, suggesting a similar mechanism.
   - The observed frequency changes by $\approx 6\mu Hz$ from high to low state, similar to the behaviour of PG1346+082.

- The high state FT contains a dominant fundamental frequency and a large number of harmonics, while the low state FT contains a dominant fundamental $\approx 5\mu Hz$ larger in frequency, and power at the first harmonic of the high state dominant peak.

4. V803 Cen

   - The FT of V803 Cen in low state consists of an unresolved band of power at $\approx$ 1500 seconds.
   - The amplitude of the 1500 second power is inversely dependent on the magnitude of the system, as with CP Eri and PG1346+082, again suggesting a common mechanism.

4. G61-29

   - We found some evidence for photometric variation at the spectroscopic period of 2790 seconds.
   - The photometric variations change in both amplitude and frequency with color.

Our list includes a large number of details of behaviour of each of the interacting binary white dwarfs. If we examine the details as a whole body, patterns common to all the IBWDs in our sample emerge.

- If the IBWD undergoes large brightness changes (PG1346+082), the high state FT contains a fundamental frequency and a large number of harmonics. If AM CVn is perpetually in high state, it too fits this pattern.

- If the IBWD undergoes outbursts, the low state FT contains a fundamental band of power and a large amplitude first harmonic of the dominant fundamental period, not necessarily corresponding to the frequency present in high state.
- The observed amplitudes of the short period variations are dependent on the magnitude of the system for IBWDs undergoing large magnitude changes. The fractional change in observed magnitudes is explained by a constant source viewed against the changing brightness system of the system. The low amplitude of the 525.6 second period of AM CVn fits the pattern if the system is bright. However, G61-29 does not display high amplitude short period variations as would be expected for an IBWD perpetually in low state.

We tried to approach each IBWD from an empirical point of view, and let the data point us to the best model for each object. If these objects form a class, we should be able to derive a general model for all IBWDs. Our attempt has not been as successful as we hoped for in a few cases; we were able to fit an object equally well with more than one model. We have found areas of agreement that bear mentioning. Each object is indeed best fit by an interacting twin helium degenerate system transferring material via an accretion disk. The IBWDs are multiperiodic, and our models must be capable of explaining this. The intermediate polar model is flexible enough to explain many of the observed behaviours of all of the IBWDs, if we allow for variations in the mass transfer rates. These binaries have such small separations that magnetic fields of 10^5 G, insignificant in hydrogen cataclysmic variables, may

play a prominent role in the disk structure of these objects. We have not found any unambiguous examples of nonradial pulsations in the IBWDs. However, we cannot rule pulsations out, either. AM CVn bears many of the signatures of pulsation.

7.2 A View of the Past and the Origin of IBWDs

Our analysis has clearly demonstrated the interacting binary white dwarf systems to be complex objects. Perhaps we can gain further insight into their mysteries by considering their origin. What are their ancestors and what are their descendants?

The secondary in the IBWDs is a helium crystal ball through which to peer into the mists of time and expose clues about the past history of the IBWDs. From our observations, we infer that the secondary in each case is a low mass ($\approx 0.04 M_{\odot}$ or less) object, based on the model proposed by Faulkner, Flannery and Warner (1972). Optical and UV spectra of each system contain no hydrogen, and are dominated by neutral helium alone (Patterson, 1992 and references therein). The accreting material must contain nearly pure helium, therefore the mass donor must be a helium object. But, the secondary is of such a small mass that if it were once a "normal" carbon/oxygen core white dwarf, it should be whittled down to well inside the carbon core (Bradley, 1993). We should be observing an accretion disk consisting of carbon and oxygen, not helium. The lack of carbon demands we discover an evolutionary path for the secondary in which its progenitor could not have reached helium ignition.

We know, through the lack of spectral radial velocity variations (Robin-

son, 1975, Solheim, 1988) and assuming Roche lobe overflow, that the mass ratio in the IBWDs must be extreme, forcing us to conclude that transfer in the IBWDs is proceeding from the less massive degenerate object to the more massive white dwarf. Since white dwarfs obey a degenerate mass-radius relation and expand as they lose mass, the mass donor must have had a larger initial radius and hence a smaller initial mass than the accretor. Its Roche lobe would therefore be smaller, so the secondary would be the first to contact its Roche lobe, as gravitational radiation slowly removed the system's orbital momentum and brought the two stars closer together. The immediate progenitor of the secondary produced a less massive relic than did the ancestor of the accreting white dwarf.

We can imagine several possible paths which could produce a white dwarf such as the mass donor in the IBWDs. For the first, we assume that the secondary's progenitor was a low mass star that did not have enough initial mass to achieve helium ignition. However, such a star would still be on the main sequence, and could not produce a white dwarf in a Hubble time (Iben, 1984).

Since a single star could not yet have formed a helium white dwarf, we must consider that the secondary in the IBWDs evolved in a binary environment. Evolution in a binary can deviate radically from the expected track of a single star. Roche overflow episodes cloud the issue of progenitor mass. The mass a component of a binary ends up with is not an accurate indicator of its mass at formation.

Since we find examples of IBWDs, it must be possible to form a he-

lium white dwarf in a binary system on timescale less than the age of the universe. On grounds of evolutionary timescales, we have already eliminated the possibility of a low mass main sequence star unable to ignite helium. The secondary must have had an initial mass of greater than about $0.5M_{\odot}$ (Kippenhahn, 1990), implying substantial mass loss during the course of its evolution. Let's consider a very generalized evolutionary track of a typical close binary system. The primary star, with initial mass anywhere from $2 - 8M_{\odot}$, will exhaust hydrogen in its core, expand to form a giant and fill its Roche lobe. The details of exactly when the star fills its lobe will determine the next fork in the path the binary is forced to. If the star fills its Roche lobe after it has formed a deep convection zone, right before helium ignition, the mass transfer will be on a timescale much quicker than the secondary envelope's thermal timescale, and a common envelope will form. Friction between the orbiting binary components and the envelope will decrease the orbital separation and drive the envelope out of the system. Transfer will proceed until the primary shrinks below its Roche lobe surface. The remnant will continue to evolve, and eventually contract until helium is ignited. If the helium burning star is below $\approx 0.75M_{\odot}$, it will not fill its Roche lobe again (Frank, 1985), and will proceed to the white dwarf phase without further mass loss.

If the primary fills it Roche lobe immediately after exhausting hydrogen, the mass transfer will be on a timescale comparable to the thermal timescale of the secondary's envelope and the secondary may accrete much of the mass lost by the primary (Frank, 1985). In cases of transfer from the more massive to the less massive star, the orbital separation will decrease.

In either case, the secondary star is now in an orbit much closer to

the primary than its original separation. It will exhaust hydrogen in its core, expand and fill its Roche lobe and begin a second stage of mass transfer. The rapid expansion of the secondary makes it likely that a common envelope will form during this phase as well. The results will be similar; the binary separation will decrease and the envelope will be driven off. We have found that, in the case of all the IBWDs, the secondary, as it contracted, did not achieve helium ignition and emerged as a helium white dwarf.

The degenerate mass donor is expanding in size as mass transfer continues in the present IBWD. Since we have shown that the transfer must be from the less massive to the more massive star, the binary separation will increase as well. If we reverse the flow of time and run the clock backwards, the components were once much closer together than they are now. Mass transfer from the more massive to the less massive star would have brought the two stars very much closer together. Whatever path we choose as the model for evolution of IBWDs, the previous history must end with the two stars very close together.

We can use the failure of the secondary to achieve helium ignition to argue in favor of double common envelope evolution. If the secondary accreted a large amount of mass directly from the primary, the secondary would have gained sufficient mass to create a helium core large enough to ignite helium after hydrogen exhaustion. The domination of helium in the IBWDs proves this did not occur. The best possible path we can find to the formation of an IBWD winds through two phases of common envelope evolution. The white dwarfs in IBWDs are relics of common envelope evolution and theoretical models of common envelope evolution being examined today must have IBWDs as a

possible an end product.

7.3 The Present Evolutionary Status of the IBWDs

Interacting objects are not static, but are constantly evolving, their futures inextricably tangled together. So it must be with the interacting twin degenerate systems. As the donor loses mass, the mass ratio of the binary changes, increasing the separation between the two components. The two stars spiral apart as they evolve. If we follow the course charted by models of IBWD systems and assume conservative mass transfer, the secondary is a degenerate object and must expand at an ever increasing rate as it continues to lose mass. Since we see IBWDs today, this obviously cannot be the case. We expect the orbital periods, mass transfer rates, and rates of change of binary separation to be bound together if mass transfer is to persist.

To first order, we find such patterns among the known IBWDs (Table 8.1). In Table 8.1, we list some parameters of the IBWDs, including an estimated $\dot{M}$. We calculated AM CVn's mass transfer rate assuming the measured $\dot{P} = 1.7 \times 10^{-11}$ was due entirely to mass transfer induced increase in the separation. We estimated $\dot{M}$ for PG1346, V803 Cen, and CP Eri by assuming the luminosity changes during outburst were due to accretion. And finally, the mass loss estimate for G61-29 comes from Nather *et al.*, (1981).

If we believe the large $\dot{M}$ for AM CVn and the identification of the photometric periods as representative of orbital periods, we do indeed see patterns among the IBWDs. AM CVn has the highest mass transfer rate, the shortest orbital period, and the highest effective temperature. PG1346+082,

Table 7.1: The Interacting Binary White Dwarf Systems

Name	Temp (K)	Magnitude (b)	Period (s)	Amp (mmi)	$\dot{M}(M_\odot)$
AM CVn	25000	14.4	1011.4	11-< 3	$4 \times 10^{-8}, 1 \times 10^{-12}$
			525.6	11	
PG1346	20000(h)	13.6-17.3	1471.3	55(l) 13(h)	2×10^{-9}
			1492.8	32	
V803 Cen	20000(h)	13.6-17.3	1600	20	2×10^{-9}
	15000(l)		175		
CP Eri		$\approx 16.7 - 21$	1800	68(h) 16(l)	2×10^{-9}
G61-29	$\leq 10000(disk)$	16.0	< 3	2790	$\approx 2 \times 10^{-11}$

V803 Cen and CP Eri have somewhat longer orbital periods and lower mass transfer rates. G61-29 has the longest orbital period of all, the lowest effective temperature, and the lowest estimate of mass transfer rate. We must note, however, that temperatures measured for IBWDs are probably disk temperatures, not temperatures of the central, accreting star.

If we imagined a single IBWD out in space evolving, we would expect the orbital period to gradually increase and perhaps the behaviour of our IBWD to go through phases of outburst. Table 8.1 demonstrates the presence of this trend in our sample of IBWDs. We propose that the distribution of IBWDs today trace out their evolutionary sequence. AM CVn should eventually begin undergoing outbursts when its orbital period reaches $\approx$ 1400 seconds, long enough to allow the formation of an the accretion disk capable of developing instabilities. The dwarf novae behaviour will cease when the orbital period reaches $\approx$ 2000 seconds, when the mass loss rate drops below the critical value necessary to create instabilities in the disk, and the temperature of the disk drops below that required for helium partial ionization (Smak, 1975).

If this evolutionary scenario of IBWDs is correct, it has profound consequences on the number distribution versus orbital period of the IBWDs. The trend of decreasing $\dot{M}$ with increasing orbital period leads us to expect decreasing rates of period change with increasing orbital periods. In other words, the IBWDs spend a good deal more time at longer orbital periods than shorter. The high mass loss systems evolve quickly to become eruptors, which evolve more slowly to become low mass transfer systems. In a given sample, we should have more systems in the same evolutionary state as G619-29. Selection effects bias our sample towards eruptors and bright systems like AM CVn. Systems like G61-29 would be hard to detect.

Our empirically implied dependence of period on mass transfer rate is in direct opposition to that predicted by models based on the assumption of conservative mass transfer. As the mass donor is whittled down in mass, its degenerate mass-radius relation demands that it expand at an ever increasing rate, increasing the transfer rate and causing the separation to increase very quickly. The increasing radius of the secondary's Roche lobe cannot keep up, (Iben *et al.*, 1986) resulting in a merger on a dynamical timescale. However, our results suggest that the mass transfer rate decreases with orbital period. The is not merely a question of having the endpoints of the sequence reversed, either. G61-29 is the only IBWD with an unambiguously identified orbital period, undeniably longer than the other systems. Some mechanism of angular momentum loss must function efficiently in the IBWDs. The IUE spectra of PG1346+082, V803 Cen and AM CVn all show narrow blue shifted absorption lines not arising from the central star or the disk. These lines are interpreted as arising from gas moving away from the system, towards us (Solheim, 1984),

indicating mass loss from the system. We cannot detect the red-shifted component arising from material moving away from us because the accretion disk is opaque and we cannot see through it. A small amount of mass loss could carry large amounts of angular momentum, slowing down the separation increase. If this interpretation is correct, the period changes we detect are convolutions of mass loss from the system and mass accretion onto the primary.

7.4 A View of the Future

We mentioned in our discussion of the previous history of the IBWDs that the mass donor will expand as mass transfer proceeds. Since the separation is also increasing, the mass transfer is self-sustaining, although it may not be conservative (see Appendix). The mass transfer will continue until the mass-radius relation of the donor changes at $\approx 0.001 M_{\odot}$ where the object loses its degeneracy. The secondary will then begin to shrink, and mass transfer will decrease dramatically.

The secondary, now Jupiter sized, will serenely orbit the primary white dwarf while the system radiates gravitational radiation. The two will spiral together and eventually transfer will increase. Although the process may be lengthy, eventually nothing will remain of the secondary star. Only a white dwarf with a helium surface layer will remain.

Solitary white dwarf stars come in different flavors. There are the hydrogen dominated DA white dwarfs, the hot DO pre-white dwarfs, and the helium dominated DB white dwarfs. There are also the occasional half-breeds, i.e. a few DA white dwarfs with some helium or metal lines and vice versa.

However, we have found no DB white dwarfs above $\approx 30,000$ K. The ratio of DBs to DAs is high in the 30,000 to 20,000 K range, but the number of DBs decreases until they essentially vanish at the cool end of the white dwarf evolution track (Fontaine, 1987). Various attempts have been made to explain this apparent chemical evolution of white dwarfs as they cool, from gravitational settling, radiative levitation, and accretion from the interstellar medium (Koester, 1987). Recently, Clemens (1993) has shown that all DA pulsating white dwarfs (DAVs) have thick ($10^{-4} M_{\odot}$) surface hydrogen layers. Since a DAV is an otherwise normal white dwarf, we can infer that all DAs have thick hydrogen envelopes. The mechanisms we listed assume thin surface layers and can no longer account for the appearance of DBs below 30000 K. We can deduce the existence of a second entry point onto the white dwarf cooling track.

All of the IBWDs, with the exception of G61-29 with measured effective temperature that is certainly the outer disk, have T_{eff} at the upper end of the DB temperature range, raising an intriguing possibility. Our evolutionary model of the IBWDs places them in the final stages of merger, the result will be a helium rich, DB white dwarf which will then proceed to cool on a white dwarf evolutionary timescale. Perhaps this represents another entry point into the white dwarf cooling track that does not begin with the hot DO stars. Perhaps the DBs have a different origin; the merging of IBWDs? The natural explanation for the lack of cool DBs(Fontaine, 1987) would be the simple fact that their evolutionary lifetimes encompass both white dwarf cooling times and binary merger times, including phases where gravitational radiation was the dominant force bringing the two stars together. The total time for merger could a be substantial fraction of the white dwarf cooling time (Wood,

1990). The temperature of the coolest DB is a measure of DB cooling time plus binary evolution time. If we assume the coolest DB is a merger and its total age is the same as the coolest observed DA white dwarf, we can calibrate an upper limit on the binary evolution timescale.

Our hypothesis of the IBWDs as the ancestors of the DB white dwarfs predicts that IBWD birthrates should compare favorably with the birthrates of the DBs. Unfortunately, birthrates depend on a knowledge of distances and lifetimes, direct measurements of which are both scarce and difficult to estimate.

We will begin our attempt to estimate IBWD birthrates with AM CVn. AM CVn can be either bright and far away, or fairly faint and close by, but not both at once. A parallax of 0.012 ± 0.007 arcseconds has been measured for the object (Vasilevskis, 1982), corresponding to a distance of 83 ± 60 pc and, assuming a bolometric correction of 2.4 magnitudes (Winget, 1981) an absolute magnitude of ≈ 7.0. At this magnitude and distance, AM CVn's luminosity is $\approx 0.1 L_{\odot}$, the luminosity of a 25000 K DB white dwarf.

If we use AM CVn as a standard candle, we can obtain relative distances to the other IBWDs, assuming the eruptors have the same luminosity in high state as AM CVn, and G61-29 has the same luminosity as the eruptors in low state. From the relative distances in Table 8.2 and using an estimated life time of 10^6 years (Patterson, 1992) we can obtain an range of estimates of the birthrate of IBWDs. If AM CVn has the luminosity of a DB white dwarf, and the parallax measurement is correct, the lower limit on the space density of IBWDs is $4 \times 10^{-7}\ pc^{-3}$ and the birthrate is $\approx 4 \times 10^{-13}\, pc^{-3} s^{-1}$. If we allow

Table 7.2: Distances of IBWDs

Name	$L_{AM} = 1.0 L\odot$	$L_{AM} = 0.1 L\odot$ parallax is correct
	Distance (pc)	Distance (pc)
AM CVn	780	87
PG1346	618	64
V803 Cen	618	64
CP Eri	2580	266
G61-29	282	160
new one	≈ 400	≈ 40

AM CVn to be bright ($1 L\odot$) and far away, the lower limit on the space density is $4 \times 10^{-10}\ pc^{-3}$, corresponding to a birthrate of $\approx 3.5 \times 10^{-15}\ pc^{-3} s^{-1}$.

To test our hypothesis of IBWDS as the progenitors of the DB white dwarfs, we must compare the two birthrates. The estimated DB birth rate is $\approx 10^{-13}\ pc^{-3} s^{-1}$ (Liebert, 1986), the same order of magnitude calculated for the IBWDs if the parallax measurement of AM CVn is correct. Much uncertainty is associated with each estimate, perhaps as much as an order of magnitude for either number. Our hypothesis is certainly not ruled out by our current observational knowledge. Indeed, the IBWDS could account for all of the DBs.

Our next logical step is to consider differences between DBs resulting from mergers and DBs that evolved as single stars. How could we separate them? Both would be helium dominated and from our limited perspective outside the surface would appear identical. However, all DBs must pass through the instability strip where helium partial ionization powers pulsation (Bradley, 1993). A DB pulsator from an IBWD progenitor would have a very different pulsation signature from a a solitary star DB relic. Accreting material trans-

fers angular momentum to the envelope of the accretor. Depending upon the coupling of the slippery degenerate core and the envelope, the rotation law of the merger DB will be quite different from a single star descendant. Rotation splits the observed pulsation model into $2l+1$ modes, separated by the rotation frequency (Unno, W., 1989). The accretor DB will be a differential rotator that will manifest itself in the rotational splitting of various modes excited in the star. Each mode samples a slightly different region of the white dwarf's interior, and sees a different rotation rate. The rotational frequency splitting for each mode of a differential rotator will be different. The Whole Earth Telescope recently observed the DB pulsator GD358. The star pulsates at over 100 frequencies. The signature of differential rotation has been found among different modes (Winget *et. al*, 1993).

A second possibility we must ponder is the difference between the thermal structure of solitary DBs and that of the DB relic of an IBWD. Any evolutionary path we consider for IBWDs must contain phases in which mass transfer between the white dwarfs does not occur, such as when the two white dwarfs were spiralling together under the influence of gravitational radiation. During this phase, the white dwarfs are cooling with typical white dwarf cooling times. The gravitational radiation timescale of an interacting binary white dwarf is $\approx 10^8 - 10^9$ years, the range depending on the initial orbital period assumed (Iben, 1984). If we imagine that the primary is a $0.6 M_{sun}$ carbon core white dwarf, it would cool from its initial temperature at formation to as little as $\approx$ 14000 K (Wood, 1990) during the gravitational radiation phase of the binary evolution. The cooling timescale increases if the primary in our IBWD is more massive. Eventually, the less massive white dwarf begins transferring material

to the compact accretor. The material falling to the surface of the accretor heats the outer layers of the star, producing a warmer surface temperature than we would predict if we knew the core temperature of the white dwarf. The depth of the heating depends on the accretion timescale.

If we took a slice from the accreting white dwarf, its thermal structure would be quite different from a slice of a "normal" DB white dwarf, perhaps affecting the normal modes of the star. When the IBWD relic finally passes through the DB instability strip, it may display different pulsation characteristics from a solitary DB. Theoretical work is underway to determine the effects of accretion heating on the normal modes of white dwarfs.

7.5 Where do We Go from Here?

The interacting binary white dwarfs are complicated objects, both in behaviour and evolution. They are laboratories of accretion, binary star evolution, and white dwarf evolution, their impact reaching deep into the foundations of astronomy. We have not heard the last of these intriguing systems.

Much work remains to be undertaken. Detailed analysis in the form of a WET campaign on another DB pulsating white dwarf is crucial. We must know if GD358 is unique, or if all DB variable (DBV) white dwarfs display the signature of differential rotation. This is vital to improve our knowledge of the origin of the helium white dwarfs.

We must improve our knowledge of the distances to the IBWDs. We must improve the parallax measurement for AM CVn, and attempt to measure the parallaxes of the other IBWDs. Perhaps we could enlist the help of the

Hubble Space Telescope.

Our evolutionary scheme for the IBWDs predicts the existence of more G61-29 type objects. We must search for these systems. A survey for cool white dwarfs is now underway at McDonald Observatory (Claver, 1993). If our scheme is correct, large numbers of G61-29 objects should show up in this survey.

We must continue monitoring each IBWD. AM CVn represents our best chance to identify a pulsing accreting white dwarf. The 525.6 second variation must be monitored to track the behaviour of $\dot{P}$ and identify any second derivative terms. A $\dot{P}$ for the 350.4 second variation will provide an important constraint on its relation to the 525.6 second period. Also, it would be nice to measure a $\dot{P}$ for PG1346+082 or V803 Cen. This is technically difficult, however, because of the mean magnitude changes of the system.

As an important test of the IBWD progenitor hypothesis, we must measure $\dot{P}$ for field DB pulsators. If some of these stars have Jupiter-sized companions we cannot detect via other mechanisms, we could detect them against a secular $\dot{P}$. The $\dot{P}$ we would measure would be a convolution of secular changes and orbital motion. If our IBWD progenitor model is correct, we would expect short timescale periodic variations in $\dot{P}$ to be superimposed on the secular cooling $\dot{P}$.

And finally, work is now underway to develop theoretical models of the accretor in these binaries. If a pulsator does exist in any of these objects, the pulsation signature may be influenced by the accreting material. It is crucial to understand the changes induced.

Chapter 8

References

Abbott, T. M. C., Opal, C. B., 1988, in Instrumentation for Ground-Based Optical Astronomy: Present and Future, ed L. B. Robinson (New York: Springer), 386.

Abbott, T. M. C., Robinson, E. L., Hill, G. J., Haswell, C. A. 1992, ApJ., 399, 680.

Abell, G. O., Morrison, D., Wolff, S. C. 1987, *Exploration of the Universe*, Saunders College Publishing, New York.

Angel, J. R. P., Landstreet, J. D. 1970, ApJ., 162, L61.

Bradley, P. A., Winget, D. E., Wood, M. A. 1992, ApJ., submitted.

Bradley, P. A., Ph. D. Thesis, University of Texas, 1993.

Becker, R. H. 1981, ApJ., 251, 626.

Burbidge, E. M., Strittmatter, P. A. 1971, ApJL., 170. L39.

Cheng, F. H., Lin, D. N. 1991, ApJ., 389, 714.

Claver, C. F., MacQueen, P. J. 1993, BAAS, 24, 1282.

Clemens, J. C., *Ph.D. Thesis*, University of Texas, Austin, Texas, 1993.

Elsworth, Y., Grimshaw, L., and James, J. F., 1982, MNRAS, 201, 45.

Elvius, A., 1975, A.&A., 44, 117.

Eracleous, M., Patterson, J., Halpern, J. 1991, ApJ., 370, 330.

Frank, J., King, A.R., Raine, D.J., 1985 "Accretion Power in Astrophysics ", Cambridge University Press.

Faulkner, J., Flannery, B. P., and Warner, B. 1972, ApJ., 175, L79.

Fontaine, G., Wesemael, F. 1987, IAU Coll. 95, 319.

Gentleman, W. M., Computer J. 1969, 11, 160.

Giclas, H. L., Burnham, R. Jr., Thomas, N. G. 1961, *Lowell Obs. Bull.*, 112, 61.

Greenstein, J. 1976, ApJ., L119.

Greenstein, J. 1986, AJ., 92, 867.

Greenstein, J., and Matthews, M. S. 1947, ApJ., 105, 85.

Iben, Icko, Tutukov, A. 1984, ApJ. Sup., 54, 335.

Iben, Icko, Tutukov, A. 1986, ApJ., 311, 742.

Iben, Icko, Tutukov, A. 1986, ApJ., 311, 753.

Jeffries, W. H., Fitzpatrick, J. E., McArthur, B. E., and McCartner, J. E. 1988, in Gaussfit: A System for Least Squares and Robust Estimation USER's MANUAL(Austin: University of Texas, Dept. of Astronomy).

Hege, E. K., Allen, C. K., Cocke, W. J. 1991, ApJ., 381, 543.

Hirose, M., Osaki, Y. 1990, PASJ, 42, 135.

Howell, S. B., Szkody, P. , Kreidl, T. J., Dobrzycka, D. 1991 PASP, 103, 300.

Humason, M. L., and Zwicky, F. 1947, ApJ., 105, 85-19.

Kepler, S. O., Robinson, E. L., Nather, R. E., and McGraw, J. T. 1982, ApJ., 254, 676.

Kepler, S. O., Steiner, J. E., Jablonski, F., 1989, IAU Colloq., 114, 443.

Kippenhahn, R., Weigert, A. 1990, Stellar Structure and Evolution (Berlin: Springer)

Koester, D., 1987 IAU Coll. 95, 329.

Krzeminski, W. 1972, Acta Astr., 22, 387.

Kurtz, D. W., Shibahashi, H., Goode, P. R., 1990, MNRAS, 247, 558.

Kurtz, D. W., Kanaan, A., Martinez, P., Tripe, P., 1992 MNRAS, 255, 289.

Lambert, D. L., Slovak, M. H. 1981, PASP, 80, 477.

Lazaro, C., Solheim, J.-E., Arevalo, M. J., 1989, *IAU Colloq. 114*, 458.

Liebert, J., Wesemael, F., Hansen, C.J., Fontaine, G., Shipman, H.L., Sion, E.M., Winget, D.E., and Green, R.F. 1986 ApJ., 309, 241.

Luyten, W. J., Haro, G. 1959, PASP, 71, 469.

Marsh, T. R., Horne, K. 1991, ApJ., 366, 535.

Mochkovitch, R. 1993, in *White Dwarfs: Advances in Observation and Theory*, M. Barstow, ed., 107.

Molnar, L. A., Kobulnicky, H. A. 1992, ApJ., 392, 678.

Nather, R. E., Warner, Brian 1969, MNRAS, 143, 145.

Nather, R. E. 1973, *Vistas Astr.*, **15**, 91.

Nather, R. E., Robinson, E. L., Stover, R. J. 1981, ApJ., 244, 269.

Nather, R. E., Wood, M. A., Winget, D. E., and Liebert, J. 1984, IAU Circ., 4021.

Nather, R. E., Winget, D. E., Clemens, J. C., Hansen, C. J., Hine, B. P. 1990, ApJ., 361, 309.

Nather, R. E., 1993, private communication

Oke, J. B., Wade, R. A., 1982 AJ., 87, 670.

Oke, J. B., Wade, R. A., 1974 Ap. J. Sup. 27, 21.

O'Donoghue, D., Kilkenny, D., 1989 MNRAS, 236, 319.

O'Donoghue, D., Wargau, W., Warner, B., Kilkenny, D., Martinez, P., Kanaan, A., Kepler, S. O., Henry, G., Winget, D. E., Clemens, J. C., Grauer, A. 1990, MNRAS, 245, 140.

Osaki, Y. 1985, A&A., 144, 369.

Osaki, Y. 1989, PASJ, 41, 1005.

Patterson, J., Nather, R. E., & Robinson, E. L. 1979, ApJ., 232, 819.

Patterson, J., Raymond, J.C. 1984, ApJ., 292, 535.

Patterson, J., Sterner, Emily, Halpern, Jules P., Raymond, John C. 1991, ApJ., 384, 384.

Patterson, J., Schwartz, D. A., Pye, J. P., Blair, W. P., Williams, G. A., Caillault, J.-P. 1992, ApJ., 392, 233.

Patterson, J., Thomas, G., Skillman, D. R., Diaz, M. 1993, ApJ. Sup., 86, 235.

Patterson, J., Halpern, J., Shambrook, A. 1993, submitted to ApJ.

Fress, W. H., Flannery, B. P., Teukolsky, S. A., Vettering, W. T., in Numerical Recipes, Cambridge University Press, New York, 1987.

Probst, R. G., 1983 Ap. J. Sup., 53, 335.

Provencal, J. L., Clemens, J. C., Henry, G., Hine, B. P., Nather, R. E., Winget, d. E., Wood, M. A., Kepler, S. O., Vauclair, G., Chevreton, M., O'Donoghue, D., Warner, b., Grauer, A. D., Ferrario L. 1988, IAU Colloquium No. 114, 296.

Provencal, J. L., Master's Thesis, Univserity of Texas and McDonald Observatory, 1990.

Robinson, E.L., Faulkner, J. 1975 ApJ., 200,L23.

Robinson, E. L., 1979, IAU Colloquium 53, White Dwarfs and Variable Degenerate Stars, ed. H. M. Van Horn and V. Weidemann (Rochester, N.Y.: University of Rochester), 343.

Robinson, E. L., Shafter, A. W. 1987, ApJ., 322, 296.

Robinson, E. L., Shafter, A. W., Balachandran, S. 1991, ApJ., 374, 298.

Shakura, N. I., Sunyaev, R. A. 1973, A&A, 24, 337.

Simon, T., Herbig, G., Boesgaard, A. M. 1985, ApJ., 551.

Smak, J. 1967 Acta. Astr., 17, 255.

Smak, J. 1975, Acta. Astr., 25, 227.

Smak, J. 1983, Acta. Astr., 33, 333.

Solheim, J. E., Robinson, E. L., Nather, R. E., Kepler, S. O. 1984, Astron. Astrophys., 135, 1-11.

Solheim, J. E., Proceedings of IAU Colloquium No. 114, (Lecture Notes in Physics, Vol. 328) 1988, 446.

Solheim, J. E., et. al 1992, in preparation.

Stover, R. J. 1983, PASP, 95, 18.

Szkody, P., Howell, S. B., Mateo, M., Kreidl, T. J. 1989, PASP, 899.

Trimble, V., Sahade, J. eds., in The Realm of Interacting Binary Stars, Kluwer Academic Publishers, 1993.

Ulla, A. M., Solheim, J. E. 1989, Ap&SS, 236, 319.

Unno, W., Oskai, Y., Anodo, H., Saio, H., Shibahashi, H., Nonradial Oscillations of Stars, University of Tokyo Press, 1989.

Van Horn, H. M., Wesemael, F. Winget, D. E. 1980, ApJL., 235, L143.

Vasilevskis, S., Harlan, E. A., Klemola, A. R., Wirtanen, C. A. 1975, *Publ. Lick. Obs.*, 22, Part 5.

Voikhanskaya, N. F. 1982, Sov. Astron., 26, 558.

Wade, R. A., Ward, M. J., Interacting Binary Stars, Cambridge University Press, 1985, 149.

Warner, B. and Robinson, E. L. 1972, MNRAS, 159, 101.

Warner, B. 1972, MNRAS, 159, 315.

Warner, B., Nather, R. E., 1972, MNRAS, 159, 429.

Warner, B., O'Donoghue, D., & Wargau, W., 1989, MNRAS, 238, 73.

Whitehurst, Robert 1988, ApJ., 32, 35.

Whitehurst, Robert 1988, MNRAS, 232, 35.

Wickramasinghe, D. T., Hintzen, P., Strittmatter, P. A., 1975, ApJ., 191.

Winget, D. E., *Ph.D. Thesis*, University of Rochester, Rochester, N.Y., 1981.

Winget, D. E., Van Horn, H. M., Tassoul, M., Hansen, C. J., Fontaine, G., and Carroll, B. W. 1982, ApJ., 252, L65.

Winget, D. E., Nather, R. E., Hill, J. Allen 1987, ApJ., 316, 305.

Winget, D.E., Nather, R.E., Clemens, J.C., Provencal, J., Kleinman, S.J., Bradley, P.A., Wood, M.A., Claver, C.F., Frueh, M.L., Grauer, A.D., Hine, B.P., Hansen, C.J., Fontaine, G., Achilleos, N., Wickramasinghe, D.T., Marar, T.M.K., Seetha, S., Ashoka, B.N., O'Donoghue, D., Warner, B., Kurtz, D.W., Buckley, D.A., Brickhill, J., Vauclair, G., Dolez, N., Chevreton, M., Barstow, M.A., Solheim, J.E., Kanaan, A., Kepler, S.O., Henry, G.W., Kawaler, S.D. 1992, ApJ., 378, 326.

Winget, D. E., Nather, R. E., Clemens, J. C., Provencal, J. L., Kleinman, S. J., Bradley, P. A., Claver, C. F., Dixson, J. S., Montgomer, M. H., Hansen, C. J., Hine, B. P., Birch, P., Candy, M., Marar, T. M. K., Seetha, S., Ashoka, B. N., Leibowitz, E. M., O'Donoghue, D., Warner, B., Buckley, D. A. H., Tripe, P., Vauclair, G., Dolez, N., Chevreton, M., Kepler, S. O., Kanaan, A., Augusteijn, T., Wood, M. A., Bergeron, P., Grauer, A. D. 1993, in press.

Wood, Janet H., Horne, K., Horne, S. 1992, 385, 294.

Wood, M. A., Winget, D. E., Nather, R. E., Hessman, Frederic V., Liebert, James, Kurtz, D. W., Wesemael, F., Wegner, G. 1987, ApJ., 313, 757.

Wood, M. A., Ph.D. Thesis, University of Texas, 1990.

Zhang, E. H., Robinson, E. L., Nather, R. E. 1986, ApJ., 305, 740.

Zhang, E. H., Robinson, E. L. 1987, ApJ., 321, 813.

Zhang, Erho, Robinson, E. L., Ramsyer, Tod F., Shetrone, Mathew D., Stiening, Rae, ApJ. 320, 714.

VITA

Judith Lucille Provencal was born on February 1, 1965 to Ronald (BonHomme) and Paulette Provencal of Biddeford, Maine. The family quickly picked up and moved to the quaint fishing and nuclear sub repairing village of Kittery, Maine, where Ronald opened an appliance store and Judi grew up. She attended R. W. Traip Academy (a public institution despite its name) and thankfully graduated in 1983, but was disappointed to watch Kittery become overrun with shopping malls and factory outlets. She then proceeded to Smith College in Northampton, MA. where, besides receiving a Bachelor of Arts in 1987, she was introduced to the world of the horse, a nearly incurable disease that afflicts her still today. Judi also enjoyed an illustrious career at Smith as intramural athletic representative for Tyler House. Her house won the prize for most participation two years in a row. Of course, it may have had something to do with the riding whip with which she coerced her fellow Smithies to participate in the activities. Judi also masquaraded as "the shadow", the infamous figure who secretly left everyone candy on Halloween. Of course, her secret identity was safe, as no one believed such a mild mannered Smithie could accomplish such an outrageous deed. After graduating from Smith, Judi moved to Texas on the advice of Susan Edwards and began her graduate career in September of 1987, cursing the Texas summer heat, the lack of real trees, and wondering why Texans insist on calling what is obviously a river a lake. In December of 1987, she met Golden, a stubborn quarter horse. In 1989, Golden moved to Judi's house, and hasn't left since. Judi received her Master of Arts in astronomy in 1990. She continued her work with the Whole Earth Telescope,

and travelled to the far reaches of the globe. After her Ph.D. defense, Judi will hitch up her diesel truck, pack her horse into a trailer, and move to Delaware to begin her post-doctoral career with Dr. Harry Shipman.

Permanent address: Rte. 4 Box 231
Georgetown, Texas 78628

This dissertation was typeset [1]with LaTeX by the author.

[1]The LaTeX document preparation system was developed by Leslie Lamport as a special version of Donald Knuth's TeX program for computer typesetting. TeX is a trademark of the American Mathematical Society. The LaTeX macro package for The University of Texas at Austin dissertation format was written by Khe-Sing The.